SPACE RESEARCH COORDINATION CENTER

A METHOD FOR SODIUM DAYGLOW MEASUREMENT USING A ZEEMAN PHOTOMETER WITH A POLAROID FILTER

BY

BRUCE WILLIAM GUENTHER

DEPARTMENT OF PHYSICS

SRCC REPORT NO. 120

NGL-39-011-002

UNIVERSITY OF PITTSBURGH

PITTSBURGH, PENNSYLVANIA

13 FEBRUARY 1970

The Space Research Coordination Center, established in May, 1963, has the following functions: (1) it administers predoctoral and postdoctoral fellowships in space-related science and engineering programs; (2) it makes available, on application and after review, allocations to assist new faculty members in the Division of the Natural Sciences and the School of Engineering to initiate research programs or to permit established faculty members to do preliminary work on research ideas of a novel character; (3) in the Division of the Natural Sciences it makes an annual allocation of funds to the interdisciplinary Laboratory for Atmospheric and Space Sciences; (4) in the School of Engineering it makes a similar allocation of funds to the Department of Metallurgical and Materials Engineering and to the program in Engineering Systems Management of the Department of Industrial Engineering; and (5) in concert with the University's Knowledge Availability Systems Center, it seeks to assist in the orderly transfer of new space-generated knowledge in industrial application. The Center also issues periodic reports of space-oriented research and a comprehensive annual report.

The Center is supported by an Institutional Grant (NsG-416) from the National Aeronautics and Space Administration, strongly supplemented by grants from the A. W. Mellon Educational and Charitable Trust, the Maurice Falk Medical Fund, the Richard King Mellon Foundation and the Sarah Mellon Scaife Foundation. Much of the work described in SRCC reports is financed by other grants, made to individual faculty members.

A METHOD FOR SODIUM DAYGLOW MEASUREMENT USING A ZEEMAN PHOTOMETER WITH A POLAROID FILTER

By

Bruce William Guenther

B.A., Gettysburg College, 1965

Submitted to the Graduate Faculty of
Arts and Sciences in partial fulfillment
of the requirements for the degree of
Master of Science

University of Pittsburgh

1969

PREFACE

The author wishes to express his gratitude to his advisor, Professor T. M. Donahue, for his guidance and support. Much of the instrument was designed by W. A. Feibelman, and electronics modifications were undertaken by E. Korpela. The author also recognizes the support, understanding and sacrifices on the part of his wife, Sue.

This research was sponsored by National Science Foundation grants GP4435 and GA1237.

TABLE OF CONTENTS

FIGURE CAPTIONS

I. INTRODUCTION

The sodium doublet emissions of 5890-5896Å have been known to be part of the airglow since 1929 when Slipher first reported measurements of a 5892Å emission from the night sky (Slipher, 1929). In 1937 Cherniaev and Vuks first reported a twilight enhancement in this wavelength (Cherniaev and Vuks, 1937). T. M. Donahue, in 1956, first calculated a sodium dayglow intensity (Donahue, 1956). Reviews of the sodium airglow literature are provided in Chamberlain (1961), Hunten (1964), and Donahue (1965).

During the day free atomic sodium emitting the yellow doublet was shown to be narrowly layered in a 5 km wide region centered at 92.4 km by a sodium vapor scattering chamber detector flown in a rocket from Wallops Island, Virginia (Donahue and Meier, 1967). During the twilight the sodium doublet has been investigated by means of a chopping wheel-wedge photometer and diffraction grating. While the sun slips below the horizon, the earth's shadow progressively sweeps from below the emitting sodium atoms through and above the emitting atoms. The sodium resonance signal measured by a detector during this time is proportional to the integral number of sodium atoms above the shadow. By differentiating this signal, the altitude profile of free atomic sodium during the twilight can be obtained. This twilight experiment shows the sodium also in a narrow layer, but indicates the twilight layer is several kilometers lower than the dayglow layer of Donahue and Meier. Several layering mechanisms have been suggested but none of them seem satisfactory. The layering mechanism is beyond the scope of this paper.

This paper will present a new method for measuring dayglow atmospheric sodium emissions with a ground based device called a Zeeman photometer. As this detector currently is used, a direct measurement of the polarization of the sodium doublet and Rayleigh scattered background is taken by placing a polaroid filter in front of the input optics into the photometer. Since both the Rayleigh scattered surface brightness and the D_2 sodium component, the $^2P_{3/2} - {}^2S_{\frac{1}{2}}$ transition which radiates at 5890Å, are polarized, and since the plane of polarization, which is perpendicular to the plane including the sun, the detector, and the observed sky, changes throughout the day as the position of the sun in the sky changes, the polarization of the signals to be measured changes throughout the day. A previous method of using the Zeeman photometer to deduce atmospheric sodium emissions which did not include a direct measurement of the polarization will be discussed here; and a comparison will be made with the new method.

The solar Fraunhofer lines contain an absorption profile such that the full width at half depth of the absorption well is about 1400 mK in both the D_1 and D_2 lines, where a mK is a milli-Kayser or 10^{-3} cm^{-1}. The intensity at the bottom of the Fraunhofer lines is about 5% the intensity which the solar spectrum would be in the absence of the Fraunhofer lines. The emissions from free atomic sodium in the earth's atmosphere will be an enhancement to the underlying Fraunhofer continuum at the center of the absorption feature, and will have a bimodal shape due to the large hfs splitting of the $^2S_{\frac{1}{2}}$ energy levels with respect to the splitting of the energy levels of the $^2P_{3/2}$ or $^2P_{\frac{1}{2}}$. The D_1 emission is the Doppler broadened profile of 4 hfs transitions, with a

Doppler width $\Delta\nu_D$ = 23 mK for T = 200°K, the temperature of the atmospheric free sodium. The D_2 emission is the sum of 6 hfs transitions.

The Zeeman photometer utilizes a sodium vapor scattering chamber between the poles of a magnet. The sodium vapor absorption cross-section strongly overlaps the emission profile of the atmospheric sodium for zero field applied across the chamber. The temperature of the vapor is maintained near 438°K so that the Doppler width of the vapor in the cell is about $\sqrt{2}$ larger than the Doppler width of the atmospheric sodium emissions. When a magnetic field is applied to the chamber, Paschen-Back effect splitting will alter the energy levels of the sodium atom so that the strong overlap of the scattering chamber zero field absorption cross-sections and the atmospheric emission cross-sections will be destroyed. At 5000 Gauss, the strongest field used for this study, the D_1 line will absorb 10^{-4} the signal it would absorb at zero field, while the D_2 line will have 1/3 the cross-section overlap which exists for the zero field. By comparing the zero field and 5000 Gauss signals measured by the Zeeman photometer, the surface brightness of the sodium emissions and Rayleigh scattered background can be determined.

When a magnetic field is applied across the vapor in the scattering chamber and a polarized beam enters the chamber, the transition probabilities for absorption are not given by the Einstein coefficients alone, but include a dependence on the angle between the axis of polarization and the axis of the applied field. Instead of calculating explicitly the transition probabilities for all angles, the method presented here assumes that all light transmitted into the scattering

chamber through the polaroid will be polarized either parallel or perpendicular to the axis of the polaroid. In that the angular dependence of the transition probabilities is $\cos^2\theta$ or $\sin^2\theta$ for p or s transitions, that is with $\Delta m = 0$ and $\Delta m = \pm 1$ between the initial and final hfs level, the polaroid is oriented at 45° with respect to the axis of the field. In this manner all changes in the degree of polarization and the plane of polarization will mean a change in the signal attenuation in the polaroid but no change in the transition probabilities.

For the calculations included in this study, a high speed digital computer (the University of Pittsburgh's IBM 7090) was used extensively.

II. INSTRUMENTATION

The Zeeman photometer used in this study to measure resonately scattered atmospheric sodium emissions basically is composed of an optical system, a scattering chamber embedded between the pole pieces of a magnet, and the supporting electronics. The scattering chamber and the electronics will be discussed later in this section.

The relation between the optical arm signal input to the scattering chamber and the optical arm signal output from the chamber to the photomultiplier tube is shown in Figure I. Although Figure I is not a scaled diagram, the input and output arms are given to scale as Figures II and III respectively.

Each optical arm includes two lenses. In the optical input arm lens B is placed at the focal point of lens A, and a solenoid actuated shutter can close onto lens B, closing the scattering system to light. All light entering the scattering chamber must pass through lens A first, and then lens B. Light baffles between the lenses are used to reduce light scatter off the walls of the cylinder supporting the input optics. When the experiment is operated with a polaroid filter, the filter is placed in front of lens A.

In the optical output arm from the scattering chamber to the PM tube, an interference filter with a 20Å band pass at 50% peak transmission and centered at 5893Å is situated between the two lenses. A glass blank adjacent to the scattering chamber on the output arm is used to guard against excessive heat diffusion onto the first lens and the interference filter. All the components of the output optics except the glass blank,

and including the photomultiplier tube viewing the scattering chamber, are mounted by means of a long aluminum cylinder, without any baffles.

Mounted on the long cylinder containing the output optics is an additional photomultiplier tube with a broad band transmission filter, with a full band pass at half intensity of 100Å. With a broad band filter, this PM tube monitors the white light or background intensity.

The scattering cell is a transparent plastic in the shape of a Wood's Horn. The front section of the cell is in a rectangular shape and is called the head or head section. The rear or tail section is shaped as a horn so that all reflections off the walls of the tail are trapped in the tail. The scattering chamber, which is injected with free atomic sodium and sealed, can be seen in Figure I. With the exception of the foremost portion of the head, the entire scattering chamber is coated with a black paint to improve the stray light scattering characteristics.

The head and tail sections of the cell are wrapped independently with heating wire. The heating wire in the head section of the cell maintains the walls of the chamber at 438°K throughout the entire operation of the Zeeman photometer. The heating coil is controlled by a thermister temperature sensing device capable of maintaining the temperature within a degree of the required value. The tail heating also controlled by a thermister temperature sensing device is alternately on and off in periods of about 15 minutes each, giving alternately periods when the scattering chamber is filled with vapor and periods when the sodium vapor is condensed in the tail section. When the tail section is being heated, the temperature in the tail is maintained 15°K below the

head section to avoid condensation of the sodium vapor on the front windows. Sodium vapor condensed on the front window would destroy the scattering characteristics of the chamber. When the tail section is not being heated, a fan mounted outside the aluminum housing containing the scattering chamber blows air onto the tail section, while the heating is maintained in the head section, to quicken the condensation of the vapor in the tail section. The scattering properties of the vapor cell are regularly monitored without any vapor in the chamber because the scattering chamber inevitably passes a stray or parasitic light signal which changes throughout the day. This parasitic signal, or I_p, is then effectively treated as an instrumental background and must be distinguished from the signal measured when the shutter is closed.

When the shutter is closed, the chamber is light tight, and there can be no scattering out of the chamber. Any signal measured when the shutter is closed must be a residual signal in the electronics of the detecting system. When the shutter is closed, we get a signal which we call the dark current. The parasitic light signal is an enhancement above the dark current when the shutter is open, but the chamber is without sodium vapor.

The scattering chamber photomultiplier tube used in this experiment is an RCA C70038D side window tube operated at a voltage of -1250 V, which is supplied by a Fluke High Voltage Power Supply. The monitor PM tube is an RCA tube operated at -850 V supplied by the same power supply. This power supply has two parallel outputs, so that the monitor voltage is supplied through a simple voltage dividing network. The signals from the PM tubes are connected to separate Keithley Electrometers which in turn drive a two channel Texas Instrument strip chart recorder. The

temperatures of the head and tail sections of the scattering chamber are monitored by Dohrmann temperature controls and two variacs supply the voltage to the heating coils. The power supply for the magnet is an Alpha Power Supply. The temporal relationships between the heating and cooling cycles of the tail, the various magnetic field settings used in this study, and the operation of the shutter are maintained by a motor driven series of cams and microswitches. A complete cycle of the cam drive includes two complete 30 minute cycles of the scattering chamber.

A complete 30 minute cycle of the scattering chamber will begin and end with the shutter closed and without any vapor in the chamber. When the shutter is opened, the wire in the tail section will begin to heat; it takes several minutes before any sodium is vaporized. Before any sodium is vaporized, the parasitic light scattering properties of the cell are monitored and the signal above the dark current counting rate is identified as I_p. When all the vapor is condensed in the tail, the cell is referred to as a cold cell.

About 13 minutes after the heating coils are turned on in the tail, an equilibrium is reached in the chamber between the evaporation and condensation of the sodium in the cell. The cell is then referred to as a hot cell. All signals measured during the hot cell configuration are measured as enhancements above the parasitic light signal. When the sodium is vaporized, magnetic fields of 1000, 3000, and 5000 Gauss are applied across the hot cell. The amplitude recorded for the zero, 1000, 3000, and 5000 G field settings give respectively I_o, I_1, I_3, and I_5. Typical responses for a cycle would include a dark current of

several 10^{-11} amps, $I_p \sim 10^{-10}$ amps, I_o about the magnitude of I_p, and I_5 about three times as large as I_o.

The ordering of cycling is given in Figure IV, which indicates that each of the three non-zero field settings is used twice in a complete cycle. In the middle of the hot cell portion of the cycle, the shutter is closed for another dark current reading. Because of the symmetry present in the cycling, data can be taken nearly simultaneously with and without a polaroid by alternating the polaroid on and off with each successive closing of the shutter.

The phototubes are placed about four feet away from the scattering chamber and magnet on the light output supporting cylinder so that the magnetic field generated at the chamber will not alter the amplification characteristics of the photomultiplier. The monitor and light input optics are pointed to the north pole, along the earth's axis, at an elevation of 45°.

The measurements taken for this paper were taken at the University of Pittsburgh's Airglow Observatory in Lynn Run State Park (-79.185° long, 40.185° lat) on 21 July 1968, 27 January 1969, and 26 July 1969.

III. RADIATIVE TRANSFER

The sodium doublet is composed of transmissions to the $3s^2S_{\frac{1}{2}}$ ground state of free atomic sodium from the $3p^2P_{\frac{1}{2}}$ and $3p^2P_{3/2}$ states for the D_1 and D_2 emissions respectively. The hyperfine structure splitting of the ground state, an interaction between the magnetic field generated at the nucleus by the elctron cloud and the nuclear spin I = 3/2, is large with respect to the hfs splitting of the $^2P_{\frac{1}{2}}$ and $^2P_{3/2}$. Using the total atomic angular momentum, $\vec{F}$, where F = J + I and J is the total angular momentum of the electron cloud, the hfs splitting for the $^2S_{\frac{1}{2}}$ results in energy levels -36.9341 mK for F = 1 and +22.160 mK for F = 2 relative to the centroid, where this energy unit, the milli-Kayser, is 10^{-3} cm^{-1} (Kusch and Taub, 1949). The $^2P_{\frac{1}{2}}$ state has two hfs components at -4.0 mK for F = 1 and +2.4 mK for F = 2 (Jackson and Kuhn, 1938), and $^2P_{3/2}$ splits into four components at -2.43 mK (F = 0), -1.76 mK (F = 1), -0.50 mK (F = 2), and +1.49 mK (F = 30) (Sagalyn, 1954) measured relative to their respective centroids.

The Zeeman diagram for free atomic sodium is the following:

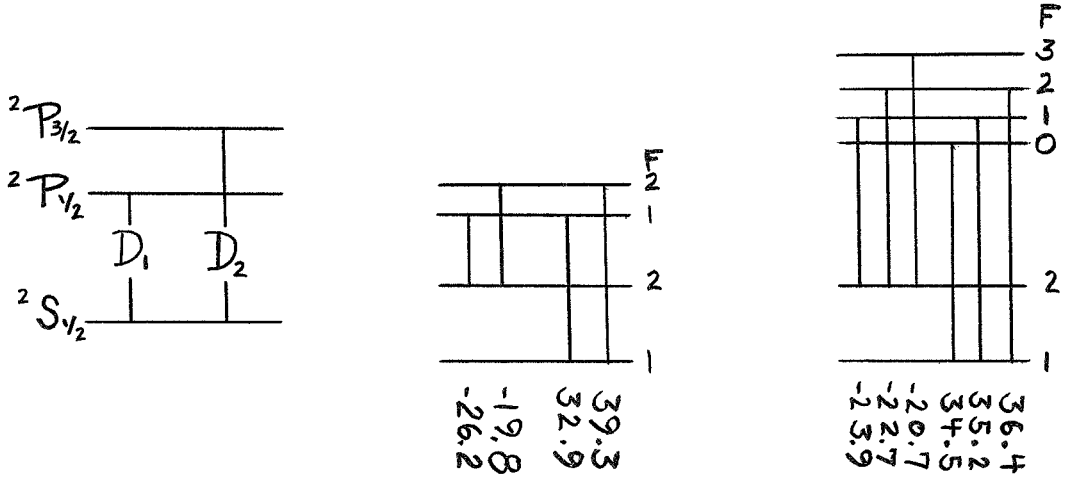

The centroids are at 16956 cm^{-1} for the D_1 and 16973 cm^{-1} for the D_2 components. Designating transitions with the less

energetic F = 2 level of the $^2S_{\frac{1}{2}}$ as D_{1a} and D_{2a} respectively for the D_1 and D_2 lines, and likewise D_{1b} and D_{2b} for the F = 1 level of the $^2S_{\frac{1}{2}}$, the relative transition probabilities at the centroid of these components are to be adjusted to give the experimentally obtained values for the absorption coefficients at 200°K of

$$\sigma_o(D_{2a}) = 8.94 * 10^{-12} \text{ cm}^2 \qquad \sigma_o(D_{1a}) = 4.47 * 10^{-12} \text{ cm}^2$$
$$\sigma_o(D_{2b}) = 5.53 * 10^{-12} \text{ cm}^2 \qquad \sigma_o(D_{1b}) = 2.72 * 10^{-12} \text{ cm}^2 . \tag{1}$$

The shape of the absorption cross-sections for the D_1 and D_2 lines can be obtained by summing the four or six Doppler temperature broadened hfs components shown in the Zeeman diagram. The Doppler width $\Delta\nu_D$ relates Boltzman's constant, the temperature, and mass of the absorbing atom by $\Delta\nu_D = (2kT/m)^{\frac{1}{2}}$, and has the value $\Delta\nu_D$ = 23 mK for sodium at 200°K. Figure V gives the shape of the Doppler profile for a Doppler width of 23 mK, calculated from e^{-x^2} where $x = \Delta\nu_D/23$ mK is the displacement from the centroid.

The following radiative transfer calculations are handled in much the same manner as in Donahue and Meier (1967). The sodium rate of emission of photons per unit volume, called the source function, is S(z) at an altitude z, and the apparent surface brightness observed at a direction is given by

$$4\pi I(z) = \int S(z')dz'/\cos\theta \tag{2}$$

where the integration is from z to the upper boundary of the medium.

We are assuming here that the sodium emission rate is produced by scattering from a beam of solar photons incident on the topside of the layer from outside the layer. For a density of scatters, $\rho(z)$, we introduce the optical depth, a distance scale called τ, defined as

$$\tau = \sigma_o \int_z^\infty \rho(z')dz' \tag{3}$$

which can be evaluated between any level z and infinity. The optical depth is the absorption cross-section evaluated at the centroid multiplied by the column abundance. For atmospheric sodium the optical depth is small, which means we expect an insignificant amount of multiple scattering. We will also treat the radiative transfer calculations as if the scattering is incoherent, i.e. a photon absorbed, either in the core or the wings of the absorption cross-section, can be reemitted anywhere in the emission cross-section independent of the frequency of absorption, and that the scattering is isotropic. That the re-emission will be incoherent and isotropic in the observers reference frame is referred to as complete frequency redistribution. A complete discussion of the accuracy of complete frequency redistribution (CFR) is given in a thesis by George Doschek, (1968), in which it is shown that CFR is an accurate approximation for problems dealing with small optical depths.

For an initial intensity $(\pi F\nu)_o$ solar photons cm^{-2} sec^{-1} in a unit frequency incident on the top of the layer at an angle whose cosine is μ_o, the initial source function S_o, the initial rate of excitation, will be given by

$$S_o = (\pi F_\nu)_o \, \Delta\nu_D \int_{-\infty}^{\infty} e^{-x^2} \, e^{-\tau e^{-x^2}/\mu_o} \, dx \tag{4}$$

for $x = (\nu - \nu_o)/\Delta\nu_D$ where ν_D is the centroid of the emission cross-section.

Introducing the Holstein radiative transfer T function (Holstein, 1947)

$$T(\tau) = \frac{1}{\sqrt{\pi}} \int_{-\infty}^{\infty} e^{-x^2} \exp(-\tau \, e^{-x^2}) dx \tag{5}$$

we get for the source function

$$S_o = (\pi F_\nu)_D \, \sqrt{\pi} \, \Delta\nu_D T(\tau/\mu_o) \tag{6}$$

$T(\tau)$ is the probability that a photon emitted in the medium will travel a depth τ without being absorbed. $T(\tau)$ is catalogued in Table I, and shown in Figure VIII.

We see then that

$$\epsilon(\Delta\tau) = \frac{2\pi}{4\pi} \int_o^1 T(\Delta\tau/\mu) d\mu \tag{7}$$

$$= \frac{1}{2\sqrt{\pi}} \int_o^1 \int_{-\infty}^{\infty} e^{-x^2} \exp(\Delta\tau \, e^{-x^2}/\mu) dx d\mu \tag{8}$$

is the probability that a resonance photon emitted is somewhere in the layer and crosses a plane $\Delta\tau$ away, measured vertically. Figure IX gives ϵ for τ less than 2.000. The probability that a photon is emitted at τ' and absorbed τ away in a layer of width $d\tau$ will be

$$H(\tau', \tau) = - \frac{\partial \epsilon}{\partial \tau} \tag{9}$$

$H(\tau',\tau)$ is readily evaluated to give

$$H(|\tau'-\tau|) = -\frac{1}{2\sqrt{\pi}} \int_0^1 \int_{-\infty}^{\infty} \frac{e^{-2x^2}}{\mu} \exp\left(-|\tau-\tau'| \frac{e^{-x^2}}{\mu}\right) dx d\mu. \quad (10)$$

For small optical thicknesses, the functions, T, ϵ, and H are most easily generated in the following manner.

If we define

$$K_1(\tau) = \tfrac{1}{2} \int_{-\infty}^{\infty} \varphi^2(x)\, E_1(\tau\varphi(x))dx \quad (11)$$

$$K_2(\tau) = \int_{-\infty}^{\infty} \varphi(x)\, E_2(\tau\varphi(x))dx \quad (12)$$

$$M_1(\tau) = \tfrac{1}{2} \int_{-\infty}^{\infty} \varphi^2(x)\, \exp(-\tau\varphi(x))dx \quad (13)$$

$$M_2(\tau) = \int_{-\infty}^{\infty} \varphi(x)\, \exp(-\tau\varphi(x))dx \quad (14)$$

with $\varphi(x)$ the line shape, here the Doppler line shape

$$E_1(\tau) = \int_1^{\infty} \frac{e^{-\tau x}}{x}\, dx \quad (15)$$

and

$$E_2(\tau) = \int_1^{\infty} \frac{e^{-\tau x}}{x^2}\, dx \quad (16)$$

then

$$K_1(\tau) = \tfrac{1}{2} \int_{-\infty}^{\infty} \varphi^2(x) \int_1^{\infty} \frac{\exp(-\tau\varphi(x)T)}{T}\, dT$$

$$= -\tfrac{1}{2} \int_{-\infty}^{\infty} \int_1^{\infty} \varphi^2(x)\, \exp(-\tau/\mu\, \varphi(x))\, d\mu/\mu$$

$$K_1(\tau) = \sqrt{\pi}\, H(\tau) \quad (17)$$

$$K_2(\tau) = \int_{-\infty}^{\infty} \int_{1}^{\infty} \frac{\varphi(x)\ \exp(-\tau\varphi(x)T)}{T^2}\, dT$$

$$= -\int_{-\infty}^{\infty} \int_{1}^{0} \varphi(x)\ \exp(-\tau/\mu\ \varphi(x))\, dx\, d\mu$$

$$K_2(\tau) = -\ 2\sqrt{\pi}\ \varepsilon(\tau) \tag{18}$$

$$M_2(\tau) = \sqrt{\pi}\ T(\tau) \tag{19}$$

(Avrett and Hummer, 1965)

From the tables of mathematical functions tabulated by Abramowitz and Stegun (1966), we find $E_2(z) = e^{-z} - z\ E_1(z)$ by recurrence relation 5.1.14 or

$$E_2 + z\ E_1 = e^{-z} \tag{20}$$

so

$$M_2 = \int_{-\infty}^{\infty} \varphi(x)\ \exp(-\tau\varphi(x))\, dx$$

$$= \int_{-\infty}^{\infty} \varphi(x)[E_2(\tau\varphi(x)) + \tau\varphi(x)E_1(\tau\varphi(x))]\, dx$$

$$M_2(\tau) = K_2(\tau) + 2\tau\ K_1(\tau) \quad . \tag{21}$$

And by 5.1.11

$$E_1(Z) = -\gamma - \ell nZ - \sum_{n=1}^{\infty} \frac{(-1)^n\ Z^n}{n\ n!} \tag{22}$$

and 5.1.12

$$E_2(z) = -Z(-\ell nZ + \psi(2)) - \sum_{\substack{m=0 \\ m\neq 1}}^{\infty} \frac{(-Z)^m}{(m-1)m!} \tag{23}$$

with $\psi(2) = -\gamma + 1$, where $\gamma = .5772$, Euler's constant, we get

$$\sqrt{\frac{1}{\pi}}\, K_1(\tau) = \tfrac{1}{2}\,\frac{1}{\sqrt{2}}\,(-\gamma - \ell n\tau + \tfrac{3}{4}) - \tfrac{1}{2}\sum_{n=1}^{\infty}\frac{(-\tau)^n}{n\; n!\;\sqrt{n+2}} \tag{24}$$

$$\tfrac{1}{2}\sqrt{\frac{1}{\pi}}\; K_2(\tau) = \tfrac{1}{2} + \frac{\tau}{2\sqrt{2}}\,(\ell n\tau + \gamma - \frac{5}{4}) - \tfrac{1}{2}\sum_{n=2}^{\infty}\frac{(-\tau)^n}{(n-1)n!\;\sqrt{n+1}} \tag{25}$$

$$T(\tau) = -\frac{1}{\sqrt{\pi}}\,[K_2(\tau) + 2\tau K_1(\tau)] \tag{26}$$

$$\varepsilon(\tau) = -\frac{1}{2\sqrt{\pi}}\; K_2(\tau) \tag{27}$$

$$H(\tau) = \frac{1}{\sqrt{\pi}}\; K_1(\tau) \tag{28}$$

The requirement of radiative equilibrium gives us an integral equation for the source function

$$S(\tau) = S_o(\tau) + \int S(\tau')H(\tau,\tau')d\tau' \quad . \tag{29}$$

The surface brightness of apparent emission rate will be given by

$$4\pi I(\tau,\mu) = \int_{\tau} S(\tau')T\,\frac{|\tau-\tau'|}{\mu}\; d\tau'/\mu \quad . \tag{30}$$

If we call the probability that a photon is emitted at level τ and escape the medium $E(\tau)$, then

$$E(\tau) = \varepsilon(\tau) + \varepsilon(\tau_o - \tau) \tag{31}$$

which can also be expressed as unity less the probability a photon is emitted at τ and absorbed elsewhere in the layer, visibly

$$E(\tau) = 1 - \int H(\tau,\tau')d\tau' \tag{32}$$

integrated over the entire layer.

Mutiplying Eq. (32) by $S(\tau)$ gives

$$S(\tau)E(\tau) = S(\tau) - \int S(\tau)H(\tau,\tau')d\tau' \tag{33}$$

which, when combined with Eq. (29) leads to

$$S(\tau) = \frac{S_o(\tau)}{E(\tau)} + \int [S(\tau') - S(\tau)] \frac{H(\tau,\tau')}{E(\tau)} d\tau' . \tag{34}$$

The integral will give a negligible contribution except where $S(\tau)$ varies rapidly near small $E(\tau)$. With small optical thickness, less than one, $E(\tau)$ will always be large and the contribution of $\frac{S(\tau')-S(\tau)}{E(\tau)}$ will be small. Also it was shown in Donahue and Meier, (1967), that S_o/E crosses over S near $\tau = \tau_o/2$. This, with the additional knowledge that T changes slowly through the interval of interest, makes S_o/E a very good approximation to S for the intensity integral (30).

We must also consider the contribution to the source function of the incident radiation which is scattered back into the layer, the scattering albedo. The geometry for the albedo problem is given in Figure X.

The flux of photons into dA at frequency x will be

$$(\pi F_\nu)_o \sqrt{\pi}\, \Delta\nu_D\, e^{-[\tau_o \varphi_o(x)/\mu_o]} \cos\varphi_1 dAdx \tag{35}$$

for the incident radiation after passage through the medium striking the element dA of a spherical surface at an angle φ_1 with respect to the surface normal. $\varphi_o(x)$ is the line shape. If we assume a Lambert's Law diffusing surface, for an albedo $\lambda, \lambda/2\pi \cos\varphi_2 d\Omega$ will be reflected into a solid angle $d\Omega$ at a distance s away. The contribution to the source

function may then be obtained from the product of the excitation probability times the photon flow back into the layer as a result of the scattering albedo from the earth's surface.

$$[(\pi F_\nu)_D \sqrt{\pi}\, \Delta\nu_D\, e^{-\tau_o \varphi_o(x)/\mu_o} \cos\varphi_1 dA] \frac{\lambda}{2\pi} \cos\varphi_2 \frac{dV}{s^2}$$

$$x\, [e^{-\tau\varphi(x)/\mu}\, k(x)]dx \tag{36}$$

gives the excitation rate at frequency x in dV a distance s from the Lambert's Law surface for an absorption coefficient k(x).

The contribution to the primary source function will be the integration over the frequency and all surface elements, so

$$S_\lambda(\tau,\mu_o) = (\pi F_\nu)_o \sqrt{\pi}\, \Delta\nu_D \frac{\lambda}{\pi} \int_{\beta_\ell}^{\pi/2} d\beta \int_{\theta_o}^{\theta} T(\tau_o/\mu_o + \tau/\mu)$$

$$x\, \cos\varphi_1 \cos\varphi_2 \sin\eta d\eta/s^2 \qquad . \tag{37}$$

If we measure this contribution in units of $(\pi F_\nu)_o \sqrt{\pi}\, \Delta\nu_D$, we have

$$R(\tau,\mu_o) = \frac{\lambda}{\pi} \int_{\beta_\ell}^{\pi/2} d\beta \int_{\theta_o}^{\theta} T\left(\frac{\tau_o}{\mu_o} + \frac{\tau}{\mu}\right) \cos\varphi_1 \cos\varphi_2 \sin\eta d\eta/s^2 \tag{38}$$

During daytime conditions $\beta_\ell = 0 = \theta_o$, and we can represent R in the following manner

$$R(\tau,\mu_o) = \frac{\lambda r_o^2 A}{2\pi} < T\left(\frac{\tau_o}{\mu} + \frac{\tau}{\mu}\right) > \tag{39}$$

where $$A = \int_{-\pi/2}^{\pi/2} \cos\varphi_1 d\beta \int_o^{\theta} \cos(\alpha + \eta)\, \sin\eta d\eta/s^2 \tag{40}$$

by using the average value of the transmission function.

$$A = \frac{2\pi \sin\theta_2}{3b^3 r^2} [(2 + b^2)(1 - b^2)^{\frac{1}{2}} - (2 + b^3)] \qquad (41)$$

with $b = \cos\theta = r_o/r$. A is explicitly evaluated in Appendix A.

This then adds to the source function giving the initial source function the form

$$S_o = T(\tau/\mu_o + R(\tau,\mu_o) \quad . \qquad (42)$$

We get H' the same way as H, namely

$$H'(\tau,\tau') = -\frac{\partial \epsilon'}{\partial \tau} \quad . \qquad (43)$$

By the additive property of R and T, we see that

$$\epsilon'(\tau,\tau') = \epsilon(\tau,\tau') + \lambda\epsilon(\tau_o - \tau + \tau_o - \tau') \qquad (44)$$

so that $$H'(\tau,\tau') = H(\tau,\tau') + \lambda H(2\tau_o - \tau - \tau') \qquad (45)$$

$$E'(\tau) = E(\tau) + (1-\lambda)\epsilon(\tau_o-\tau) + \lambda\epsilon(2\tau_o- \tau) \quad , \qquad (46)$$

We now have $S(\tau)$ for values of λ and μ, the observation angle. We can then compute the surface brightness

$$4\pi I(\tau,\mu) = \int_0^{\tau_o} S(\tau')T(\tau'/\mu)d\tau' \quad .$$

One plot of $4\pi I$ vs τ with λ as a parameter, is given in Figure XI.

The effect of some of the parameters can be seen by comparing Figures X-XII. In Figure X for a solar zenith angle of 24° the relative enhancement of the intensity as viewed at the bottom of the layer, for any given albedo, compared with the case of no albedo, is independent of the optical depth. Figure XI shows the same situation as a function of

solar zenith angle, and Figure XII converts solar zenith angle to local time. Figure XIII is for the equinoxes at Laurel Mountain.

Some other important features of these curves are the linear relationship for small τ of $4\pi I$ on τ, and the flat shape of Figure XI for small solar zenith angles. Figure XII then predicts only a slight change in intensity around local noon for a fixed sodium number density. When the linearity of $I(\tau)$ is considered, we can readily get the change in time of τ around local noon because then $I(t)$ and $\tau(t)$, where t is the time near local noon, will have essentially the same shape. Also, since the rate of change of the solar zenith angle is smaller around local noon in the summer than in the winter,

$$\frac{4\pi I(t_1)}{4\pi I(t_2)} \approx \frac{\tau(t_1)}{\tau(t_2)}$$

is a good approximation for more hours about local noon in the summer than in the winter.

The parameter least certain in this calculation is the albedo λ; however, a paper is soon to be published giving a complete mapping of the albedo at several wavelengths, including 5893Å (private communication, W. Fowler and E. Reed, 1969). This paper will be based on an optical experiment on the Polar Orbiting Geophysical Observatory IV where the optical axis is in the Nadir (pointing toward the earth).

For a continuum solar flux of π x 205 photons/cms^2 sec per sec^{-1} near the D lines (Allen, 1955) with a residual percentage of flux at the center of the D lines of 5.0% and 4.4% for D_1 and D_2 (McNutt and Mack, 1962), we get input fluxes of

$$(\pi F_\nu)_o \sqrt{\pi}\, \Delta\nu_D = \begin{matrix} 40 \times 10^9 \text{ photons cm}^{-2}\text{sec}^{-1} & D_1 \\ 35 \times 10^9 \text{ photons cm}^{-2}\text{sec}^{-1} & D_2 \end{matrix} . \tag{47}$$

For a scattering albedo $\lambda = 0.15$, and $\tau = .23$ in the D_2 channel, we have

$$4\pi I = \begin{matrix} 7.6 & D_1 \\ \times 10^9 \text{ photons cm}^{-2}\text{sec}^{-1} & \\ 13 & D_2 \end{matrix} \tag{48}$$

in the sodium channels for the surface brightness from the sodium resonance scattering.

To get a measure of the surface brightness for the Rayleigh scattered background light, we wish to calculate the brightness of a point, B.

The brightness can be resolved into two components, the primary scattered light, B_p, and the multiply scattered light, B_m (Tousey and Hulburt, 1947).

$$B = B_p + B_m \tag{49}$$

These are evaluated as the following

$$B_p = \frac{3}{4\pi} I_o' \exp(-\beta' \sec\zeta) \frac{1 + \frac{1-\delta}{1+\delta}\cos^2\varphi}{3 + \frac{1-\delta}{1+\delta}} \times \frac{\exp(-\beta x_1 \sec\zeta) - \exp(-\beta x_1 \sec\xi)}{1 - \sec\zeta\cos\xi} \tag{50}$$

where the parameters are the following,

the illumination of the sun $I_o' = 13,600$ foot-candles

the polarization defect of air $\delta = 0.04$

the angle between the vector to the sun and the vector to the place of observation

$$\varphi = \cos^{-1}(\cos\zeta\cos\xi + \sin\zeta\sin\xi\cos z)$$

where z is the bearing of the sun with respect to the point of observation, ζ the sun's zenith angle, and ξ the zenith angle of the part of the sky under observation

$x_1 = 8.00$ km is the thickness of the atmosphere above the viewing instrument

$\beta' = 0.023$ the absorption coefficient of ozone

$\beta = 0.0126/\text{km}$ attenuation coefficient of air

t is the total thickness of the atmosphere

Extra parameters are present here so that this calculation can be made for the situation when the viewing instrument is not on the earth's surface.

The multiple scattered component is given as

$$B_m = \frac{1}{B\pi}(a_1 + b_1 + a_o)(1 - \exp(-\beta x_1 \sec\xi)) \tag{52}$$

and

$$a = \frac{I_o' \cos\zeta}{1 + gt}\{(1 + gt)(C-CX) - gx(C-CT+T)\} \tag{53}$$

$$b = \frac{I_o' \cos\zeta}{1 + gt}\{(1 + gt)(C-CX+X) - (gx+1-r)(C-CT+T)\} \tag{54}$$

$$g = (1-r)(1-\eta)\beta \qquad X = \exp(-\beta x \sec\xi)$$

$$C = \eta + (1-\eta)\cos\zeta \qquad T = \exp(-\beta t \sec\zeta)$$

where

$$a_1 = a(x=x_1)$$

$$b_1 = b(x=x_1)$$

$$b_o = b(x=o)$$

r = 1.5 the earth s reflectivity

η = ½ which means that ½ of the radiation streams downward in a layer .

It is worth noting here that as the zenith angle of the sun becomes greater than 90°, this analysis for the Rayleigh scattered background fails. The B_m component then goes negative and the B_m contribution predicted by this theory cannot be understood. It is also important to realize that a singularity exists in B_p where

$$B_p \sim \frac{\exp(-\beta^* \lambda_1/\cos\zeta) - \exp(-\beta^* x_1/\cos\xi)}{1 - \cos\xi/\cos\zeta}$$

where again ξ is the zenith angle of observation and ζ is the zenith angle of the sun. The computer solution to this singularity, properly an indeterminate point, is very sensitive to $(\zeta - \xi)$ and will give problems only where this difference is smaller than 10^{-3} rad. Yet the surface brightness is a smoothly varying function and we can let $\zeta_p = \xi_p + \epsilon$ where $\epsilon \sim .1°$ or 1.7×10^{-3} rad, the surface brightness would not be expected to change appreciably over this interval, but the solution would no longer be indeterminate.

Figures XIII, XIV, and XV give the surface brightness of the Rayleigh scattered background for Laurel Mountain for a subsolar local

noon latitude of 23.5°, 8.9°, and -5.2° respectively, where North latitudes are positive. Notice that all these figures predict a relatively constant surface brightness around local noon, although both the intensities and the shapes for times greater than 3 hours from local noon differ.

IV. POLARIZATION

The treatment of the polarization of the Na emission is somewhat complicated. The Zeeman fine structure components are given below to help us in this calculation.

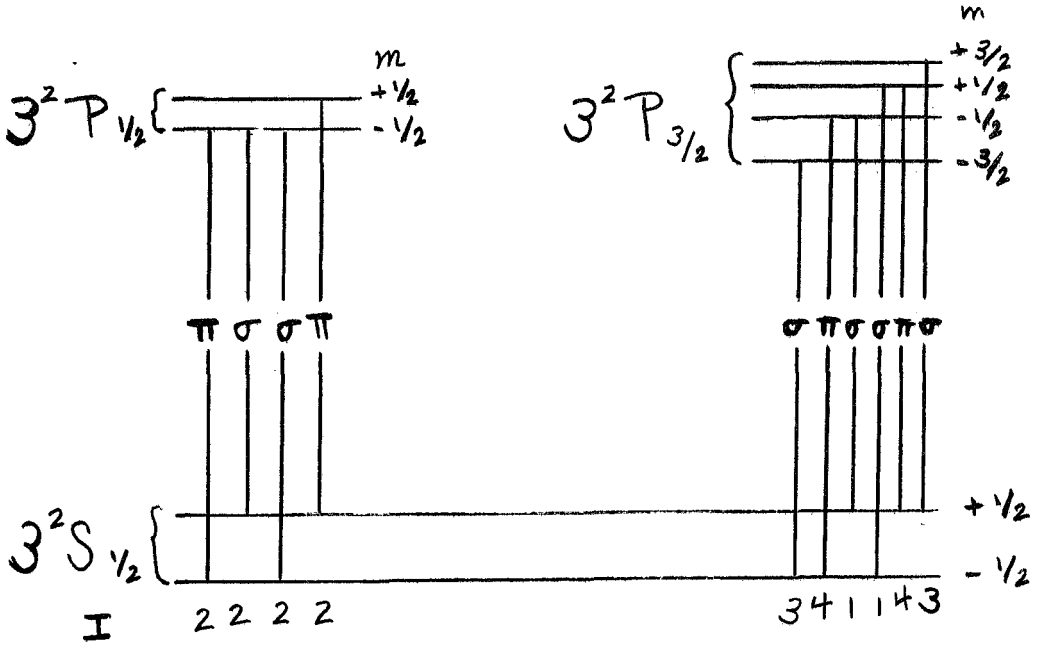

From the equal mixing of the upper and lower states in the D_1 line it is apparent that this line will be unpolarized, and will not be affected by a magnetic field. That this line is unpolarized has been experimentally verified (Pringsheim and Gaviola, 1924). The mixing of the D_2 line is somewhat more complicated, and we wish to get an analytic expression for the polarization as a function of the scattering angle.

For scattering $\perp$ to the beam

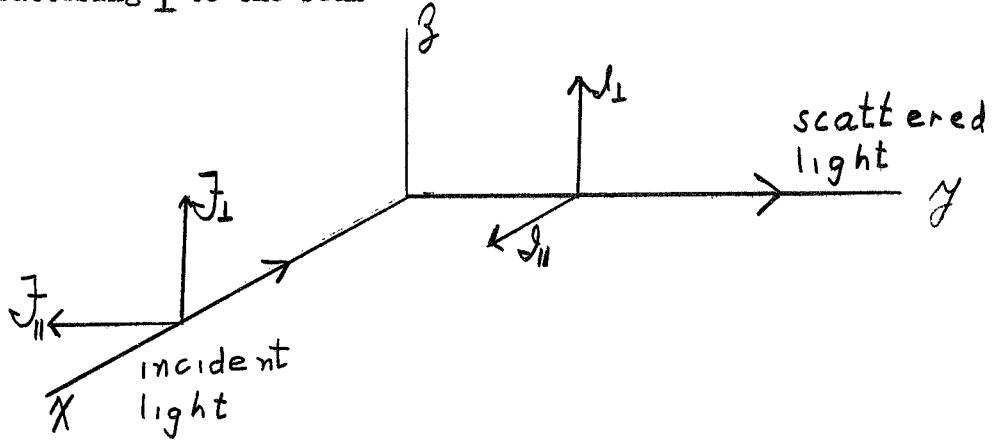

where $\perp$ and $||$ refer to the orientation of the electric field of the light with respect to the plane of scattering.

If the incident light has a flux of $\pi\mathcal{J}_\perp$ and is continuous in wavelength.

$$\mathcal{S}_\perp = \frac{c\mathcal{J}_\perp}{\tilde{\omega}(^2S)} \; A_\pi^{F'M'} \; A_{\pi F'M'} \tag{55}$$

$$\mathcal{S}_{||} = \frac{c\mathcal{J}_\perp}{\tilde{\omega}(^2S)} \; \tfrac{1}{2} A_\pi^{F'M'} \; A_{\sigma F'M'} \tag{56}$$

$\tilde{\omega}(^2S)$ is the statistical weight of the ground state.

The total transition probability is not a function of M' or F'. $\mathcal{S}_{||}$ is

$$A = A_\pi^{F'M'} + A_\sigma^{F'M'} \tag{57}$$

corrected to account for the σ component radiating with half the

efficiency which the π component radiates, when the transition probabilities are used.

If we define the auxiliary quantities

$$\alpha(F') = \frac{c}{4\tilde{\omega}(^2S)} \left(A_{\pi}^{F'M'} A_{\pi}^{F'}{}_{M'} + (2F' + 1)/3\, A^2\right) \tag{58}$$

$$\beta(F') = \frac{c}{4\tilde{\omega}(^2S)} \left(\frac{3}{2} A_{\pi}^{F'M'} A_{\pi}^{F'}{}_{M'} - \frac{2F'+1}{6} A^2\right) \quad . \tag{59}$$

If the emitted light is to be unpolarized when we observe the radiation, perpendicular to the field,

$$\sum_{M'} A_{\pi}^{F'M'} = \tfrac{1}{2} \sum_{M'} A_{\sigma}^{F'M'} \tag{60}$$

$$\sum_{M'} \left(A_{\pi}^{F'M'} + A_{\sigma}^{F'M'}\right) = (2F' + 1)\, A \quad . \tag{61}$$

We can then rewrite the following

$$\mathcal{I}_{\perp} = \sum_{F'} (\alpha(F') + 2\beta(F')) \tag{62}$$

$$\mathcal{I}_{\parallel} = \sum_{F'} (\alpha(F') - 2\beta(F')) \tag{63}$$

(Chamberlain, 1961).

The degree of polarization for light with incident polarization $\perp$ to the plane of scattering, scattered through an angle $\pi/2$, is given by

$$P(\pi/2) = \frac{\mathcal{I}_\perp - \mathcal{I}_{||}}{\mathcal{I}_\perp + \mathcal{I}_{||}} = \frac{4 \sum_{F'} \beta(F')}{2 \sum_{F'} \alpha(F')} \tag{64}$$

If we consider also the case for the electric field of the incident light along the y axis, then

$$\begin{aligned} \mathcal{I}_\perp = \mathcal{I}_{||} &= \frac{c\mathcal{F}_{||}}{\tilde{\omega}(^2S)} \tfrac{1}{2} A_\pi^{F'M'} A_{\sigma F'M'} \\ &= \sum_{F'} [\alpha(F') - 2\beta(F')] \mathcal{F}_{||} \end{aligned} \tag{65}$$

If $\mathcal{F}_\perp = \mathcal{F}_{||}$, the incident light is unpolarized,

$$P_o\left(\frac{\pi}{2}\right) = \frac{\sum_{F'} \beta(F')}{\sum_{F'} [\alpha(F') - \beta(F')]} = \frac{P_\perp(\pi/2)}{2 - P_\perp(\pi/2)} \quad . \tag{66}$$

Now looking at scattering in an arbitrary direction,

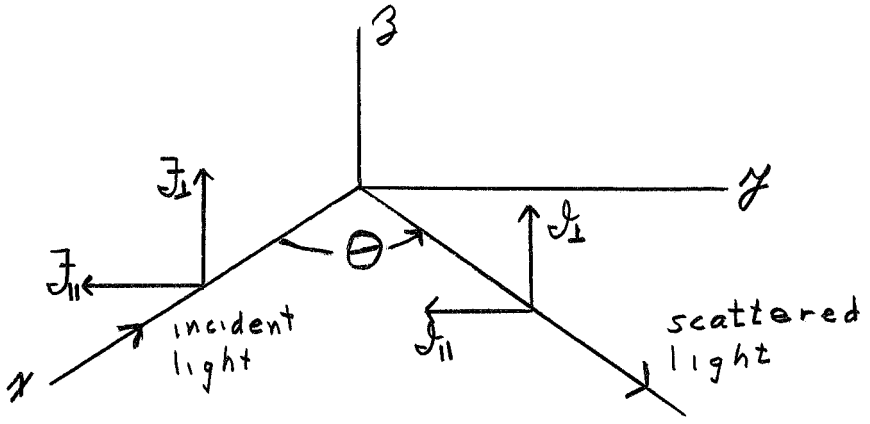

we get

$$\begin{Bmatrix} \mathcal{I}_{\parallel} \\ \mathcal{I}_{\perp} \end{Bmatrix} = \sum_{F'} \left\{ 4\beta(F') \begin{Vmatrix} \cos^2\theta & 0 \\ 0 & 1 \end{Vmatrix} + [\alpha(F') - 2\beta(F')] \begin{Vmatrix} 1 & 1 \\ 1 & 1 \end{Vmatrix} \right\} \begin{Bmatrix} \mathcal{J}_{\parallel} \\ \mathcal{J}_{\perp} \end{Bmatrix}$$

(Chandrasekar, 1950) (67)

for an incident flux of $\pi \mathcal{J}$. This gives the generalization of $P_o(\pi/2)$ for any angle to

$$P_o(\theta) = \frac{\sum_{F'} \beta(F')\sin^2\theta}{\sum_{F'}[\alpha(F') - \beta(F')\sin^2\theta]}$$

$$= [1/(\{\sum_{F'} \alpha(F') \csc^2\theta / \sum_{F'} \beta(F')\} - 1)] \quad . \tag{68}$$

For I = 3/2, Heydenburg, Larrick, and Ellett, (1932) have calculated

$$P_{\perp}(D_2|\tfrac{\pi}{2}) = \left. \frac{2 \sum_{F'} \beta(F')}{\sum_{F'} \alpha(F')} \right|_{D_2} = 0.186 \quad .$$

Putting this into Eq. (68), we get the expression

$$P_o(D_2|\theta) = \frac{1}{\frac{\csc^2\theta}{.093} - 1} \tag{69}$$

giving the polarization of D_2 for scattering through an arbitrary angle θ, which is the angle between the vector from the observing point to the

point of observation and the vector from the sun to the point of observation. Figure XVII gives the geometry for this scattering problem.

β is the inclination of the viewing instrument. The dashed lines in Figure XVI are coplanar and define the plane of scattering. From the law of sines, for this planar triangle, we see $\alpha = \alpha'$. We get α from the following equation

$$\alpha = \cos^{-1}(\cos\theta_s'\cos\theta_{Na} + \sin\theta_s'\sin\theta_{Na}'\cos\Delta\varphi') \tag{70}$$

where φ is the azimuth, θ_s the angle of the sun, and θ_{Na} the angle of observation, and the primes tell us to measure these angles at the point of observation. But $\varphi = 0$, for viewing to the north, which reduces Eq. (70) to the following

$$\alpha = \cos^{-1}(\cos(el)\cos 45° + \sin(el)\sin 45° \cos Z)$$

or

$$\cos\alpha = \frac{\sqrt{2}}{2}(\cos(el) + \sin(el)\cos Z) \tag{71}$$

where the angles el and Z are the elevation and bearing of the sun from the point of observation. Appendix B gives two ways to calculate these angles. It is this angle in Eq. (71) which we must evaluate and use in the expression for the polarization of the D_2 line.

Figure XVI also allows us to evaluate the angle of observation as measured at the bottom of the sodium layer.

$$\frac{\sin 135°}{|\underline{r}_{Na}|} \quad \frac{\sin\theta obs}{6.36(3)}$$

But $|\underline{r}_{L\text{-}Na}| = 0.09(3)$

$$6.36 < |\underline{r}_{Na}| < 6.45 \quad \times 10^3$$

so that $\theta obs = 45°$ is a good approximation.

The polarization of the Rayleigh scattered background is easily handled. The background was calculated in terms of the primary scattered light and the multiple scattered light, B_p and B_m. If we define the quantity γ,

$$\gamma = (D+B_m/2B_p\ (1+D))/(1+B_m/2B_p\ (1+D)) \tag{72}$$

$$\text{where } D = \delta + (1-\delta)\cos^2\alpha$$

then we get $B = B_{\perp} + B_{||}$

$$B_{\perp} = \frac{1}{1+\gamma} B$$

$$B_{||} = \frac{\gamma}{1+\gamma} B$$

where the $\perp$ and $||$ refer to the orientation of the electric vectors with respect to the plane of polarization. α is given by Eq. (71).

V. TREATMENT OF THE SCATTERING CELL

Before we can handle data we must understand what happens to radiation entering the vapor cell. It is assumed that the σ and π components will be rescattered into the phototube with the same efficiency, even though we know we have an optically thick vapor where multiple scatterings will occur, and that π components are not allowed to scatter in the direction of the magnetic field. There is evidence that tends to support this approximation. That both components scatter into the PM tube with equal efficiency does not mean that the ratio of π and σ components entering the PM tube be the same as the ratio of these components entering the scattering chamber. From the Zeeman fine structure diagrams we see that no upper state can decay to the ground state by only a π transition. All states which can emit a π photon also can emit a σ photon in decaying to the spin complemented ground level. This means then that in the multiple scattering process, the scattering of σ components is preferred. This will not mean necessarily that we will record more counts for every kilorayleigh* of σ photons entering the vapor cell than for π photons coming into the cell.

If this reasoning is in error, then for thicker vapor, viz. more multiple scattering, this approximation gets worse. Gadsden et al. (1966) have shown data where the error between calculated and observed intensities at 4000 G measured as a function of zero G intensities drops by only about a factor of 2 when the sodium vapor pressure drops by a

---

*A kilorayleigh is an apparent column emission rate of 10^9 photons/cm^2 sec.

factor of 10. In addition to the above argument this experimental evidence indicates this assumption does not introduce significant errors.

The monitor and the sodium light inputs are equipped with polaroid transmission filters usually aligned with their axis at 45° with respect to the direction of the field. With these polaroids we consider that all photons transmitted through the filter have their electric vectors aligned at 45° with respect to the field. Since the p and s transition probabilities have an angular dependence of $\cos^2\theta$ and $\sin^2\theta$, we expect that the total absorption profiles simply will be given by the relative absorption profiles of the p and s components. Thus, by putting polaroids over the light inputs in this analysis, we reduce the dependence of the changing plane of polarization to just the relative transmissions through the polaroid.

For the atmospheric sodium emissions we have the same situation. The relative D_1 transmissions will be unchanged, because they are unpolarized. The D_2 relative transmissions will depend on the degree of polarization, which depends on the scattering angle "alone", it being a function of the time of day and the date. The treatment of the absorption will be invariant with respect to the relative intensities transmitted through the polaroid.

Table II, III, and IV give the relative transmission for Rayleigh scattered brightness for 3 dates throughout the year. These tables also give the azimuth and elevation of the sun, the scattering angle, the brightness of the Rayleigh scattered light, and the relative brightness of the primary scattered component.

The absorption cross-sections for the sodium vapor are obtained by integrating over the four hyperfine structure components for the D_1 line and the six hyperfine components for the D_2 line, Doppler broadened by a temperature of $T = 438^{\circ}K$. Once again the line shape is given by $\exp(-x^2)$ where $x = (\nu-\nu_o)/\Delta\nu_D$ with $\Delta\nu_D = 23$ mK(T=200 K) and $(\nu-\nu_o)$ is the displacement from the centroid in milliKaysers. These zero field absorption coefficients for the absorption in the cell are the same as the atmospheric sodium emissions except that these are for a higher temperature. These profiles are given in Figures XVII and XVIII.

For the absorption cross-sections as a function of the field strength, we use the Back-Goudsmit calculations. Jackson and Kuhn (1938) showed that a complete Back-Goudsmit pattern is obtained for the sodium vapor with a field of 2000 G.

For an applied field H_o, the condition that strong field Back-Goudsmit interaction correctly predicts the absorption cross-section is given by

$$H_o \gg 10^{-3}\ \overline{H(0)} \tag{73}$$

where H(0) is the field induced at the nucleus by the orbiting electrons of the atom, evaluated in some appropriate time averaged method. The strong field case will effectively decouple the nuclear moment and the extranuclear moment. It is important to realize that a complete Paschen-Back pattern can be realized without a complete decoupling of these moments. The complete decoupling will result, incidentally, in a symmetric pattern about the centroid. A complete Paschen-Back pattern, without a complete spin-spin decoupling for an intermediate field will not generally result in a symmetric pattern.

For sodium,

$$\overline{H(0)}\ {}^2P_{3/2} = 2.5 \times 10^4 \text{ G}$$

$$\overline{H(0)}\ {}^2P_{1/2} = 4.2 \times 10^4 \text{ G} \qquad (74)$$

$$\overline{H(0)}\ {}^2S_{1/2} = 1.3 \times 10^5 \text{ G} \quad \text{(Kopfermann, 1958)}$$

so that

$$10^{-3}\ \overline{H(0)} = \begin{matrix} 25\ {}^2P_{3/2} \\ 42\ {}^2P_{1/2} \\ 103\ {}^2S_{1/2} \end{matrix} .$$

Based on this we choose to use strong field calculations for $^2P_{3/2}$ and $^2P_{1/2}$, but will use the intermediate field calculations for the $^2S_{1/2}$.

For strong field calculations

$$\Delta W_H = m_J g_J \mu_B H_o \qquad (75)$$

where $\mu_B = 0.927 \times 10^{-20}$ ergs/gauss, is the Bohr magneton and

$$g_J = \begin{matrix} 4/3\ {}^2P_{3/2} \\ 2/3\ {}^2P_{1/2} \\ 2\ {}^2S_{1/2} \end{matrix} \qquad (76)$$

we then get for 5000 G

$$\begin{matrix} {}^2P_{3/2} & m_J = \pm 3/2 & \Delta W_H = \pm 468 \text{ mK} \\ & m_J = \pm 1/2 & \Delta W_H = \pm 157 \text{ mK} \end{matrix} \qquad (77)$$

$$^2P_{1/2} \qquad m_J = \pm 1/2 \qquad \Delta W_H = \pm\ 78\ \text{mK} \tag{78}$$

displacement from the centroid.

For the intermediate field case for $^2S_{1/2}$

$$\Delta W_H = \frac{A}{2} I \pm \tfrac{1}{2} g_J \mu_B H_o \mp I\, g_I' \mu_B H_o \qquad m = \pm (I + \tfrac{1}{2})$$

or

$$\Delta W_H = I \frac{\delta W_o}{2I+1} \pm (\tfrac{1}{2} g_J - I g_I') \mu_B H_o \tag{79}$$

for $$\delta W_o = \frac{A}{2} (2I+1)$$

where $g_I' = \frac{m_e}{m_p} g_I$ and $g_I = 1.48$ (Millman, 1940) A is given by

$$A = \frac{\mu_I \overline{H(0)}}{I\ J} = \frac{\mu_n\ g_I\ \overline{H(0)}}{J} \tag{80}$$

where μ_I is the nuclear magnetic moment, μ_n is the nuclear magneton, $\mu_n = 5.0493 \times 10^{-24}$ ergs/gauss = 25.5×10^{-3} mK/1000 G. J is the quantum number of the Zeeman fine structure being split, ½ for $^2S_{1/2}$,

$$A = 10\ \text{mK} \quad .$$

For all other values we must use

$$\Delta W_H = -\frac{\delta W_o}{2(2I+1)} - m g_I' \mu_B H_o \pm \frac{\delta W_o}{2} \sqrt{1 + \frac{4m}{2I+1}\ x + x^2}$$

with

$$x = \frac{g_J - g_I'}{\delta W_o} \mu_B H_o \tag{81}$$

$$\text{for } m = ((I-\tfrac{1}{2}), \cdots (I+\tfrac{1}{2})).$$

For 5 kG, we then get 8 components at the following displacements from centroid, in mK, for $^2S_{\frac{1}{2}}$

255.9	-211.6
242.5	-228.1
228.4	-243.2
212.8	-257.6 .

Figure XIX gives the qualitative behavior of the hyperfine levels, and shows that each Zeeman fine structure component for 5000 G is composed of 4 hyperfine lines. Since sodium has a nuclear spin of $I = 3/2$, we expect each fine structure line to be composed of 4 hyperfine lines, equally intense. Two ways then are suggested to calculate the relative intensities of the 16 hfs D_1 components and the 24 hfs D_2 components.

One way to calculate these cross-sections would be to assign relative intensities for each hfs emission from the zero field case, and then keep track of each line as it shifts in the magnetic field. The cross-sections will be the sums from 16 and 24 transition probabilities. Another way to calculate these cross-sections would be to look at the 5000 G pattern and recognize that these are four and six Zeeman fine structure transitions, each split into four equally intense hyperfine structure lines. The relative intensities of each transition then can be determined by the relative intensity of each fine structure component. We can get the Zeeman fine structure relative intensities from the usual Zeeman intensity rules:

$$J \rightarrow J \text{ transition}$$

$$\begin{aligned} \Delta m &= 0 \qquad & I &= 4\ Am^2 \\ \Delta m &= \pm 1 \qquad & I &= 4A[(J+1)J - m(m \pm 1)] \end{aligned} \tag{82}$$

$$J \rightarrow J + 1 \text{ transitions}$$

$$\begin{aligned} \Delta m = 0 \qquad & I = 4B[(J+1)^2 - m^2) \\ \Delta m = \pm 1 \qquad & I = B[(J \pm m + 1)(J \pm m + 2)] \quad . \end{aligned} \tag{83}$$

The good quantum numbers for the above is m_j, because the grouping of the Zeeman hfs lines into Zeeman fine structure lines is by means of m_j as in Figure XIX. With these relative intensities for the transitions in hand for 5000 G we can then work backwards for the 1000 G and 3000 G field situations. For the 1000 G case we do not expect that this profile obtained in the above manner will be completely accurate, in that at 1000 G a Paschen-Back pattern is not obtained completely.

The relative transition strengths A and B can then be evaluated in the following manner. From the zero field case we already have evaluated the value of the constant which takes the zero field relative intensities to the actual cross-sections, and we also have evaluated the total area under the cross-section curve. The appropriate constant which takes the relative intensities for the Paschen-Back case into the cross-section can be obtained by requiring the total area under this curve equal the total cross-section for the zero field case. Each of these integrations are performed on the D_1 and D_2 components separately. These cross-sections are shown in Figures XX-XXV. The width of each transition is for a temperature of 438°K.

Although we now know how the surface brightness of the Rayleigh scattered background changes throughout the day, and how the transmission through the polaroid of the background changes due to the changing plane of polarization, we must also investigate the profile for this source to find the amount of background absorbed at various phases of the operation.

To take into account the profile for the Fraunhofer lines, we use

$$I_\nu = I_o(d + b(\Delta\nu)^2) \tag{84}$$

where $I\nu$ then is the spectral radiance at wave number ν, I_o is the continuum spectral radiance, without the Fraunhofer lines, and $\Delta\nu$ is the distance from the centroid of the atmospheric resonance line.

Donahue and Stull (1959) give weighted averages of

$$\begin{aligned} d_{D_1} &= 0.063 & b_{D_1} &= 1.72 \times 10^{-6}\ (mK)^{-2} \\ d_{D_2} &= 0.054 & b_{D_2} &= 1.07 \times 10^{-6}\ (mK)^{-2} \end{aligned} \tag{85}$$

taken from Priestley's data.

The same source gives expressions for the shift of centroid of the Fraunhofer lines with respect to the lab frame. These show at the latitude of Laurel Mountain, that the centroid will be displaced upward in energy by 25-28 mK under daytime conditions during the year by virtue of the earth's orbital motion, and the Fraunhofer lines will be decreased by no more than 2 mK due to the earth's rotational motion.

Since the transmission of radiation through a distance ρ is given by $\exp(-k_\nu\rho)$ where k_ν is the absorption coefficient at ν, then $I - \exp(-k_\nu\rho)$ must be the radiation absorbed at ν. For any given consideration, the total radiation absorbed will be

$$\int \Delta I_\nu d\nu = \int d_\nu I_\nu (1 - \exp(-k\nu\rho))$$

where I_ν will be the atmospheric sodium emission or Rayleigh background, and k_ν will be the absorbing profile. ΔI was evaluated in intervals of one mK, and was numerically integrated by Simpson's rule.

First for the daytime sky, the following absorptions were calculated, per unit I_o. Table V gives these values as a function of the parameter Q, which is the displacement of the Fraunhofer centroid.

For the sodium absorption,

$$\Delta I_\nu = I_\nu(1 - \exp(-k_\nu d))$$

was approximated by

$$\Delta I_\nu = I_\nu k_\nu d \tag{86}$$

With the use of (86), we get

H	D_1	D_2
0	9.14(-10)	3.68(- 9)
1	5.01(-10)	2.70(- 9)
3	4.49(-10)	1.08(- 9)
5	2.18(-13)	3.89(-10) .

The actual depth of the sodium vapor used for this calculation is not important, but the value 2 cm was used. It is important to realize that for the sodium signal absorption the two channels are normalized separately to the number of photons in each channel. For the Rayleigh scattered background brightness D_1 and D_2 are both normalized to the continuum background brightness I_o. They need not be handled separately for the background.

VI. DATA ANALYSIS AND RESULTS

When the polarization is measured directly with a polaroid over the light input arm, the data is decomposed according to the following.

$$I_{D_1}^{\alpha} = I_{N_a}^{'\alpha}(D_1) + I_R^{'\alpha}(D_1)$$

$$I_{D_2}^{\alpha} = I_{N_a}^{'\alpha}(D_2) + I_R^{'\alpha}(D_2)$$

where $I_{N_a}^{'\alpha}(D_1)$ is the counting rate in the D_1 channel at α field configuration from the sodium signal and $I_R^{'\alpha}(D_1)$ the counting rate from the Rayleigh scattered background into the D_1 channel at α field configuration.

The contribution to the counting rate equals the product of the relative absorption coefficient times the emitted signal from the sodium atoms and the scattered background, that is:

$$I_{N_a}^{'\alpha}(D_1) = A^{\alpha}(D_1)I_{N_a}(D_1) = A_1^{\alpha}I_{N_a}(D_1)$$

$$I_{N_a}^{'\alpha}(D_2) = A^{\alpha}(D_2)I_{N_a}(D_2) = A_2^{\alpha}I_{N_a}(D_2)$$

$$I_R^{'\alpha}(D_1) = B^{\alpha}(D_1)I_R(D_1) = B_1^{\alpha}I_R(D_1)$$

$$I_R^{'\alpha}(D_2) = B^{\alpha}(D_2)I_R(D_2) = B_2^{\alpha}I_R(D_2) \quad .$$

The relative absorption coefficients are calculated directly from

$$\mathcal{A}^{\alpha}(D_i) = [\int d\nu I\nu(1-\exp(-k_{\nu}^{\alpha}\, d))]_{D_i}$$

where the $\mathcal{A}$'s are the A's when $I\nu$'s are the sodium emission profiles, and the $\mathcal{B}$'s are the B's when $I\nu$'s correspond to the Rayleigh scattering. The $\mathcal{A}$'s are calculated per unit intensity of the incoming signal.

In detail the counting rate equations for the four field configurations of 0,1,3, and 5 thousand Gauss are

$$I_o = A_1^o I_{N_a}(D_1) + A_2^o I_{N_a}(D_2) + B_1^o I_R(D_1) + B_2^o I_R(D_2)$$

$$I_1 = A_1^1 I_{N_a}(D_1) + A_2^1 I_{N_a}(D_2) + B_1^1 I_R(D_1) + B_2^1 I_R(D_2)$$

$$I_3 = A_1^3 I_{N_a}(D_1) + A_2^3 I_{N_a}(D_2) + B_1^3 I_R(D_1) + B_2^3 I_R(D_2)$$

$$I_5 = A_1^5 I_{N_a}(D_1) + A_2^5 I_{N_a}(D_2) + B_1^5 I_R(D_2) + B_2^5 I_R(D_2)$$

and $$A_1^o = \int d\nu I\nu (I - \exp(-k_\nu^o d))$$

where $I\nu$ is the sodium profile for T = 200°K in the D_1 channel and k_ν^o is the sodium profile for T = 438°K, H = 0, in the D_1 channel, given respectively in Figures XVIII and XIX.

These relative coefficients, evaluated by a Simpson integration with an integration of 1 mK, are as follows

	A_1	A_2	B_1	B_2
0	156.3	321.2	9.18	6.38
1	161.2	159.3	18.94	14.8
3	17.0	290.6	37.17	43.84
5	1.32(-2)	122.7	66.62	94.84

For B_1 and B_2 the shift of the Fraunhofer solar lines relative to the terrestrial sodium lines as a result of the earth's revolution and rotation used here was 24 mK, and the orientation of the electric field of the incoming light was taken as 45° with respect to the axis of the magnetic field.

It is desirable to use additional information, all of which has been discussed before, to simplify this set of equations. For the Rayleigh scattered light we assume that the spectral radiance I_o in the neighborhood of the D lines is constant, and that the polarization of these scatterings is the same for both channels. This allows us to say $I_R(D_1) = I_R(D_2) = I_\omega$.

For the sodium signals we can write $I_{N_a}(D_2) = fI_{N_a}(D_1)$ where we can explicitly calculate f. For small optical depths, that is for sodium number densities around 30×10^9 which give $\tau = .15$ at the D_1 line and $\tau = .30$ at the D_2 line, the source function $4\pi I/(\pi F_\nu)_o \sqrt{\pi}\, \Delta\nu_D$, is essentially linear with τ. For this case, which will hold for cases where the sun's path through the sodium is not too long, $f = \dfrac{I_{N_a}(D_2)}{I_{N_a}(D_1)}$. Evaluated without the polaroid, we get f = 3.6. For transmission of the unpolarized D_1 line through our model polaroid we get 65%, independent of the orientation of the plane of polarization. The D_2 line is polarized as a function of the scattering angle, and will have a transmission through the polaroid dependent on the scattering angle and the orientation of the plane of polarization.

The polarization of the D_2 line measures the excess number of photons with the electric field in the plane of polarization. Thus for a polarization γ, we can consider the D_2 line as a superposition of two beams, an unpolarized beam of strength $(1-\gamma)$, and a beam of strength γ

with the electric field in the plane of polarization. The transmission through the polaroid of the $(1-\gamma)$ is 65%, however the transmission of the γ beam will be a function of the orientation of the plane of scattering with respect to the axis of the polaroid. The axis of the polaroid is inclined 45° to the east of the north when the Zeeman photometer is looking to the north. Thus, for a scattering plane inclined η to the east of north, the projection onto the axis of the polaroid will be $\cos(\frac{\pi}{4} - \eta)$. Our model calls for the transmission through the polaroid along the axis of .9 and a transmission of .4 through the polaroid perpendicular to the polaroid axis. Since the plane of polarization is 90° from the plane of scattering, and the plane of polarization is to the west in the AM and to the east in the PM, the transmission in the AM will

$$.4\cos(\tfrac{\pi}{4} - \eta) + .9\left|\sin(\tfrac{\pi}{4} - \eta)\right|$$

and in the PM we have

$$.9\cos(\tfrac{\pi}{4} - \eta) + .4\left|\sin(\tfrac{\pi}{4} - \eta)\right| \quad .$$

The solar elevation is catalogued as a function of hours from local noon, and is always positive.

The point of this discussion is to investigate the transmission of the D_2 line relative to the D_1 line. The expression is given by

$$f = \mathcal{D} * \frac{1}{.65} * \left[(1-\gamma) * .65 + \gamma \left\{ \begin{matrix} .4\cos(\frac{\pi}{4} - \eta) + .9\left|\sin(\frac{\pi}{4} - \eta)\right| \\ .9\cos(\frac{\pi}{4} - \eta) + .4\left|\sin(\frac{\pi}{4} - \eta)\right| \end{matrix} \right\} \right]$$

where $\mathcal{D} = \dfrac{4\pi I(\tau = 2\tau_o)}{4\pi I(\tau = \tau_o)} * \dfrac{13}{7.2}$. The extra term 13/7.2 is the factor

which normalizes the number of solar photons in the D_2 channel to the number of photons in the D_1 channel.

These calculations of f can then be summarized in the following manner. We are interested in writing $I_{N_a}(D_2)$ as a function of $I_{N_a}(D_1)$, transmitted through the polaroid. This is accomplished by defining an effective transmission coefficient for an equivalent unpolarized D_2 beam, defined in the following manner.

$$f = \mathcal{O} * \xi * \frac{1}{.65}$$

$$\xi = \frac{(1 - \gamma)*.65 + (4\cos(\frac{\pi}{4} - \eta) + .9|\sin(\frac{\pi}{4} - \eta|*\gamma}{(1 - \gamma)*.65 + (.9\cos(\frac{\pi}{4} - \eta) + .4|\sin(\frac{\pi}{4} - \eta)|*\gamma}$$

for the actual $I_{N_a}(D_2)$ with a polarization defined by

$$\gamma = P_o(D_2|\theta) = \frac{9.3(-2)\sin^2\theta}{1-9.3(-2)\sin^2\theta}$$

with the sun at a solar elevation η and scattering angle θ. We can then write $I^{\alpha} = (A_1 + fA_2)^{\alpha} I_{N_a}(D_1) + g(B_1 + B_2)^{\alpha} I_{\omega}$ (87)

for our four-field configurations,

$$I_0 = (156.3 + f*321.2)I_{N_a}(D_1) + g*15.56I_{\omega}$$

$$I_1 = (161.2 + f*159.3)I_{N_a}(D_1) + g*33.74I_{\omega}$$

$$I_3 = (17.0 + f*290.6)I_{N_a}(D_1) + g*81.01I_{\omega}$$

$$I_5 = (.0137 + f*122.7)I_{N_a}(D_1) + g*161.46I_{\omega} \quad .$$

In these equations for I^{α}, the g for the Rayleigh scattered background is analgous to the f for the resonately scattered sodium. The g gives the percentage of Rayleigh scattered background transmitted through the polaroid.

Applying the new method to data from 21 July 1968 yields Figure XXVIII. The calculated I_{ω} obtained from I_3 and I_5 has been suppressed for all but one measurement because all calculated I_{ω} showed remarkable agreement. The calculated I_{N_a} on the figure show a marked decrease in the later after afternoon hours. Comparison with Figure XXIX suggest a decrease in sodium atom density at six hours from local noon to about 1/3 the number density at local noon. The abundance at three hours from midday indicates no change from the midday value.

When the polarization is not directly measured, data is handled in a manner described by Gadsden et al. (1966). At the top of Figure XXVII the calculated surface brightness and the measured surface brightness are shown. The parasitic signal, I_p, as well as I_o and I_{5000} also are shown with a calculated profile of I_{N_a} obtained from this data.

The hot cell reading I_o is decomposed in the following manner, $I_o = I_{N_a} + I_{\omega}$ where I_{ω} is the Rayleigh scattered contribution to the zero field signal. This component is evaluated by measuring the instrumental response to white light when there is an insignificant contribution from I_{N_a} at 5000G as a function of the response at zero field. R_o/R_{5000} can be evaluated by observing directly at the sun. The relative absorption coefficients predict $R_o/R_{5000} = .29$, which compares favorably with the measured value of .26. One then expects

$$I_{\omega} = R_o/R_{5000} * I_{5000} \tag{88}$$

Thus the calculated sodium emission profile in Figure XXVI is given by

$$I_{N_a} = I_o - I_{\omega} = I_o - \frac{R_o}{R_{5000}} I_{5000} \quad . \tag{89}$$

Since I_p follows the expected I_{ω} profile more accurately through the day, I_p is normalized to I_{5000} at ± 3 hours from local noon (where the plane of polarization is at 45°) and replaces I_{5000} in Equation (88). Figure XXVIII gives the apparent emission rate as a function of time from local noon for 21 July for $\lambda = .15$, $\tau_o = .115$. This predicts that $4\pi I$ evaluated 6 hours from local noon will drop to 88% of $4\pi I$ at local noon, where the data show a slight increase in I_{N_a}. This increase may be caused by data scatter or the smoothing profile applied to I_p and I_o. These data indicate essentially a constant sodium column density throughout this afternoon.

The analogous exercise for data from 27 January 1969, Figures XXX and XXI, using only the new method indicated that the free atomic sodium number density at 3 hours after local noon has fallen to about 75% of its value about local noon. For times greater than three hours after local noon on this date the solar zenith angle gets relatively large and increases rapidly. The shape of $\tau(t)$ will not be the same as $4\pi I(t)$. On this day data was taken only with 45° polarization so no direct comparison between old and new reduction methods can be made.

Figure XXXII shows the effect as a function of local time of different β's, the coefficient of aerosol scattering, for 26 July 1969 on the surface brightness and the transmission through a polaroid. Figure XXXIII gives a third β as well as the measured values from the monitor for that day. Figure XXXIII shows great similarity between the predicted and measured values for the surface brightness from the Rayleigh background.

Figure XXXIV shows the measured values for 26 July 1969 needed to calculate I_{N_a} by the old method, and shows the calculated I_{N_a} values. Here the sodium abundance at three hours before local noon is 90% of its value at local noon, and at six hours before local noon is 57% of its local noon value. This method also predicts a minimum abundance at 5½ hours before local noon of 46% of its midday value.

Figure XXXV gives data taken on 26 July 1969 with a polaroid and allows direct comparison with the old method. With the polaroid abundance at six hours before local noon is 67% the local noon value, compared with a 57% value by the previous method. The three hour before local noon value obtained was 92% compared with 90% of the midday value by the old method. The absolute minimum abundance shown by the new method is much less pronounced than indicated by the previous method, and the time of that minimum is moved about ½-hour closer to local noon. The intensity profiles from three hours previous to local noon through midday are quite similar for both methods.

Before concluding more attention must be given to the purpose of this study and what these conclusions imply about the published literature. Data analysis performed without a direct measure of the polarization is plagued by not knowing exactly how to handle a rotating plane of polarization. Since the π and σ transition probabilities contain $\cos^2\theta$ and $\sin^2\theta$ terms, changes in θ throughout the day can change the absorption coefficients for I_{5000}, where θ is the angle between the plane of polarization of the incident radiation and any magnetic field applied across the vapor. The method of Gadsden et al. (1966) was to use I_p rather than I_{5000} because I_p was shown to follow the expected $I_\omega(t)$ more accurately than I_{5000}. Further by normalizing I_p to I_{5000} for the plane

of polarization at 45°, one expects fairly good results. For instance this method was able to correct previous work which indicated an anomalous midday minimum in sodium abundance. An interesting feature predicted by that method was statistically a ratio of about 1.31 for the abundance at three hours after local noon to three hours before local noon.

This new method is designed to handle the polarization directly. The assumption used in this study was that all polarization effects could be handled by simply varying the amount of signal transmitted through the polaroid as a function of the polarization of the incident beam. All the light which was transmitted through the polaroid was considered to have the electric field aligned at 45° with respect to the axis of the magnetic field. With this method, I_p no longer traces the surface brightness transmitted through the monitor polaroid.

By looking at the pair of equations I_o and I_{5000}, we see that both methods should give nearly the same results.

$$I_{N_a} = \left(I_o - \frac{B_1^o + B_2^o}{B_1^5 + B_2^5} I_5 \right) * \left[(A_1^o + f*A_2^o) \left\{ 1 - \frac{A_1^5 + f*A_2^5}{A_1^o + f*A_2^o} \frac{B_1^o + B_2^o}{B_1^5 + B_2^5} \right\} \right]^{-1}$$

$\frac{B_1^o + B_2^o}{B_1^5 + B_2^5}$ is simply the response at zero field relative to the response at 5000G. Since the bracketed term is nothing more than a scale factor, this is the same equation as $I_{N_a} = I_o - I_\omega$, except we do not make the substitution of I_p for I_{5000}. This method, however, can yield an abundance

with only one complete cycle; the old method requires several hours of data, and should include data near three hours before or after local noon.

Further, by making a composite of the three days for which data are reported using the direct measure of the polarization, the sodium column abundance appears to be essentially symmetric, at least for near midsummer, about local noon when measured as a function of the midday abundance. The value at six hours from midday is about 67% of its noon value and this abundance grows to about 90% of its midday value three hours from local noon. The one day in January quoted here shows the abundance as a function of midday abundance to be much more active, the value at three hours from midday being about 67% the midday value. If the source function of free atomic sodium were dependent on the solar zenith angle, this is what would be expected since the solar zenith angle of 68° for 27 January at three hours from midday is the same as the solar zenith angle at about five hours from midday on 26 July.

What is indicated by this data, but not conclusively shown because of the few days quoted, is that the abundance is symmetric throughout the day about the midday, and the rate of change of the abundance changes throughout the year. Although the old method again shows an excess abundance at three hours after local noon compared to the value three hours before local noon for the July data, the new method shows no excess.

APPENDIX A

The evaluation of Eq. (41) in more detail follows below

$$R(\tau,\mu_o) = \frac{r_o^2\lambda}{\pi}\int_{\beta_\ell}^{\pi/2} d\beta \int_{\theta_o}^{\theta} T\left(\frac{\tau_o}{\mu_o} + \frac{\tau}{\mu}\right) \cos\psi_1 \cos\psi_2 \sin\eta d\eta/s^2 \ .$$

The appropriate coordinate system is shown in the Figure X .

The circle for which the plane perpendicular to the sun's rays cuts the earth's surface is defined by $\tan\theta_o = \tan\eta\sin\beta$.

We then want to evaluate

$$\int_{\beta}^{\pi/2} \cos\varphi_1 \, d\beta \int_{\theta_o}^{\theta} \frac{\cos(\eta+\alpha)}{\chi^2} \sin\eta d\eta$$

where

$$\cos\varphi_1 = \sin\eta\sin\beta\cos\theta_o - \cos\eta\sin\theta_o$$

which determines the projection of the element of area in the direction of the sun.

β_ℓ is the point at which the parallel of latitude defined by η intersects the great circle defined by θ_o.

in the daytime $\beta_\ell = -\pi/2$, at noon,

which makes the integral

$$\int_{-\pi/2}^{\pi/2} \cos\varphi_1 d\beta \int_{o}^{\theta} \frac{\cos(\alpha+\eta)}{\chi^2} \sin\eta d\eta \ .$$

It is sufficient to consider the reflection for the noon case because the scattering back into the layer in the daytime will be from that part of the earth's surface which is at noon. As the lower atmosphere begins to be screened by the earth's shadow, then this approximation no longer holds; however, then the daytime analysis is replaced by a twilight analysis, but

$$\int_{-\pi/2}^{\pi/2}(\sin\eta\sin\beta\cos\theta_o - \cos\eta\sin\theta_o)d\beta = -\pi \sin\theta_o\cos\eta$$

we have

$$\frac{\pi \sin\theta_o}{r^2}\int_1^b\left\{\frac{\cos^2\eta}{(1 + b^2 - 2b\cos\eta)^{3/2}} - \frac{\cos\eta}{(1 + b^2.2b\cos\eta)^{3/2}}\right\} d(\cos\eta)$$

$$= \frac{2\pi \sin\theta_o}{3b^3 r^2}\{(2 + b^2|\lambda - b^2)^{\frac{1}{2}} - (2 + b^3)\}$$

$$R(\tau,\mu_o) = \frac{r_o^2 \lambda A}{2\pi} < T(\frac{\tau_o}{\mu} + \frac{\tau}{\mu})> \quad .$$

APPENDIX B

Two ways to calculate the azimuth and elevation of the sun as measured at the point of observation.

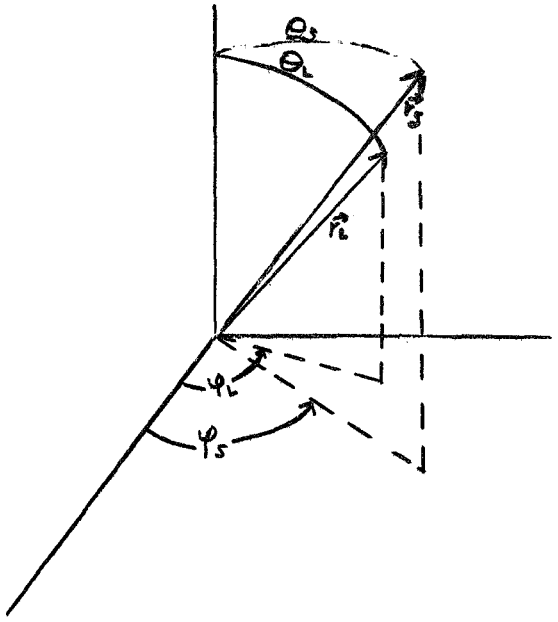

if $\underline{r_s}$ is the radius vector to the sun from the earth's center and $\underline{r_L}$ the radius vector to the point of observation.

The elevation will be given by

$$\zeta = \left[- \tan^{-1} \left(\frac{R_s - R_L}{R_s + R_L} \right) \left(\cot \frac{\theta}{2} \right) \right] + \frac{\pi}{2} + \frac{\theta}{2}$$

where

$$\theta = \cos^{-1}(\cos\theta_L \cos\theta_s + \sin\theta_L \sin\theta_s \cos\Delta\varphi)$$

and the azimuth of bearing

$$z = \sin^{-1}\left[\frac{\sin\Delta\varphi}{\sin\theta}\sin\theta_s\right]$$

which is measured from the South, West being positive.

If we prefer to rotate coordinate systems, instead of doing solid Geometry, we can use the following equivalent relations

$$\theta = \cos^{-1}(\cos\theta_L\cos\theta_s + \sin\theta_L\sin\theta_s\cos\Delta\varphi)$$

$$\begin{aligned} R_1' &= R_s(\cos\theta_L\cos\theta_s + \sin\theta_L\sin\theta_s\cos\varphi_L\cos\varphi_s \\ &\quad + \sin\theta_L\sin\varphi_L\sin\theta_s\sin\varphi_s) - R_L(\cos^2\theta_L \\ &\quad + \sin^2\theta_L\cos^2\varphi_L + \sin^2\theta_L\sin^2\varphi_L = R_s\cos\theta - R_L \end{aligned}$$

$$\begin{aligned} R_2' &= R_s(-\cos\theta_s\sin\theta_L + \cos\theta_L\cos\varphi_L\sin\theta_s\cos\varphi_s \\ &\quad + \cos\theta_L\sin\varphi_L\sin\theta_s\sin\varphi_s) - R_L(\sin\theta_L\cos\theta_L\cos^2\varphi_L \\ &\quad + \sin\theta_L\cos\theta_L\sin^2\varphi_L - \sin\theta_L\cos\theta_L) \\ &= R_s(\cos\theta_L\sin\theta_s\cos\Delta\varphi - \cos\theta_s\sin\theta_L) \end{aligned}$$

$$\begin{aligned} R_3' &= R_s(\cos\varphi_L\sin\theta_s\sin\varphi_s - \sin\varphi_L\sin\theta_s\cos\varphi_s) \\ &\quad + R_L(\sin\theta_L\sin\varphi_L\cos\varphi_L - \cos\varphi_L\sin\theta_L\sin\varphi_L) \\ &= R_s\sin\theta_s\sin\Delta\varphi \end{aligned}$$

$$\Delta\varphi = \varphi_L - \varphi_s$$

where R_1', R_2', R_3' are respectively the x,y,z components of the difference vector measured in the rotated coordinate system where

$$\underline{R}_L = R_L(1,0,0).$$

$$|\underline{R}| = [R_1^2 + R_2^2 - 2\underline{R}_1 \cdot \underline{R}_2]^{\frac{1}{2}}$$

and then

$$\text{Azimuth} = \tan^{-1} \frac{R_2'}{R_1'}$$

$$\text{Elevation} = \cos^{-1} \frac{R_1'}{R} \quad .$$

APPENDIX C.

The optical scattering coefficient $\sigma_{\varphi\lambda}$ is given by

$$i_{\varphi\lambda} = \sigma_{\varphi\lambda} i_{\lambda}$$

using the Rayleigh scattering cross section

$$\sigma_{\varphi\lambda} = \frac{2\pi^2}{n\lambda^4} (\mu_{\lambda}-1)^2 (1 + \cos^2\varphi)$$

n and μ_{λ} are molecular density and refractive index of the air.

Adjusting for the polarization defect (Dawson, 1941, yields the correct cross-section

$$\sigma_{\varphi\lambda} = \frac{2\pi^2}{n\lambda^4} (\mu_{\lambda}-1)^2 \frac{6(1+\delta)}{6-7\delta} (1 + \frac{1-\delta}{1+\delta} \cos^2\varphi) \quad .$$

TABLE I.

τ	$T(\tau)$	$\epsilon(\tau)$	$H(\tau)$	$W(\tau)$*
10^{-3}	9.99 (-1)	4.97 (-1)	2.33	
10^{-2}	9.92 (-1)	4.81 (-1)	1.52	
10^{-1}	9.31 (-1)	3.93 (-1)	7.27 (-1)	9.70 (-2)
$2*10^{-1}$	8.68 (-1)	3.33 (-1)	5.09 (-1)	1.78 (-1)
$5*10^{-1}$	7.08 (-1)	2.25 (-1)	2.61 (-1)	4.22 (-1)
10^{0}	5.13 (-1)	1.36 (-1)	1.18 (-1)	6.16 (-1)
$2*10^{0}$	2.89 (-1)	6.49 (-2)	3.99 (-2)	8.65 (-1)
$5*10^{0}$	8.94 (-2)	1.95 (-2)	5.06 (-3)	1.18
10^{1}	3.58 (-2)	8.51 (-3)	1.07 (-3)	1.40
$2*10^{1}$	1.56 (-2)	4.15 (-3)	2.28 (-4)	1.58
$5*10^{1}$	5.47 (-3)	1.42 (-3)	2.89 (-5)	1.83
10^{2}	2.64 (-3)	6.60 (-4)	6.61 (-6)	2.00
10^{3}	2.16 (-4)	5.10 (-4)	5.42 (-8)	2.44
10^{4}	1.86 (-5)	4.50 (-4)	4.46 (-10)	2.72

*$W(\tau) = \int_0^{\tau} d\tau' T/\tau)$.

TABLE II.

Lat. 23.5°N

June 19 $\beta = 0.0126/km$

June 26

Hours from local noon	Brightness	% Transmission	$\frac{B_p}{B}$	Azimuth	Elevation	Scattering Angle	γ
6.0	108.9	.474	.761	71.7	75.1	91.9	.176
5.5	114.1	.516	.786	76.0	69.6	85.1	.166
5.0	119.7	.558	.806	80.3	64.0	78.3	.185
4.5	126.7	.596	.824	84.8	58.3	71.6	.230
4.0	135.2	.626	.839	89.4	52.6	64.9	.294
3.5	137.8	.645	.846	85.6	46.9	63.7	.306
3.0	139.2	.657	.850	80.0	41.2	63.2	.310
2.5	140.4	.662	.853	73.5	35.6	62.8	.314
2.0	141.3	.661	.856	65.6	30.3	62.4	.318
1.5	142.0	.655	.858	55.4	25.3	62.1	.321
1.0	142.5	.646	.859	41.6	24.0	61.9	.323
0.5	142.8	.637	.860	23.0	17.9	61.8	.324
0.0	142.9	.633	.860		16.7	61.7	.325

TABLE III.

Lat. 0°N

March 21 $\beta = 0.0126/km$

September 23

Hours from local noon	Brightness	Transmission	B_p/B	Azimuth	Elevation	Scattering Angle	γ
6.0	calculation fails for this hour						
5.5	83.2	.408	.653	85.1	84.3	89.4	.248
5.0	103.6	.448	.736	80.2	78.6	88.8	.192
4.5	111.1	.490	.772	75.0	73.0	88.2	.169
4.0	114.8	.530	.792	69.6	67.5	87.6	.157
3.5	117.0	.566	.804	63.7	62.3	87.1	.150
3.0	118.5	.595	.812	57.2	57.3	86.6	.146
2.5	119.5	.619	.818	50.0	52.7	86.2	.144
2.0	120.2	.637	.822	41.8	48.6	85.8	.142
1.5	120.7	.650	.825	32.7	45.1	85.5	.141
1.0	121.0	.658	.827	22.6	42.4	85.3	.140
0,5	121.2	.662	.828	11.5	40.7	85.2	.140
0.0	121.3	.663	.828		40.2	85.2	.140

TABLE IV.

Lat. 5.2°S

October 31 $\beta = 0.0126/km$

February 11

Hours from local noon	Brightness	Transmission	$\frac{B_p}{B}$	Azimuth	Elevation	Scattering Angle	γ
6.0		Calculation gives negative B_m					
5.5		Calculation gives negative B					
5.0	77.4	.406	.633	72.7	85.2	98.6	.282
4.5	102.3	.441	.728	67.6	79.8	98.0	.214
4.0	110.7	.481	.766	62.2	74.6	97.5	.187
3.5	114.6	.517	.787	56.5	69.7	96.9	.172
3.0	116.8	.549	.800	50.2	65.1	96.5	.163
2.5	118.2	.575	.808	43.3	60.9	96.1	.156
2.0	119.0	.596	.813	35.9	57.2	95.7	.152
1.5	119.6	.612	.817	27.7	54.2	95.4	.149
1.0	119.9	.623	.819	18.9	52.0	95.2	.146
0.5	120.1	.629	.821	9.6	50.5	95.1	.146
0.0	120.2	.631	.821		50.1	95.1	.145

TABLE V.

TABLE V.

D_1	H \ Q	0	25	-25	28	-28	in mk
	0	9.89 (-8)	9.99	9.99	10.0	10.0	$x10^{-8}$
	1	2.04 (-7)	2.06	2.06	2.06	2.06	$x10^{-7}$
in 10^3G	3	4.70 (-7)	4.70	4.70	4.71	4.70	$x10^{-7}$
	5	8.91 (-7)	8.90	8.90	8.92	8.91	$x10^{-7}$

D_2	H \ Q	0	25	-25	28	-28	in mk
	0	8.55	8.65	8.65	8.68	8.68	$x10^{-8}$
	1	1.98	2.01	2.00	2.01	2.01	$x10^{-7}$
in 10^3G	3	5.10	5.14	5.13	5.15	5.14	$x10^{-7}$
	5	10.64	10.7	10.7	10.7	10.7	$x10^{-7}$

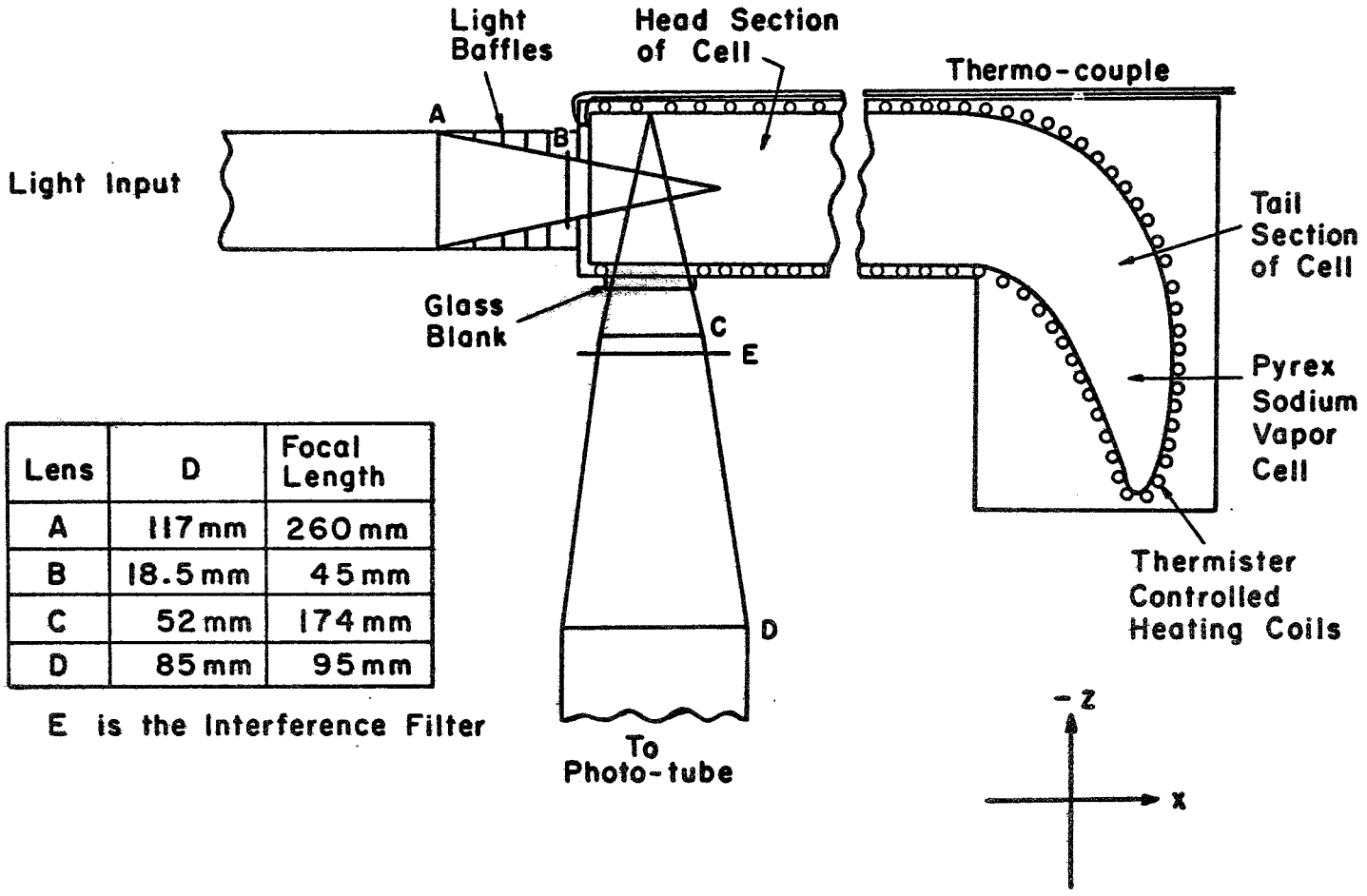

Lens	D	Focal Length
A	117mm	260mm
B	18.5mm	45mm
C	52mm	174mm
D	85mm	95mm

E is the Interference Filter

Figure I.

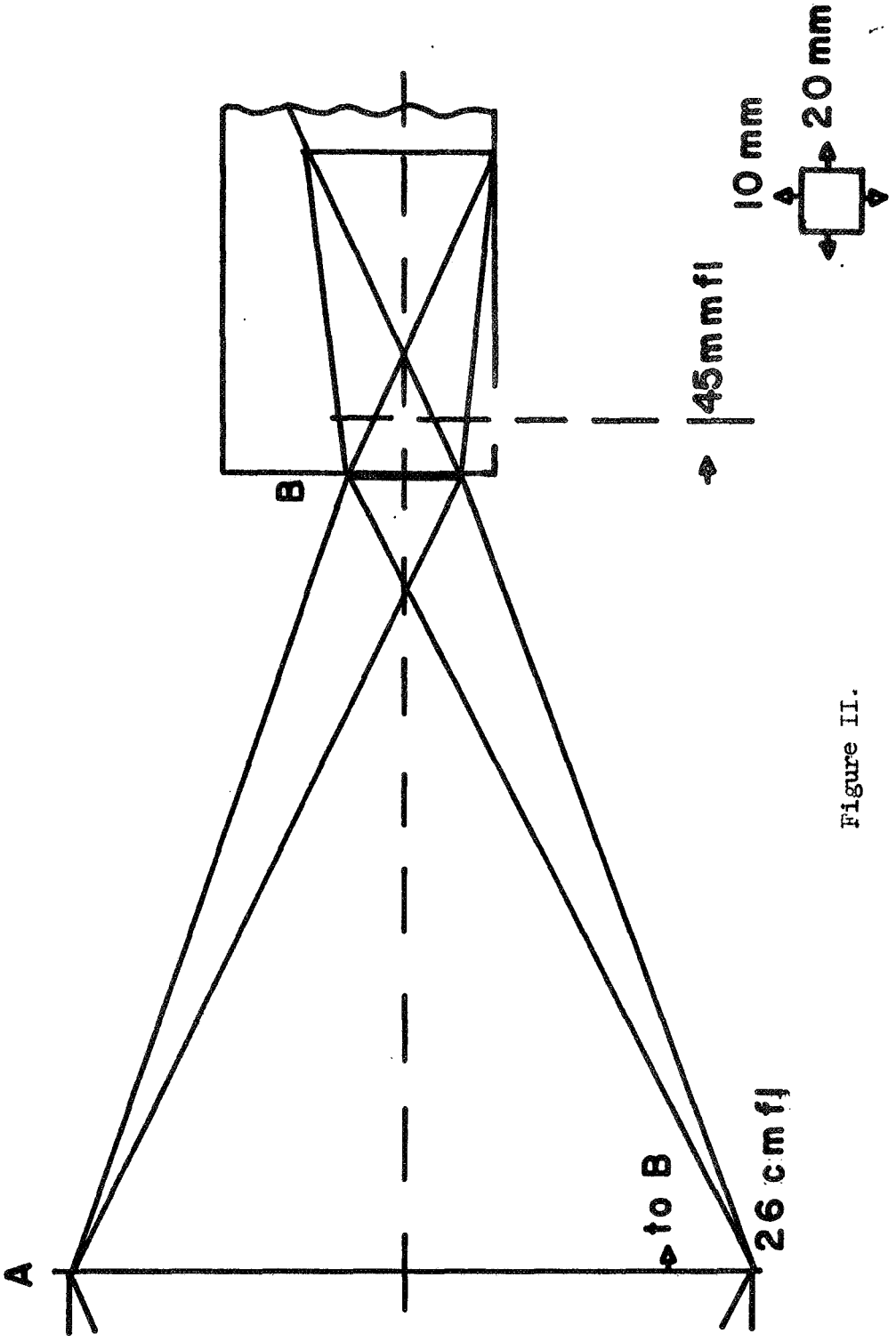

Figure II.

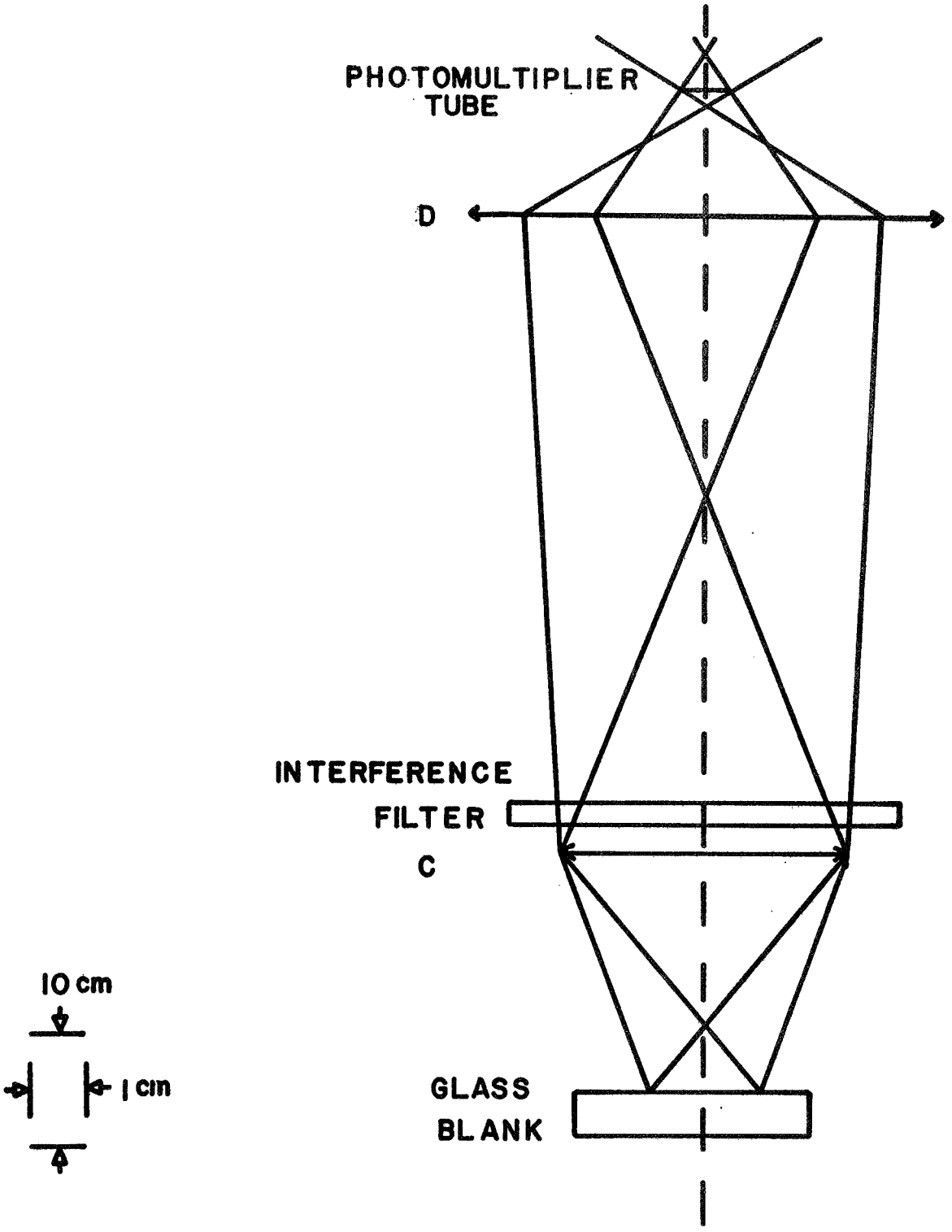
PHOTOMULTIPLIER
TUBE
D
INTERFERENCE
FILTER
C
GLASS
BLANK
10 cm
1 cm

Figure III.

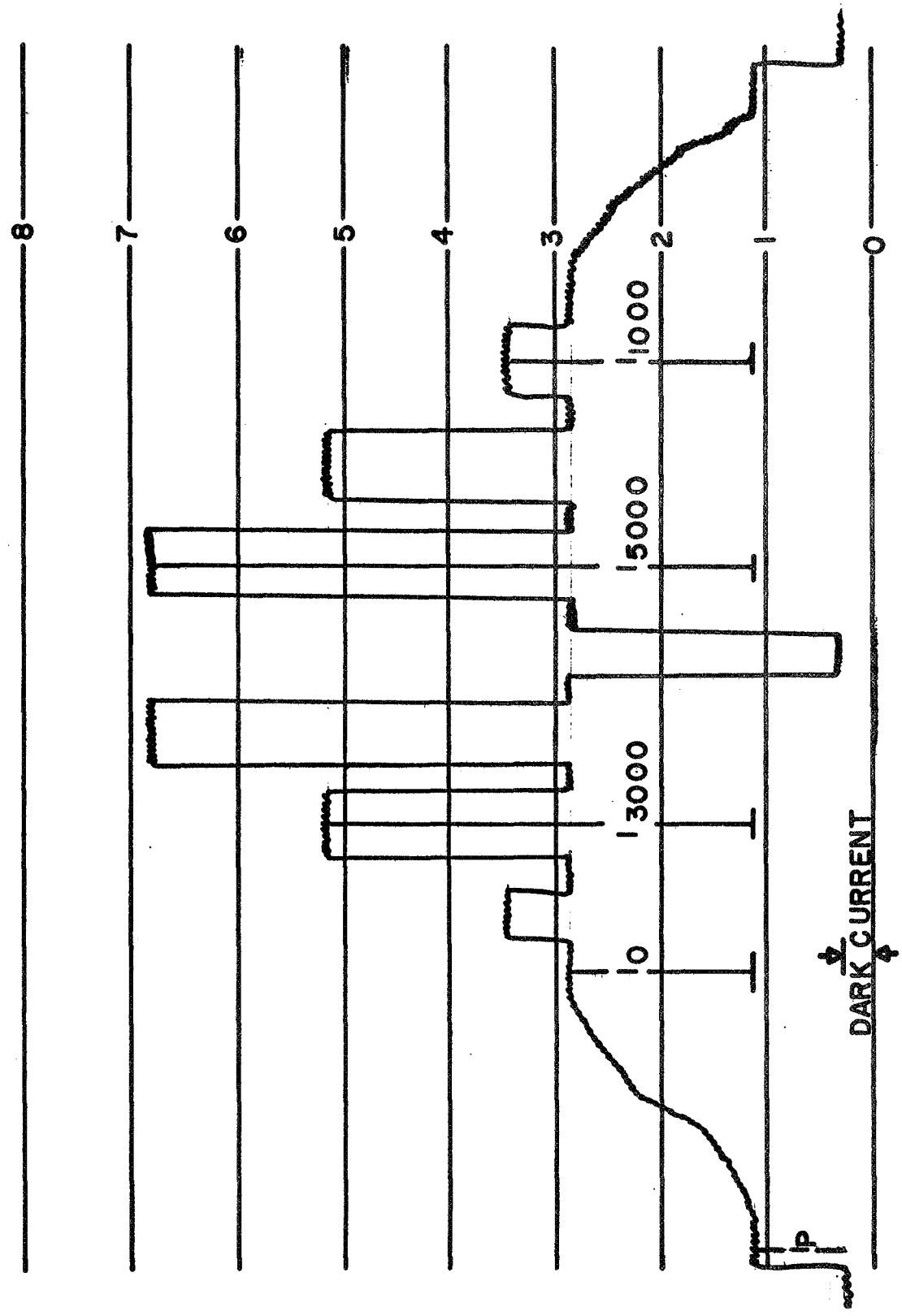

Figure IV.

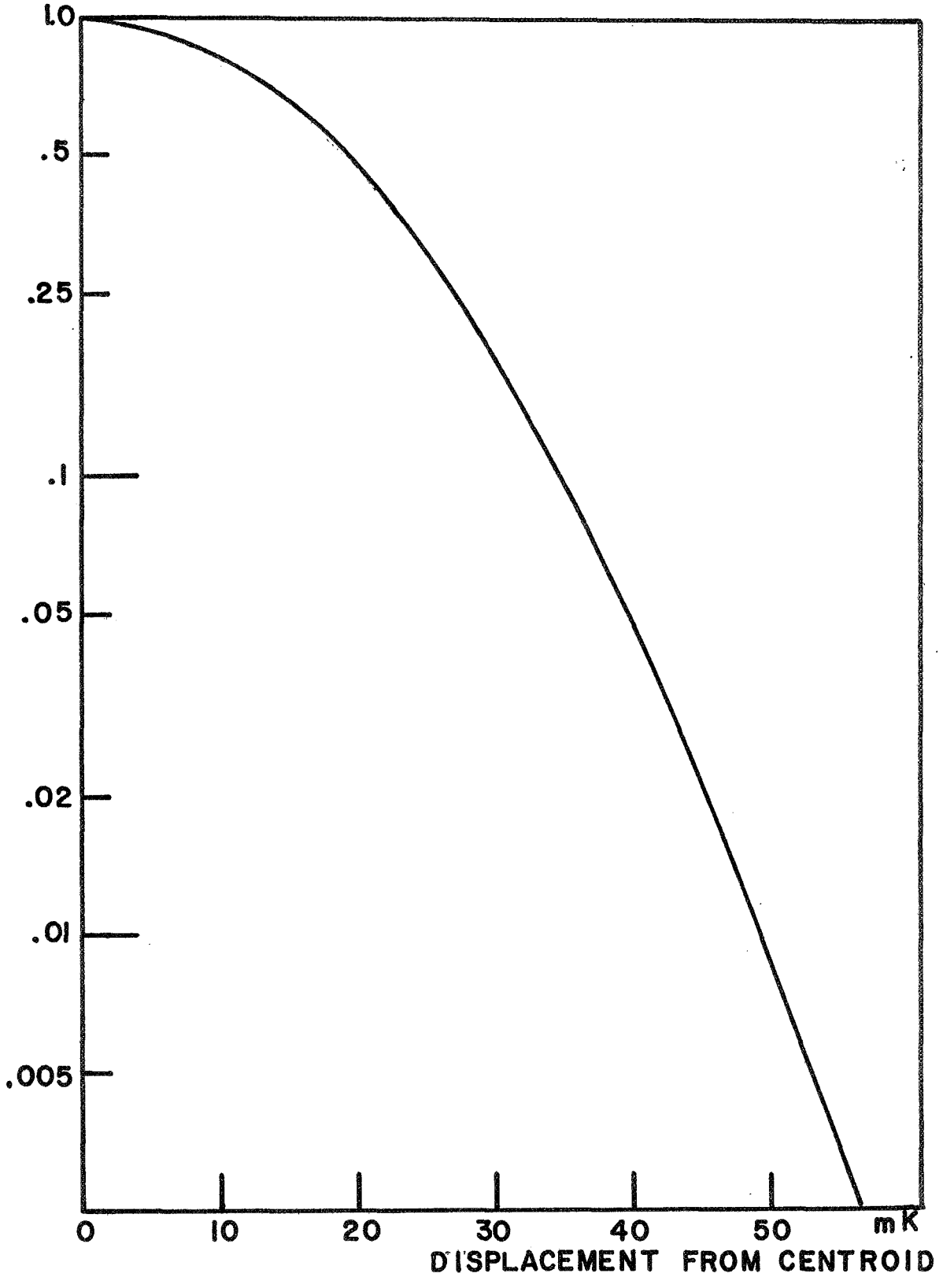
1.0
.5
.25
.1
.05
.02
.01
.005
0
10
20
30
40
50
mK
DISPLACEMENT FROM CENTROID

Figure V.

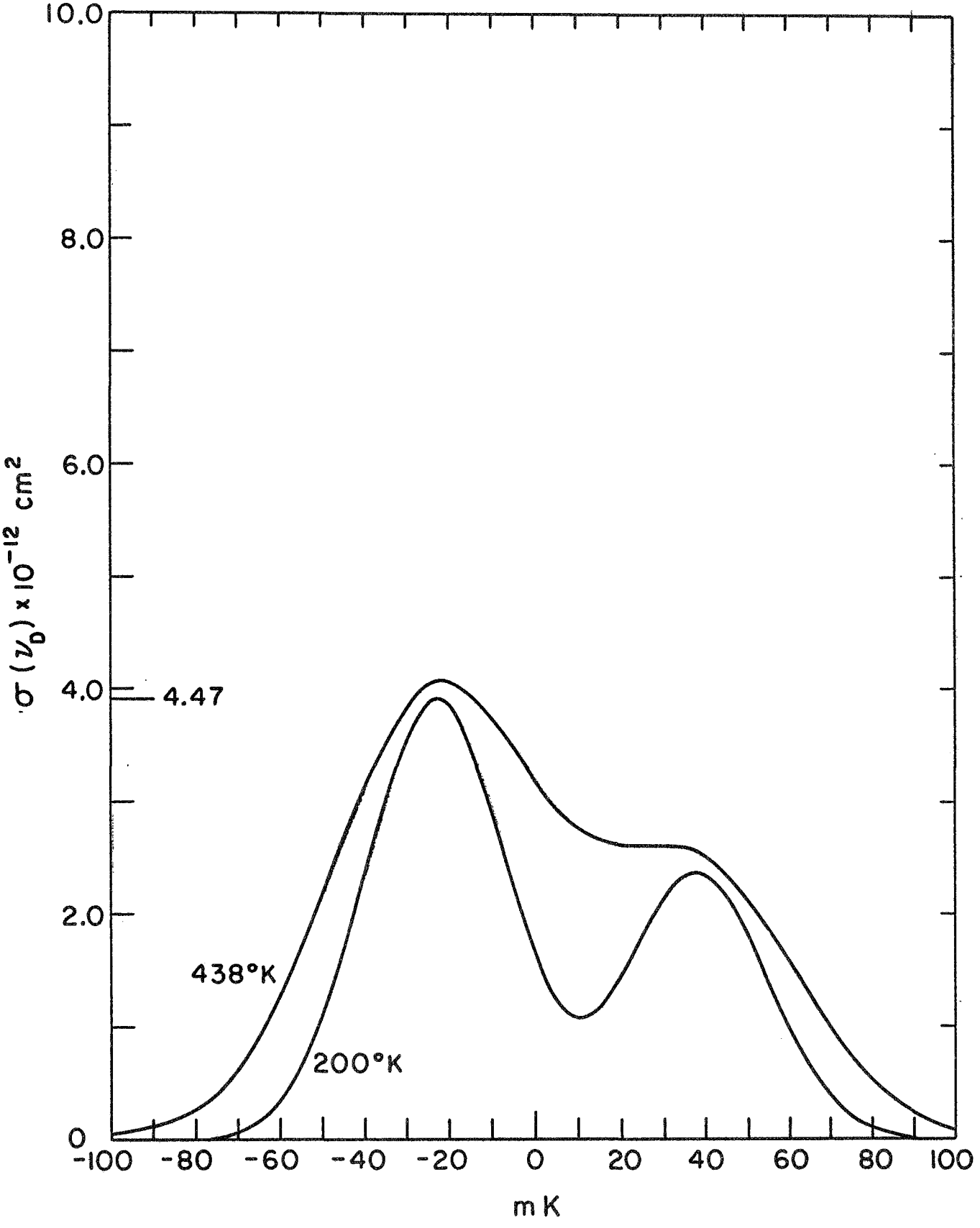
10.0
8.0
6.0
4.0
2.0
0
σ (ν0) x 10⁻¹² cm²
4.47
438°K
200°K
-100
-80
-60
-40
-20
0
20
40
60
80
100
m K

Figure VI.

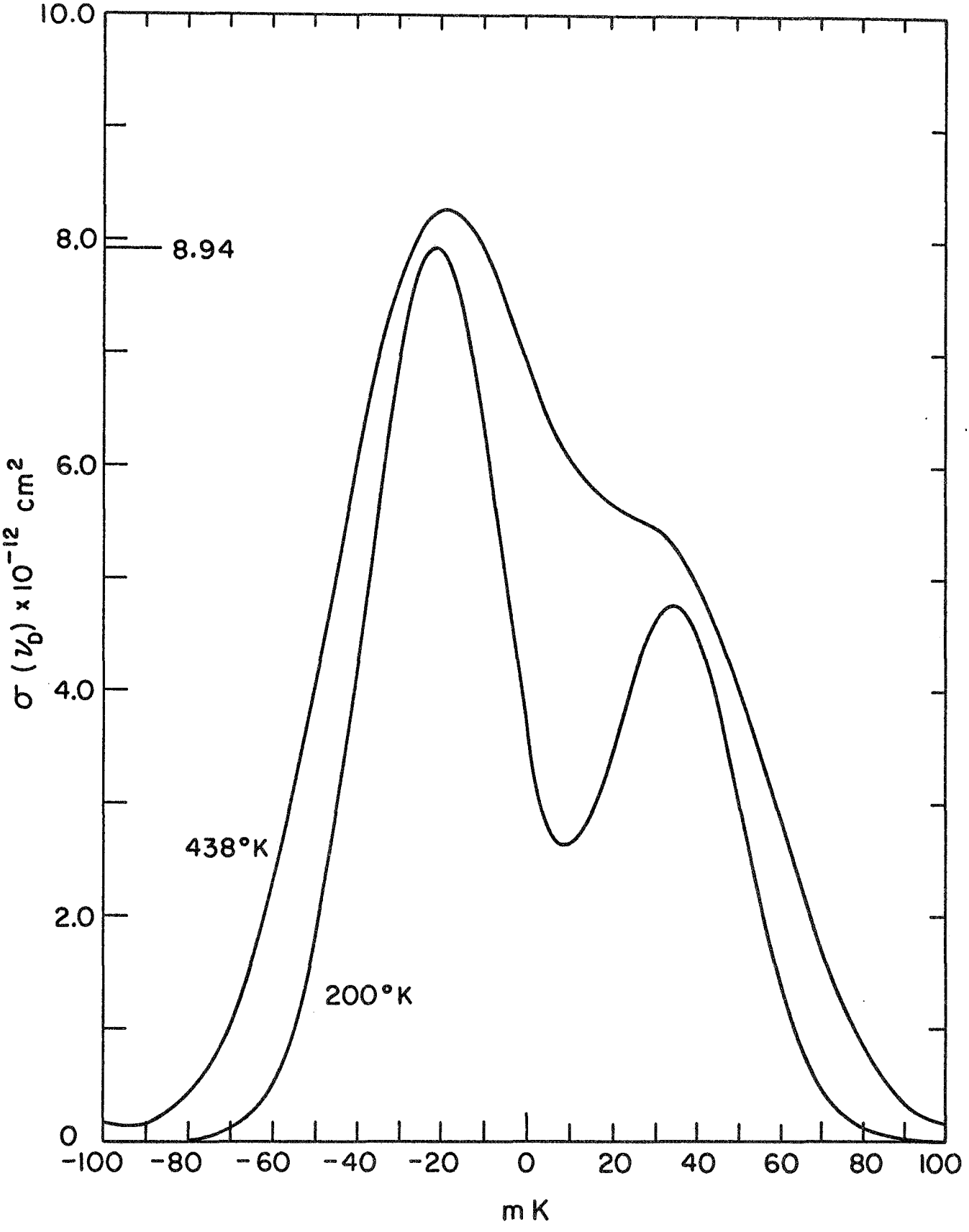
10.0
8.0
8.94
6.0
4.0
2.0
0
σ (ν_D) x 10^-12 cm^2
438°K
200°K
-100
-80
-60
-40
-20
0
20
40
60
80
100
m K

Figure VII.

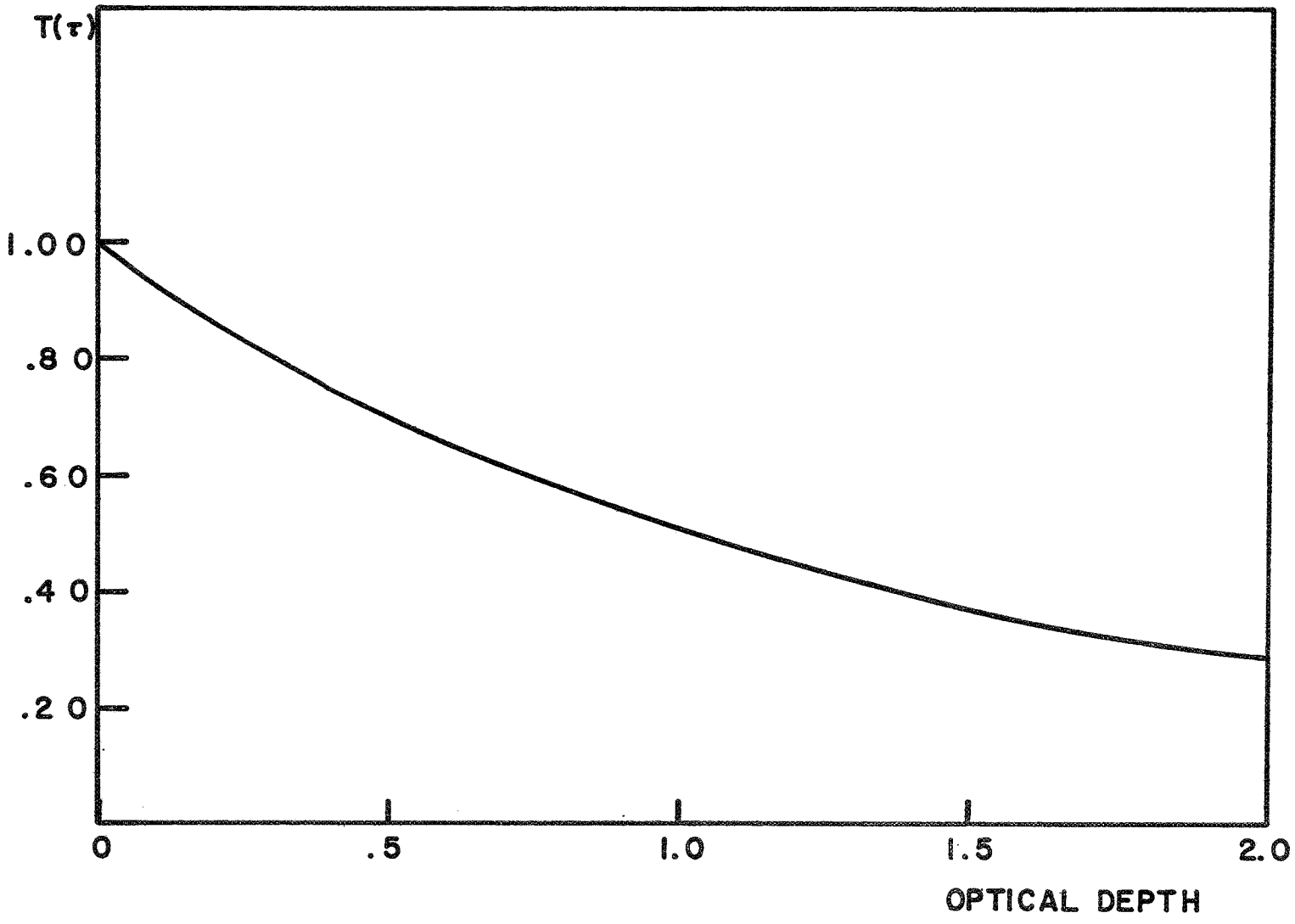

Figure VIII.

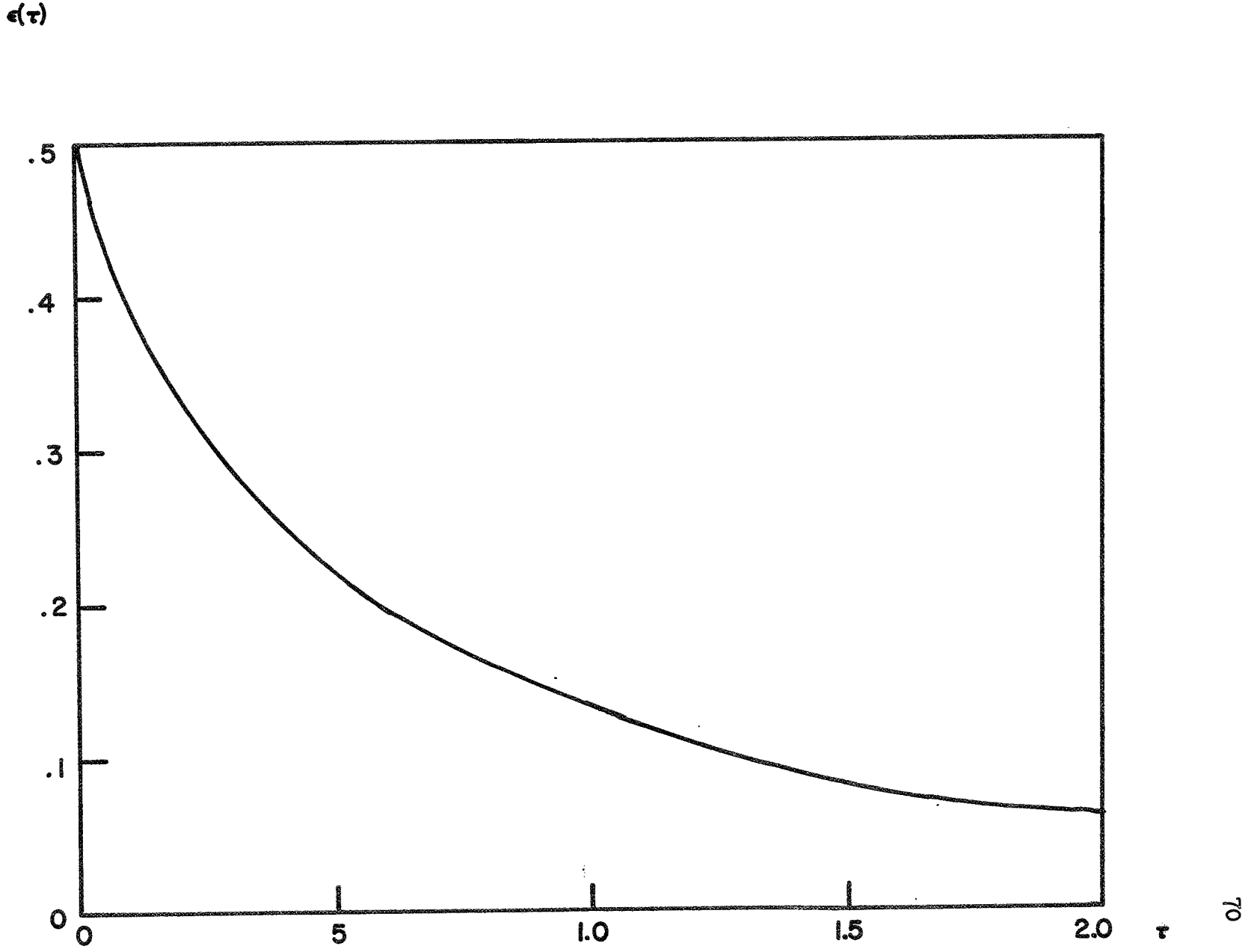

Figure IX.

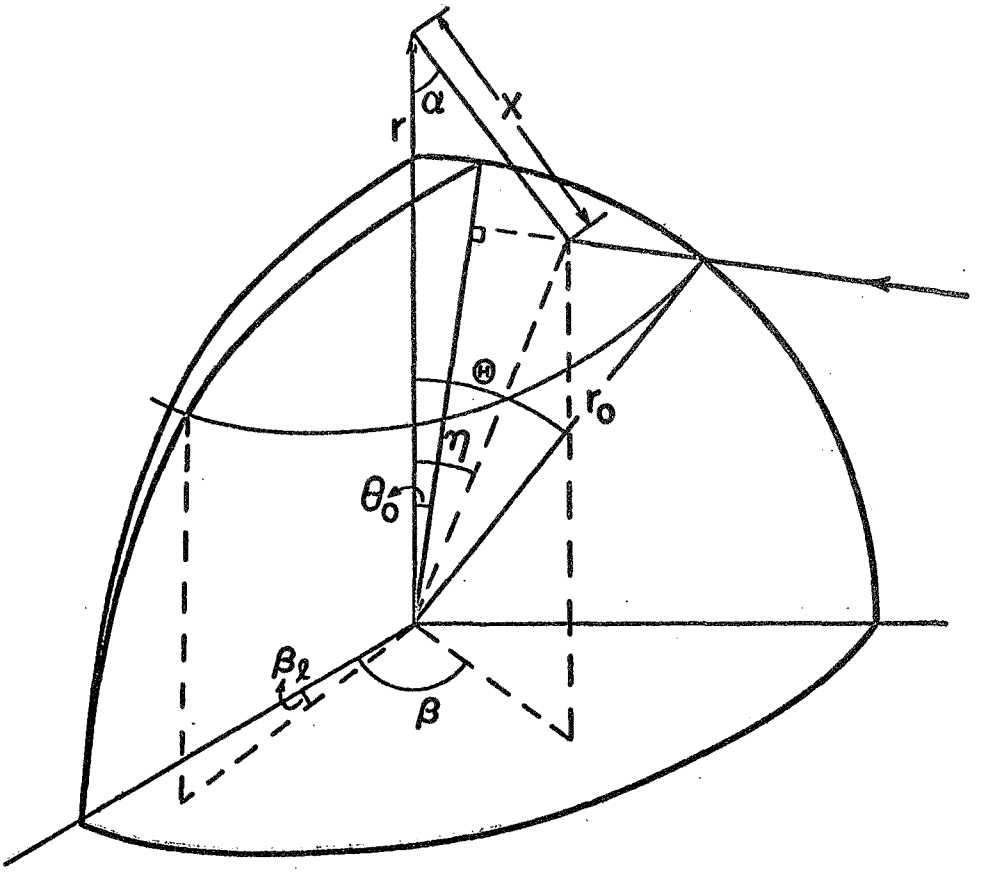

Figure X.

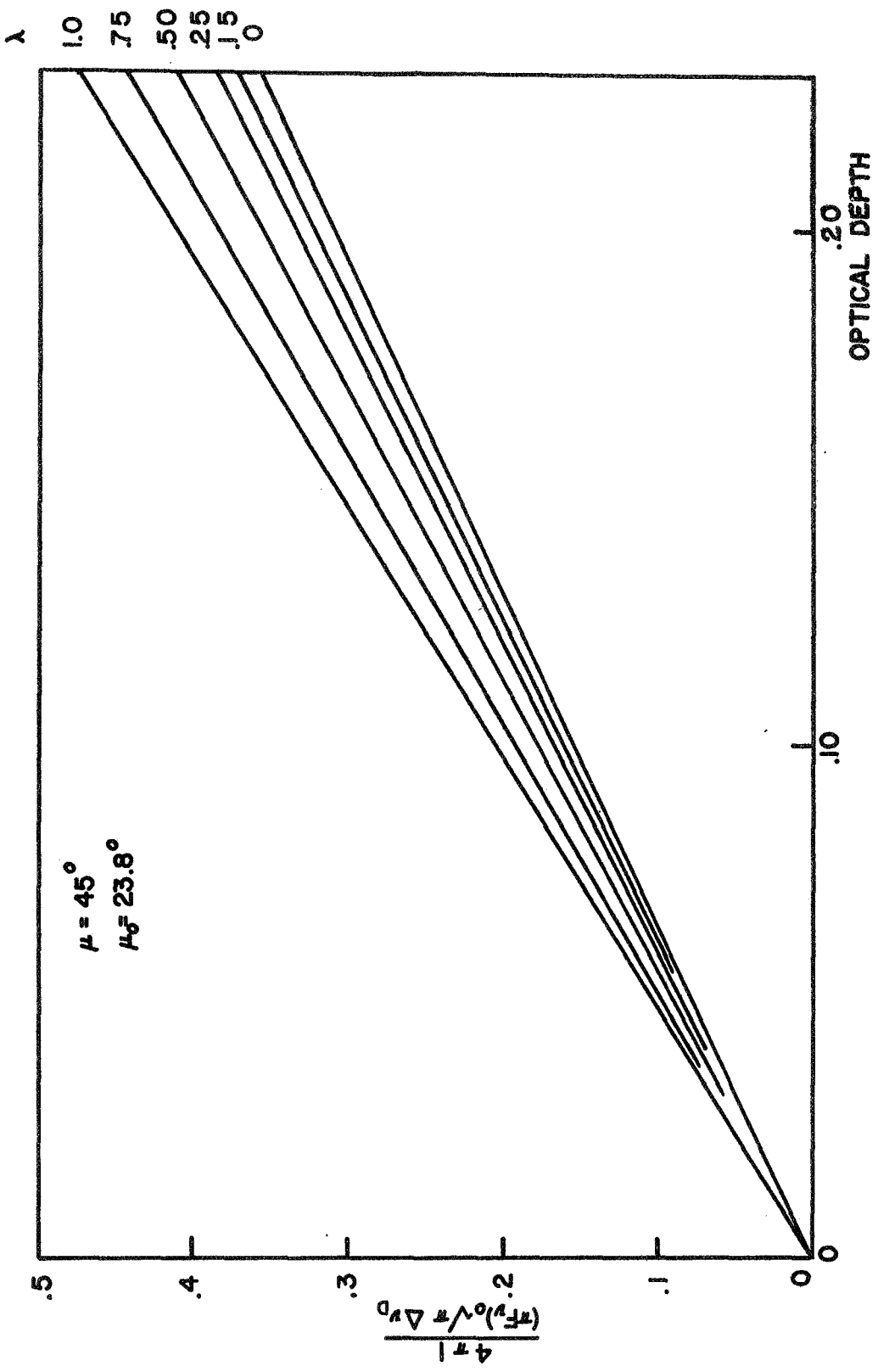
λ
1.0
.75
.50
.25
.15
0
μ = 45°
μ₀ = 23.8°
0
.10
.20
OPTICAL DEPTH
0
.1
.2
.3
.4
.5
4π I / (πF_ν)₀ √π Δν_D

Figure XI.

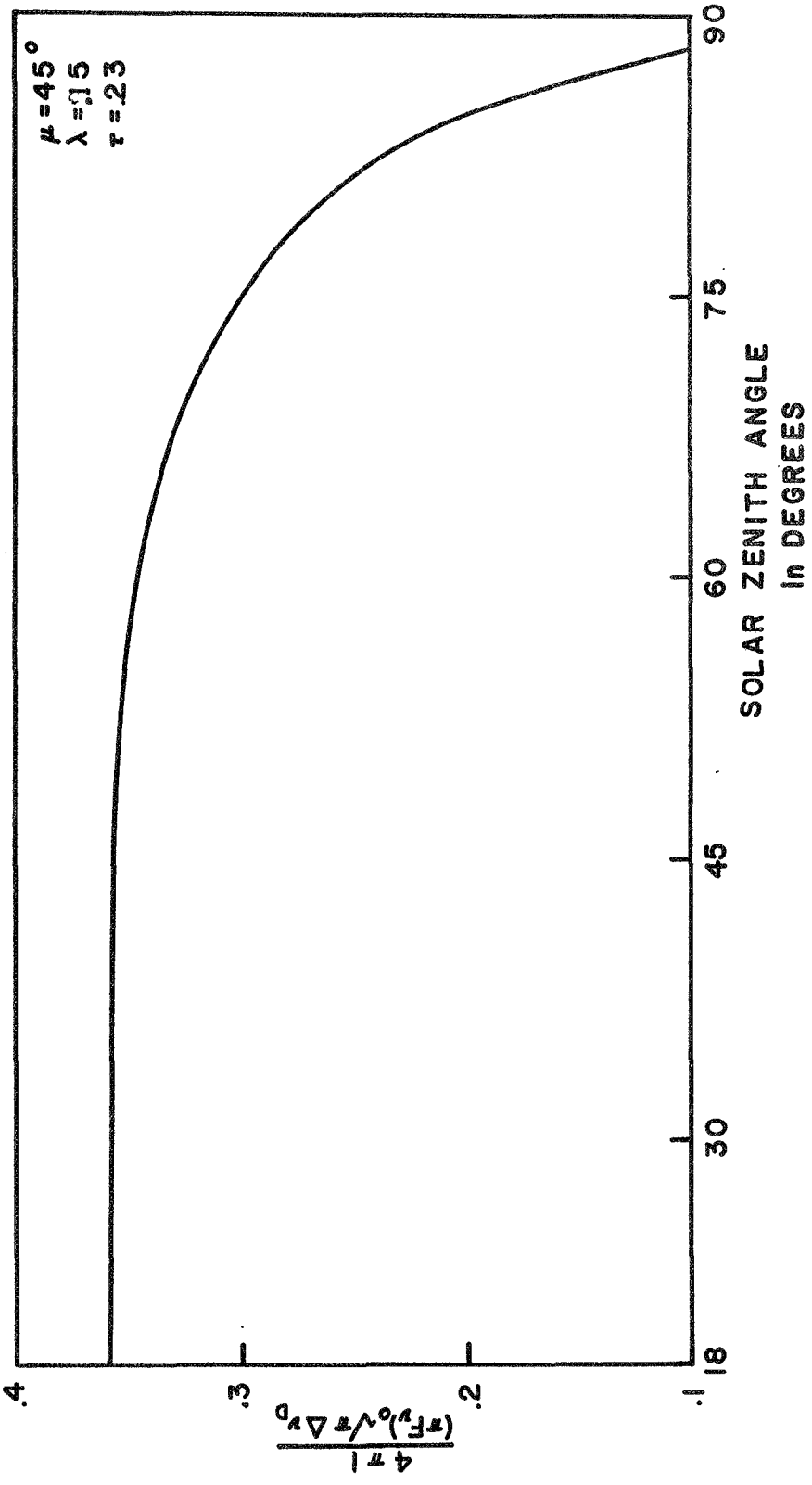
μ=45°
λ=.15
τ=.23
SOLAR ZENITH ANGLE
In DEGREES
18
30
45
60
75
90
.1
.2
.3
.4
$\frac{4\pi I}{(\pi F_\nu)_0 \sqrt{\pi \Delta \nu_D}}$

Figure XII.

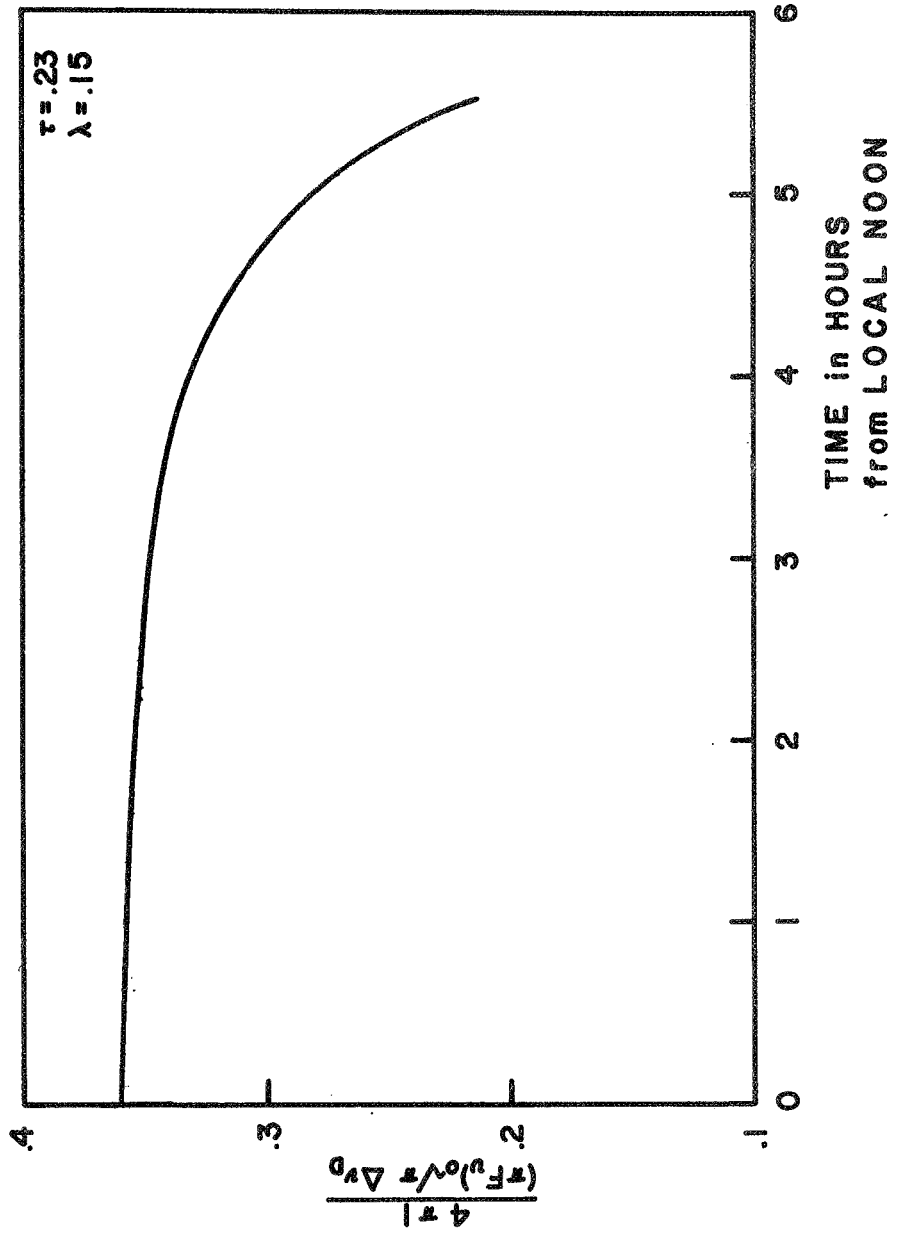
τ=.23
λ=.15
.4
.3
.2
.1
0
1
2
3
4
5
6
TIME in HOURS
from LOCAL NOON
4 π I
(π F_u)_o √π Δν_D

Figure XIII.

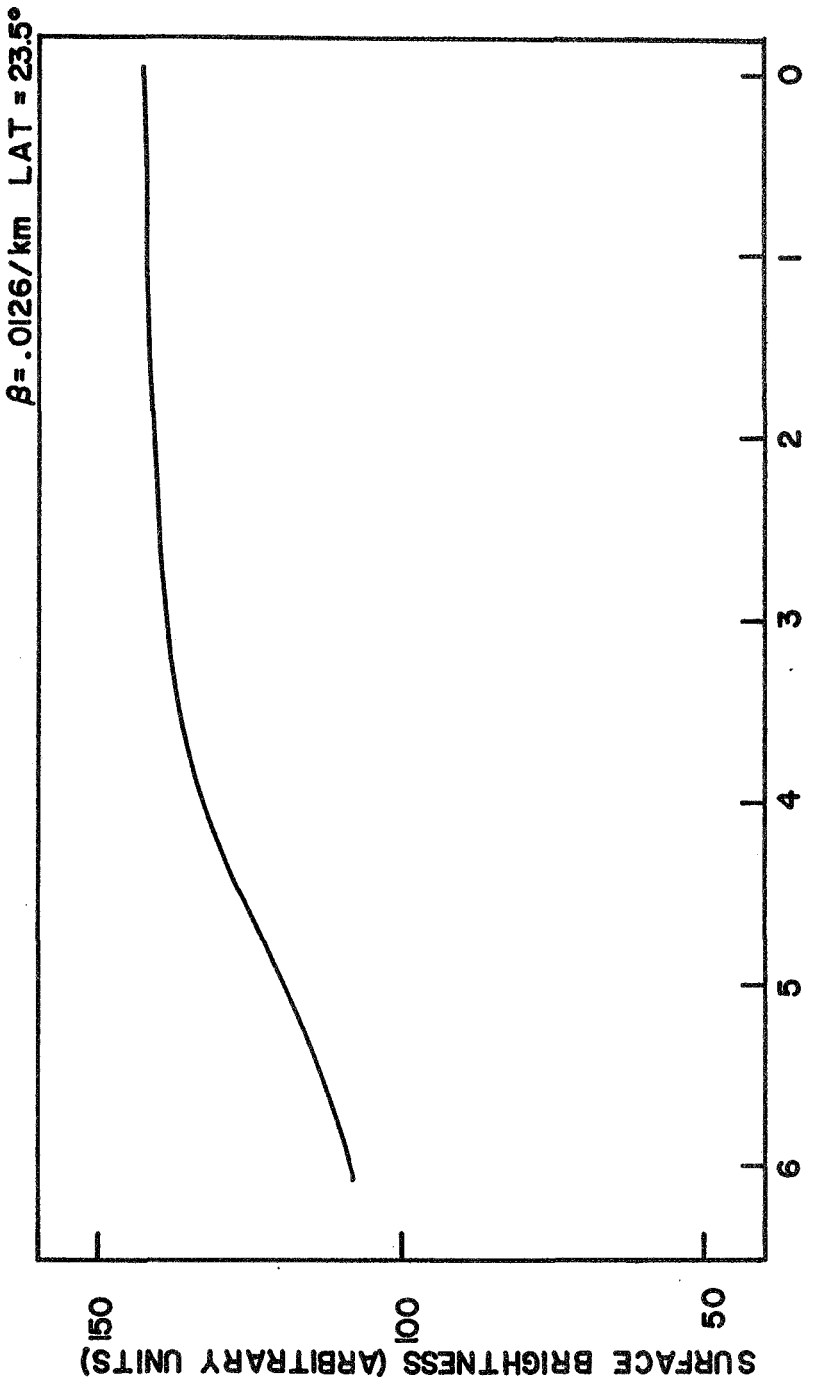
β=.0126/km LAT = 23.5°
SURFACE BRIGHTNESS (ARBITRARY UNITS)
150
100
50
0
1
2
3
4
5
6
TIME in HOURS
from LOCAL NOON

Figure XIV.

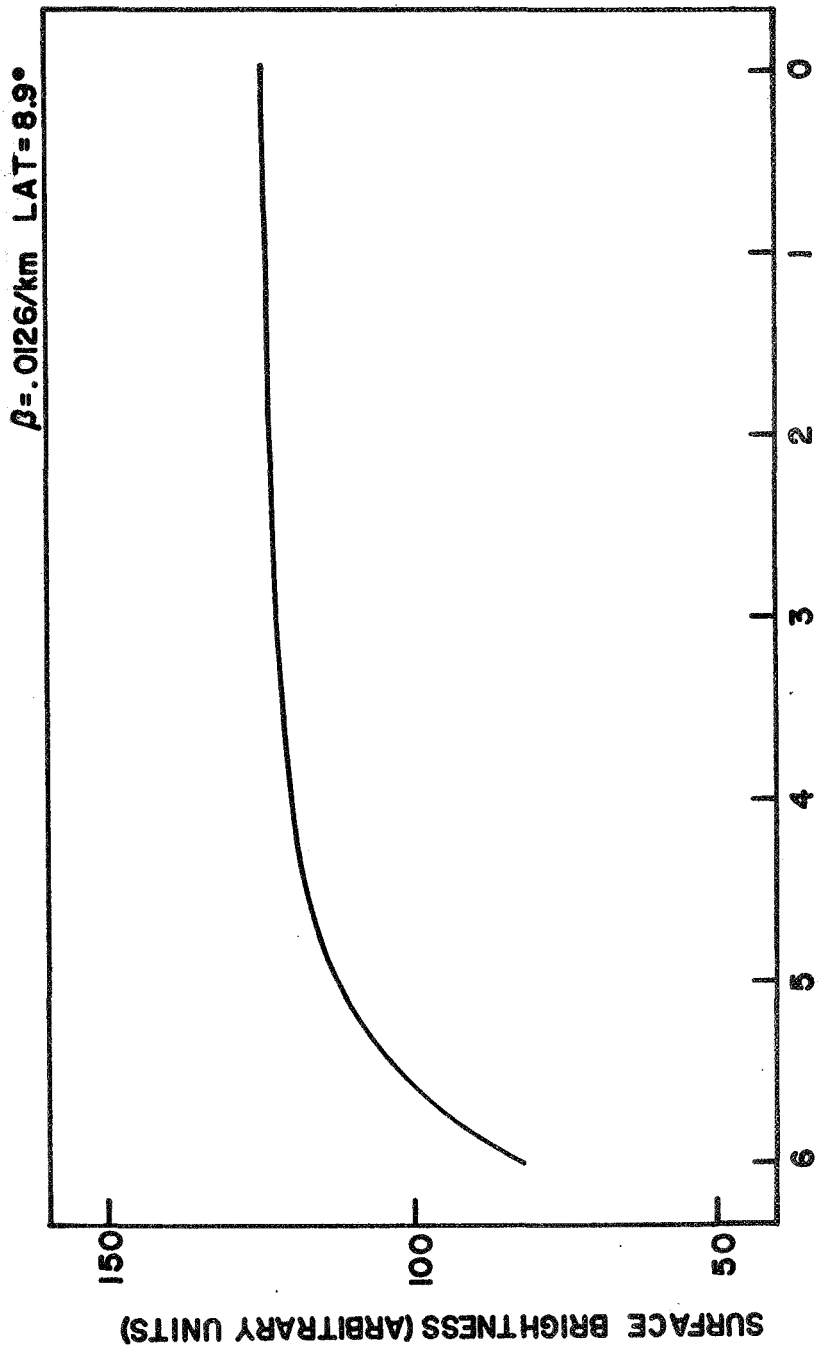
β=.0126/km LAT=8.9°
SURFACE BRIGHTNESS (ARBITRARY UNITS)
150
100
50
0
1
2
3
4
5
6
TIME in HOURS
from LOCAL NOON

Figure XV.

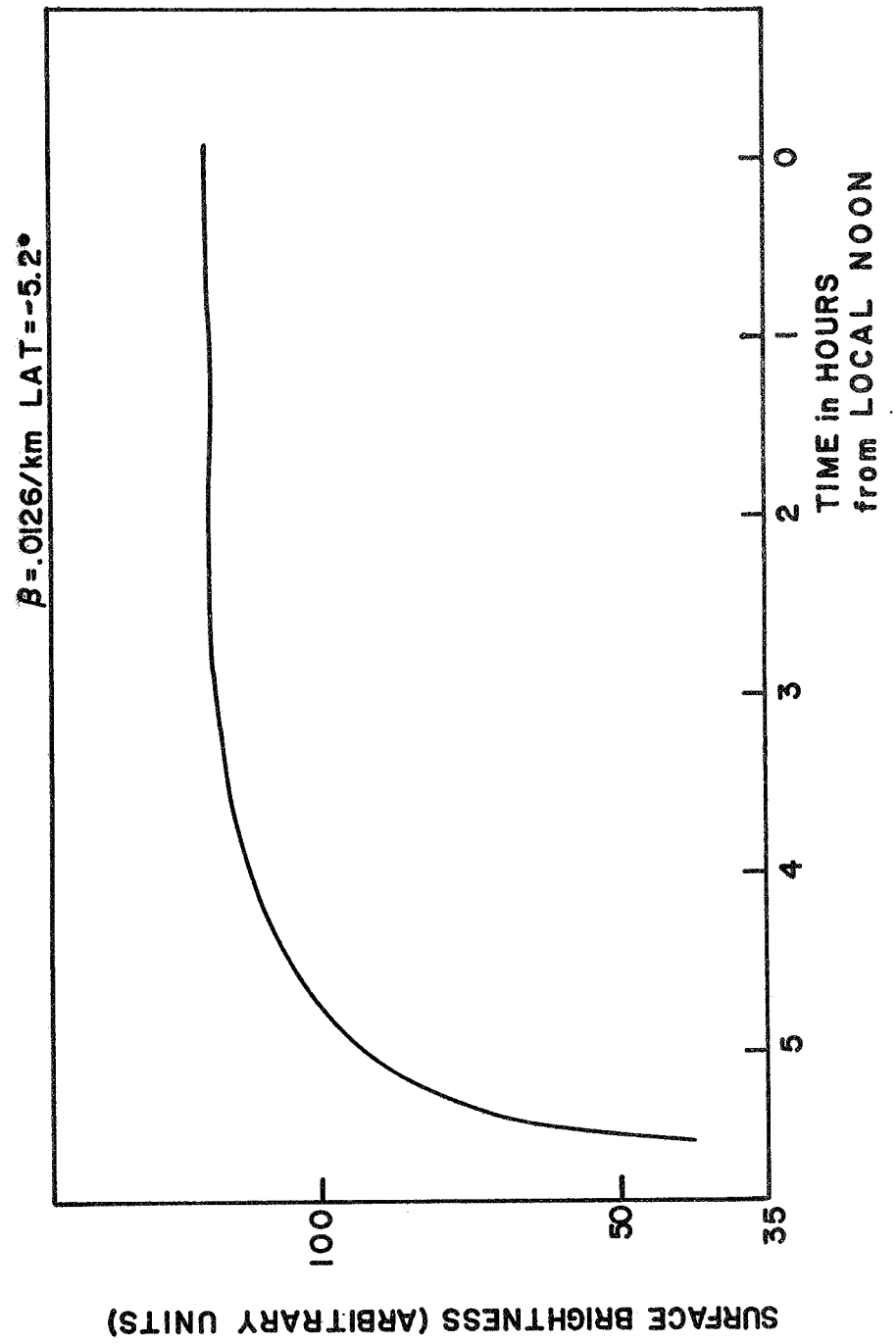
β=.0126/km LAT=-5.2°
SURFACE BRIGHTNESS (ARBITRARY UNITS)
100
50
35
0
1
2
3
4
5
TIME in HOURS
from LOCAL NOON

Figure XVI.

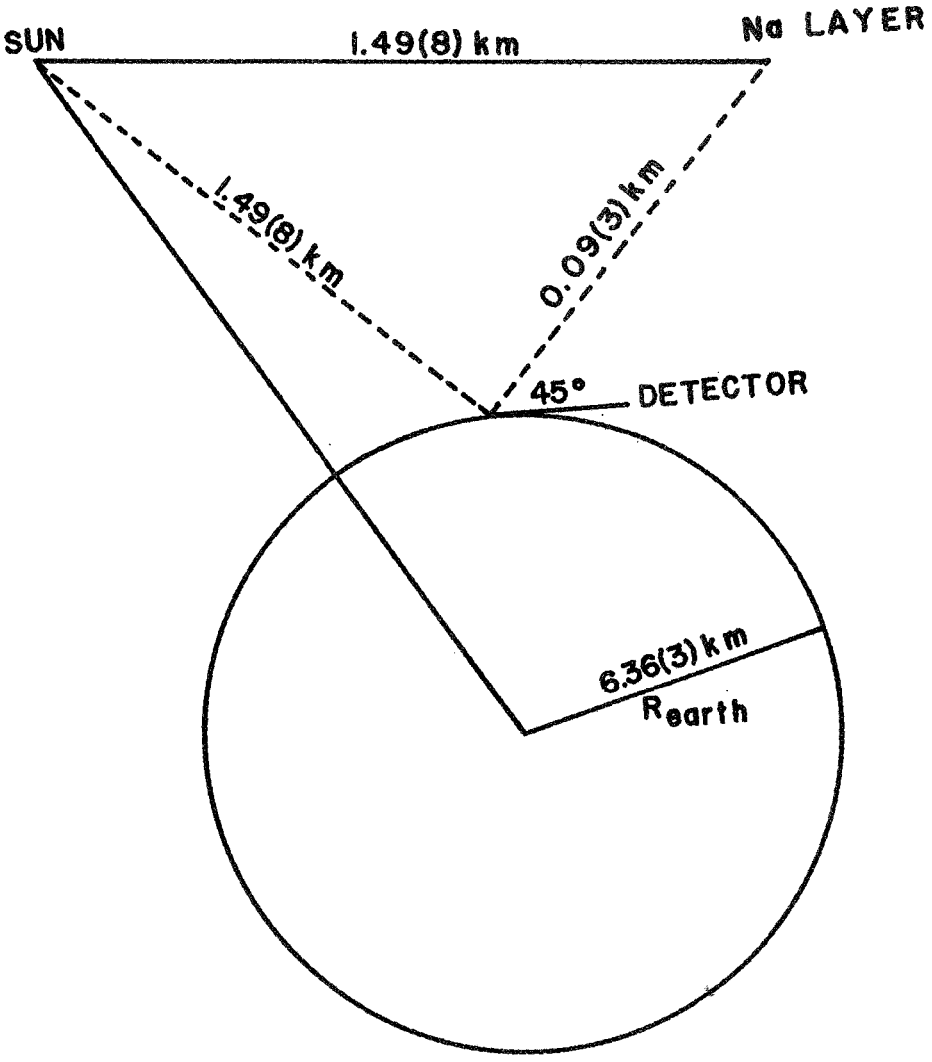
SUN
1.49(8) km
Na LAYER
1.49(8) km
0.09(3) km
45°
DETECTOR
6.36(3) km
Rearth

Figure XVII.

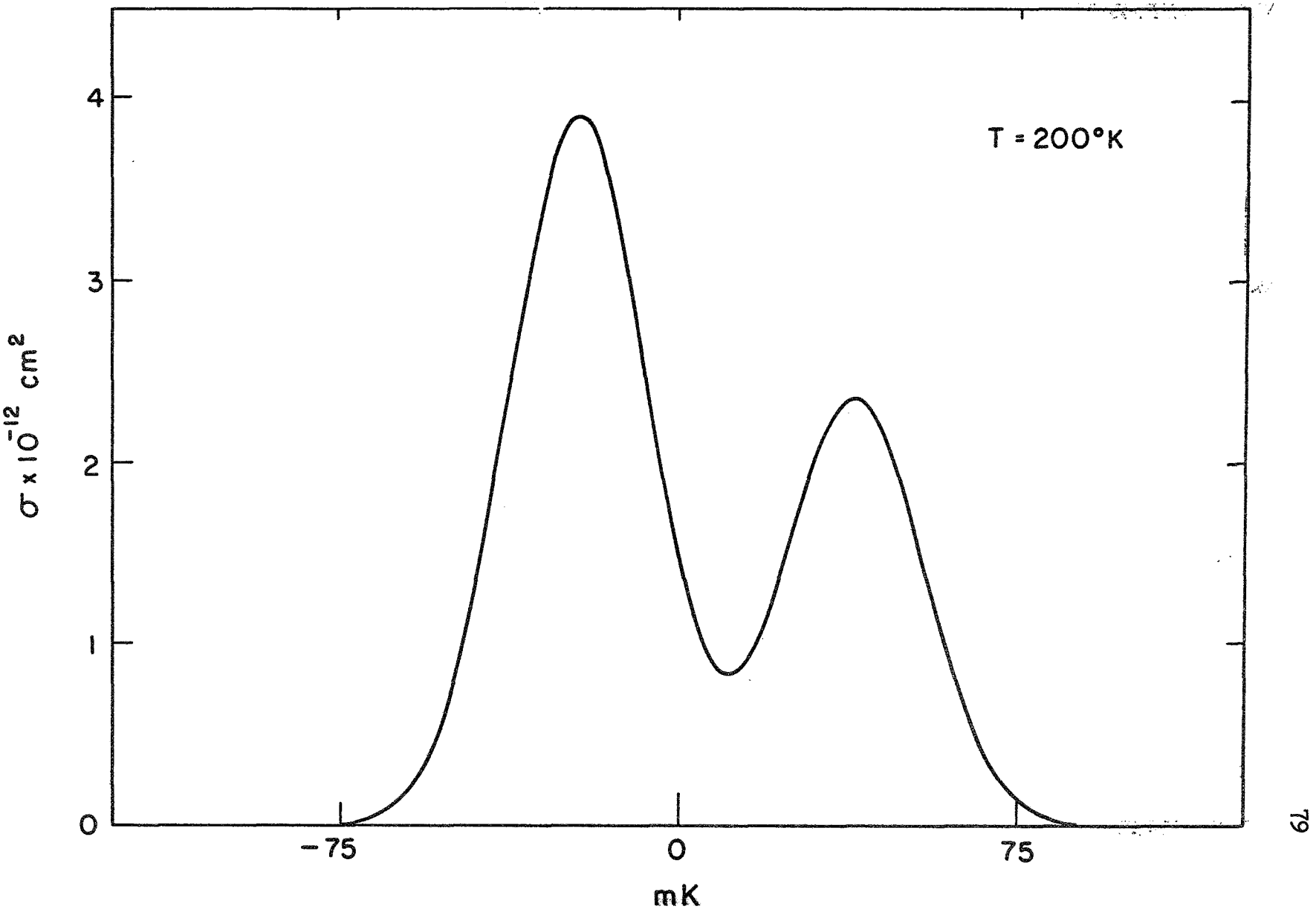

Figure XVIII.

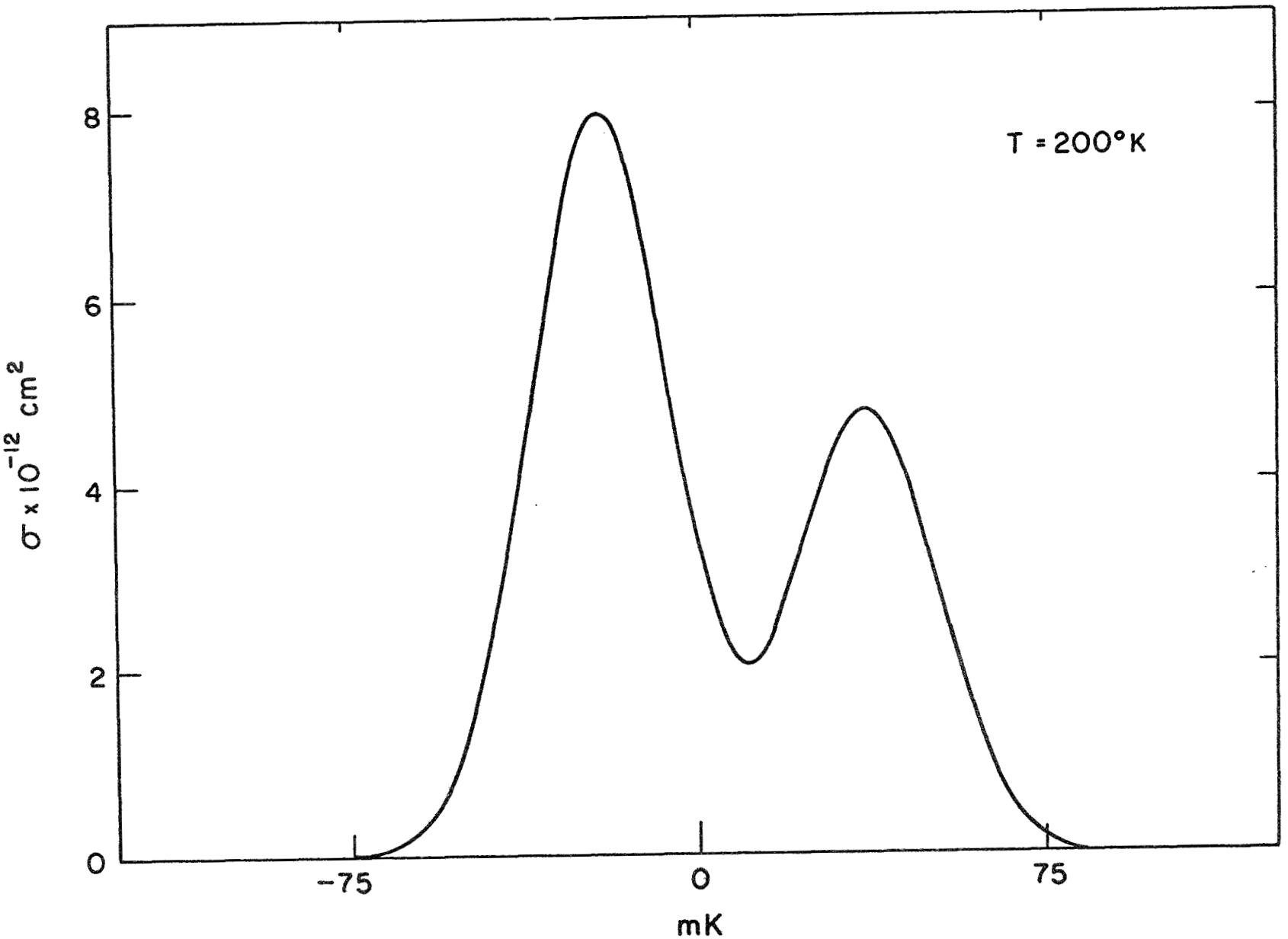

Figure XIX.

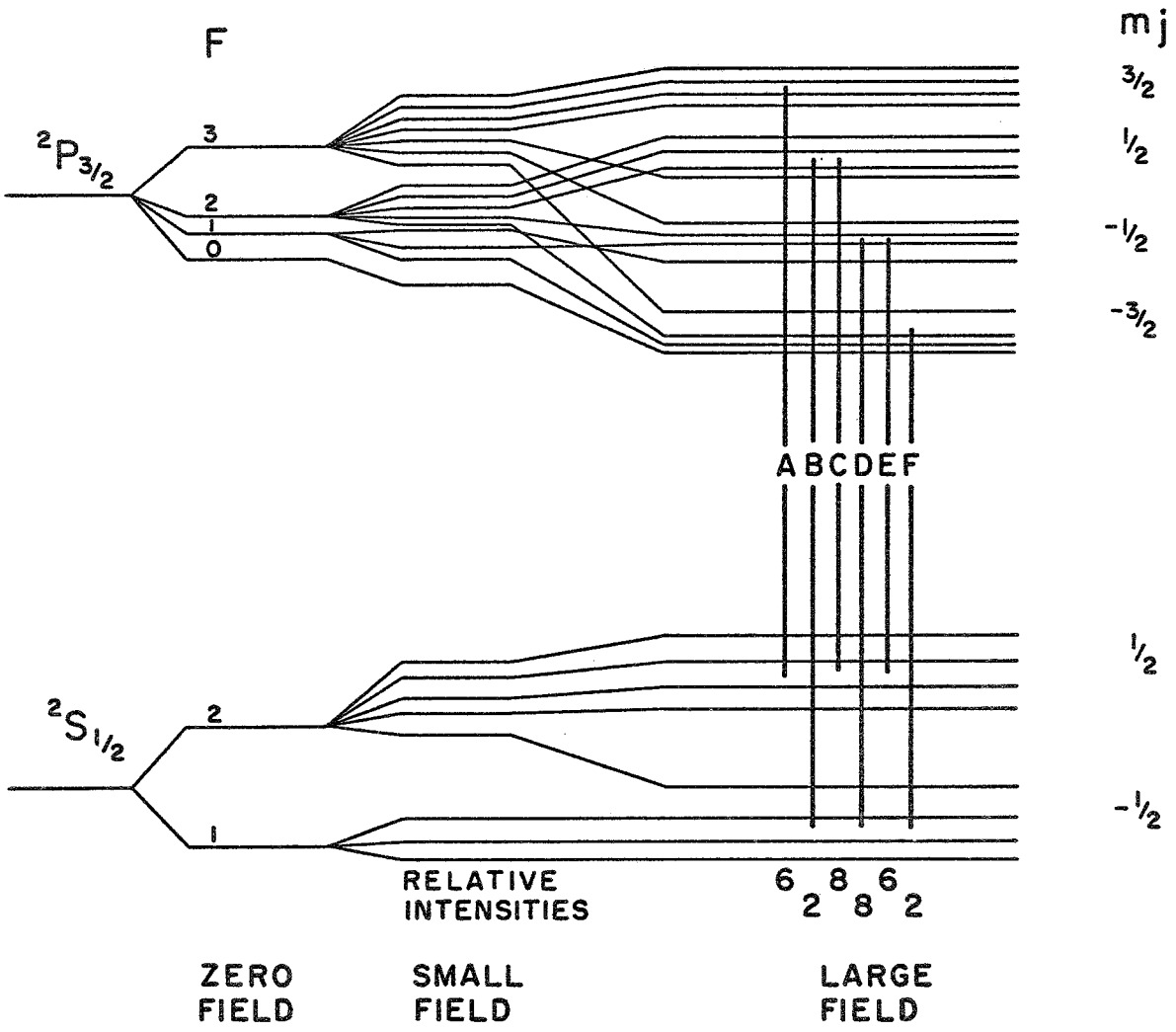
F
mj
$^2P_{3/2}$
3
2
1
0
3/2
1/2
-1/2
-3/2
A B C D E F
$^2S_{1/2}$
2
1
1/2
-1/2
RELATIVE INTENSITIES
6 8 6
2 8 2
ZERO FIELD
SMALL FIELD
LARGE FIELD

Figure XX.

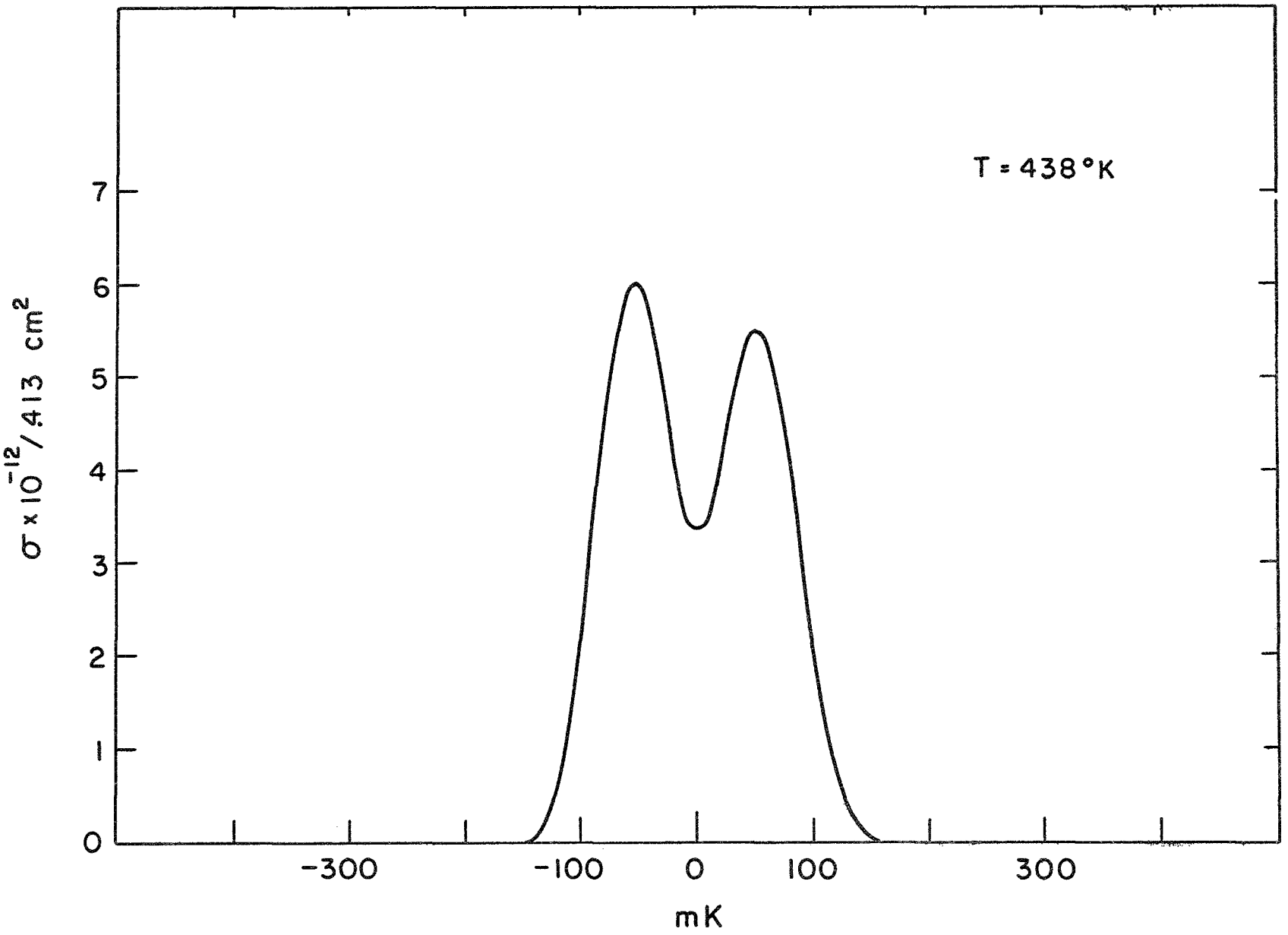

Figure XXI.

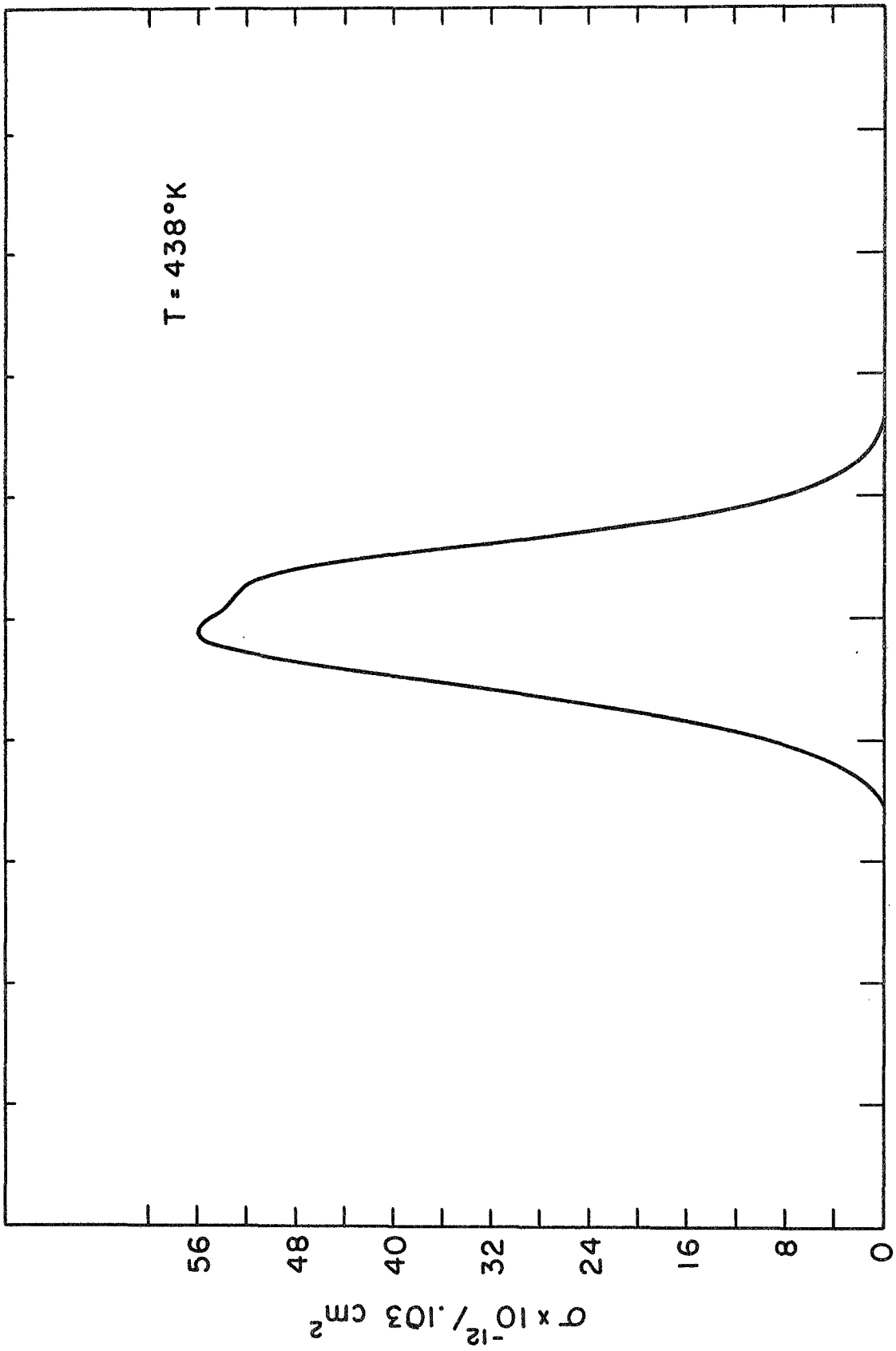

Figure XXII.

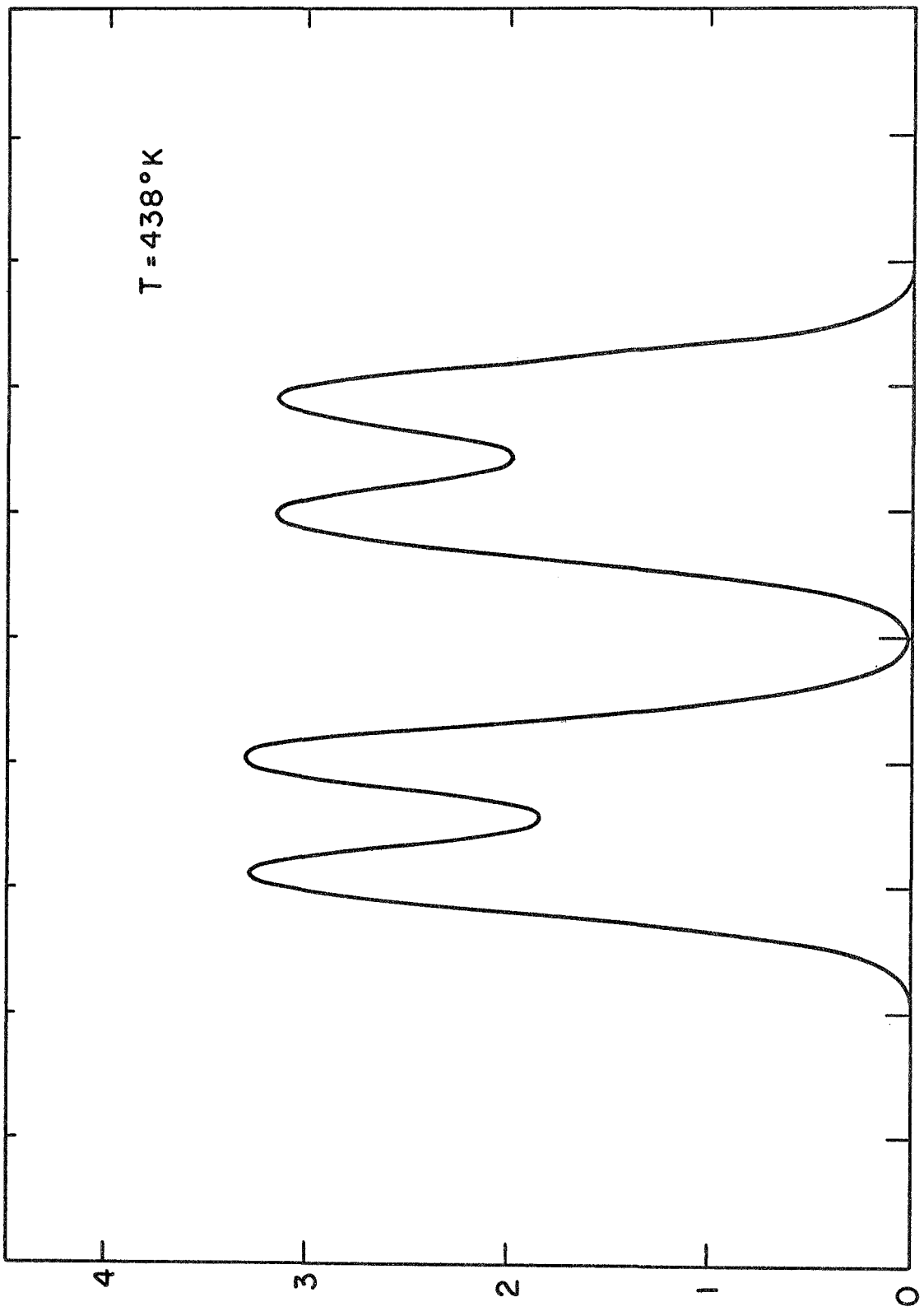

Figure XXIII.

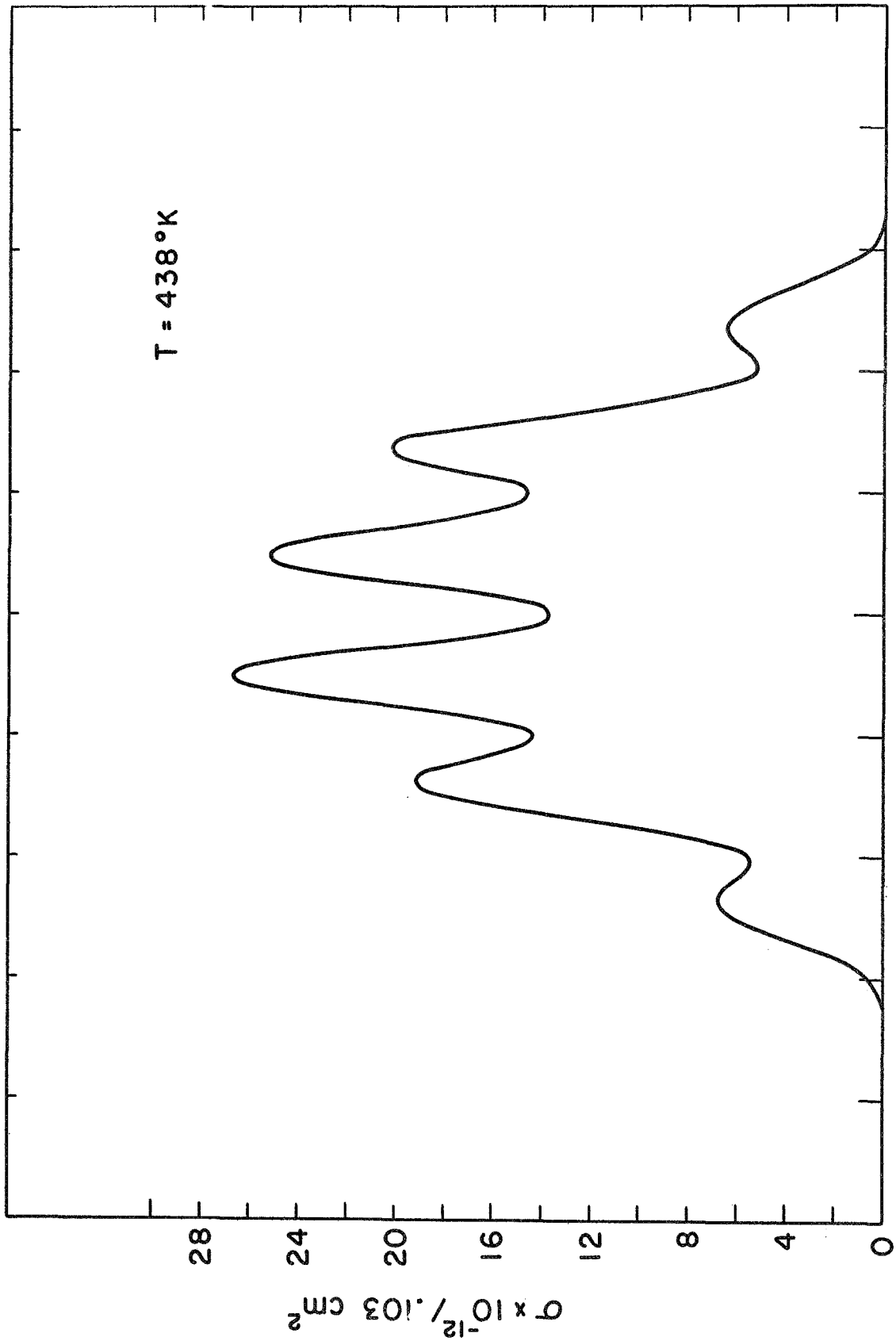

Figure XXIV.

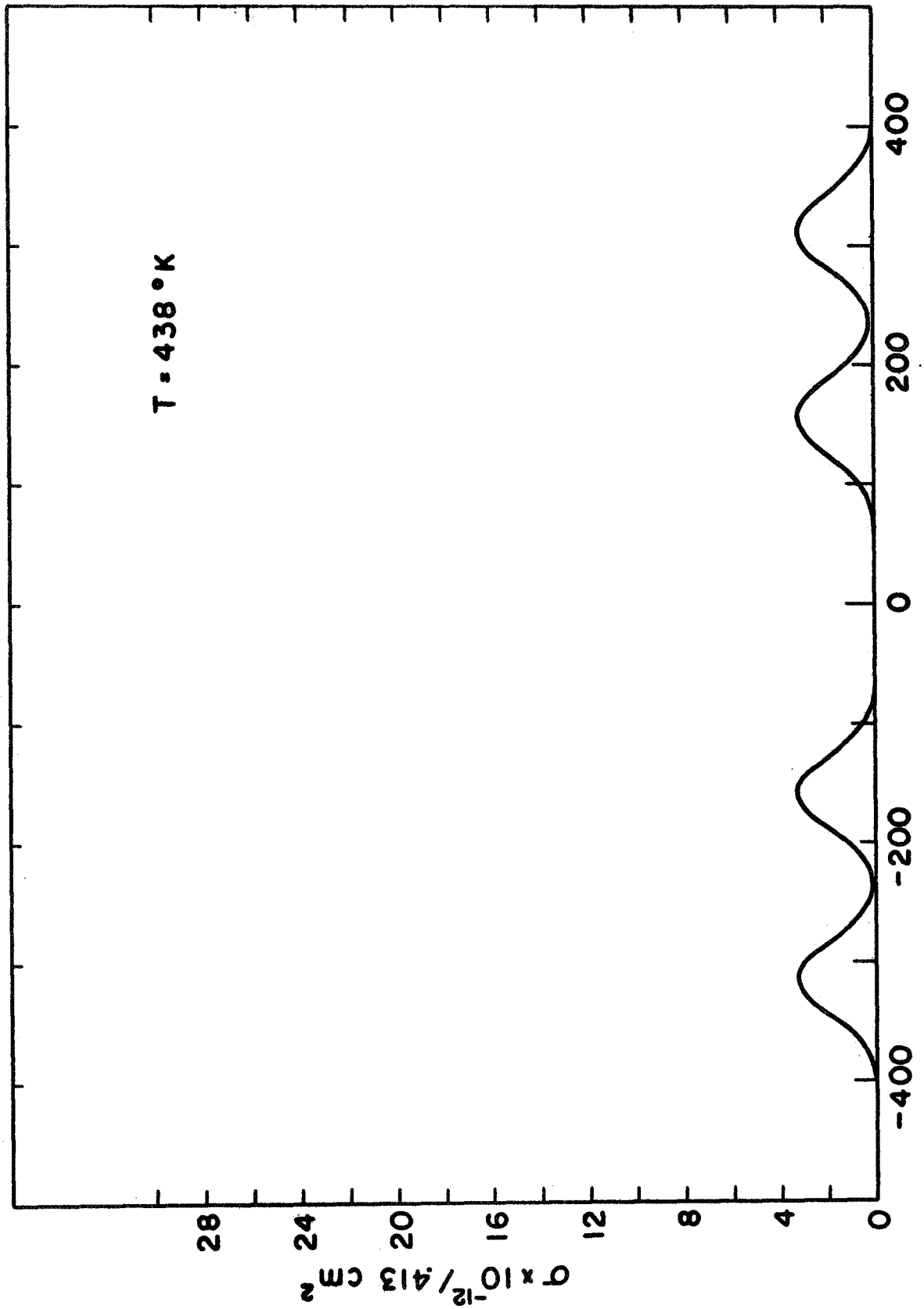

Figure XXV.

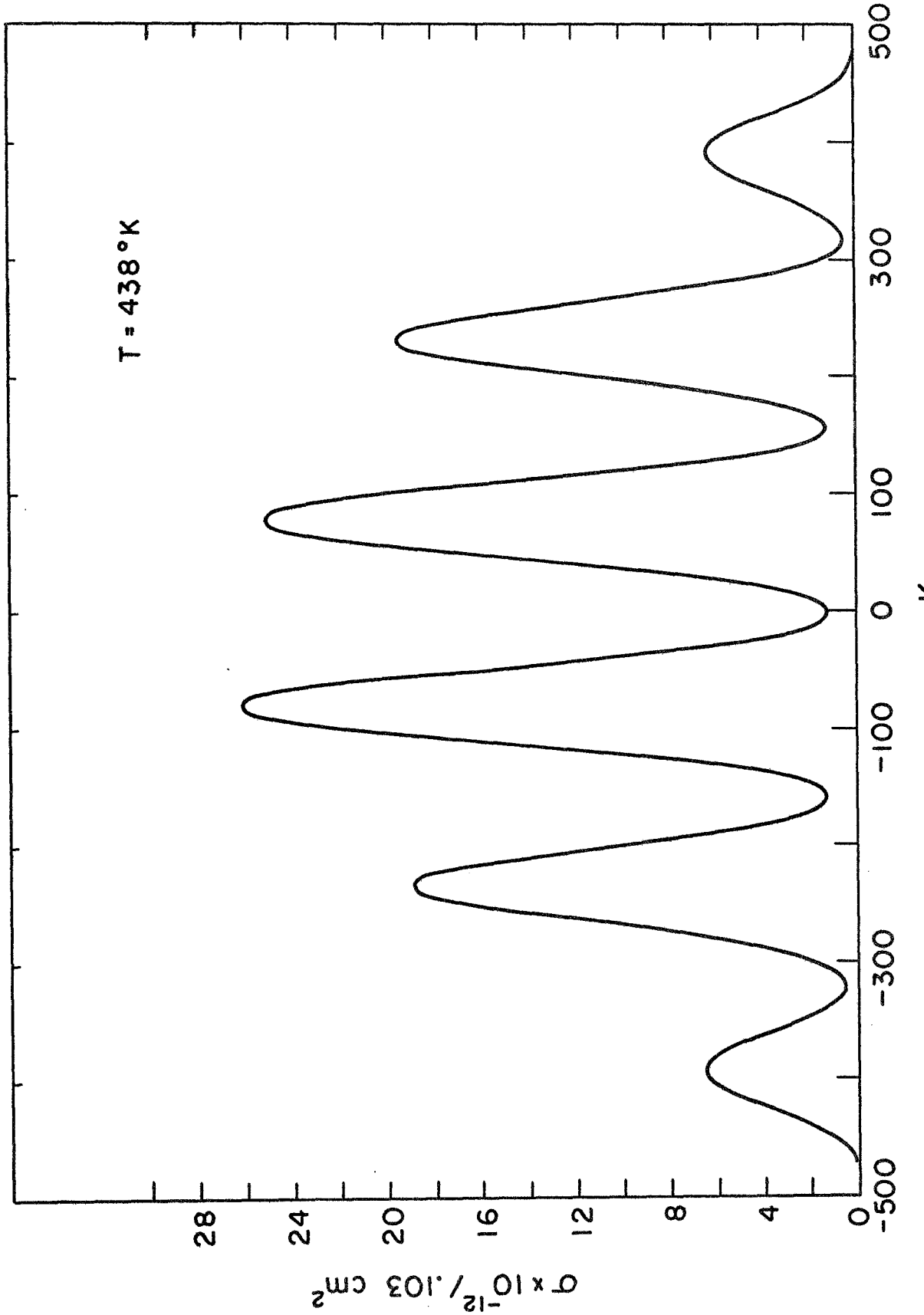
T = 438°K
σ x 10⁻¹²/.103 cm²
0
4
8
12
16
20
24
28
-500
-300
-100
0
100
300
500
mK

Figure XXVI.

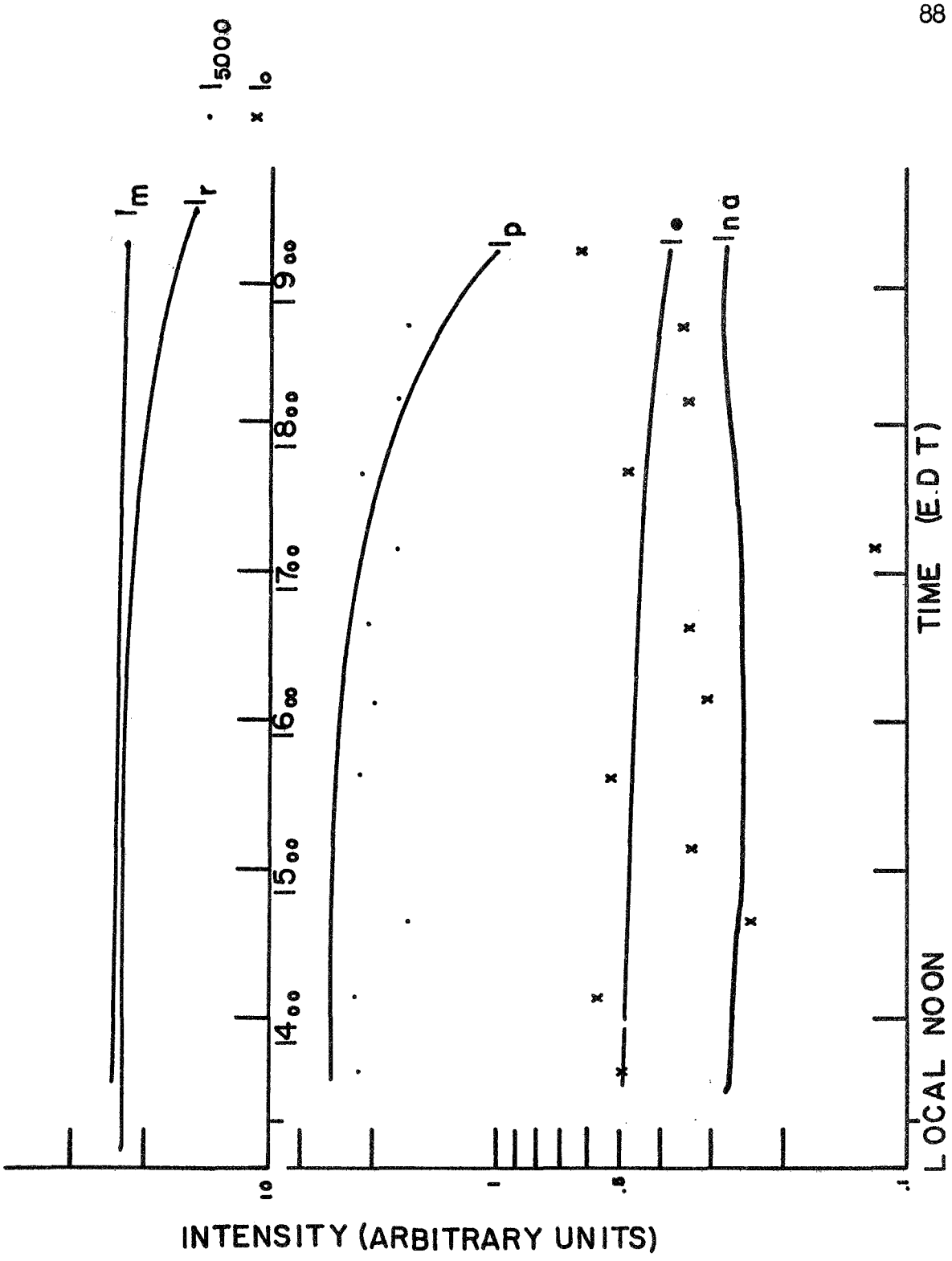

Figure XXVII.

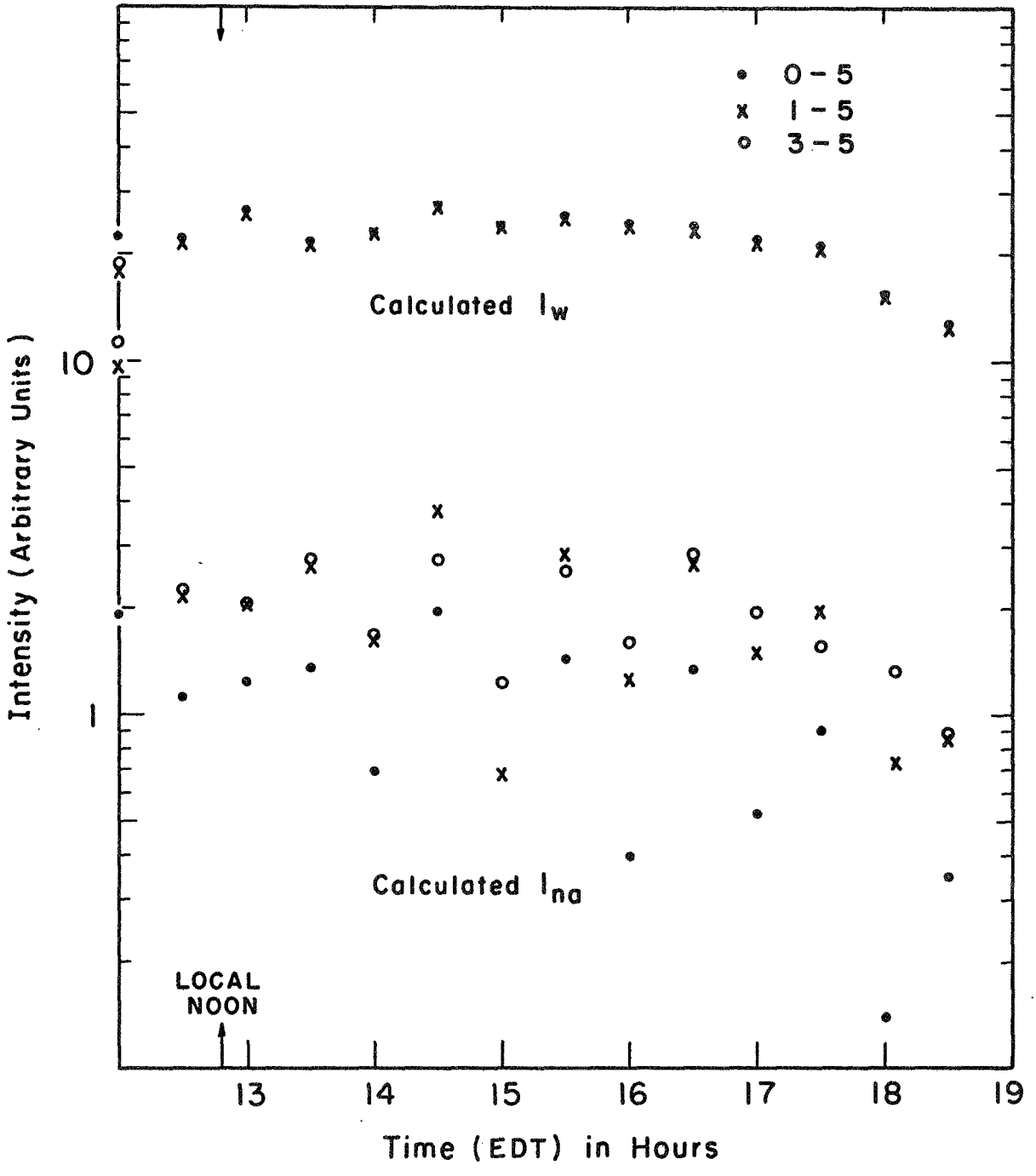

Figure XXVIII.

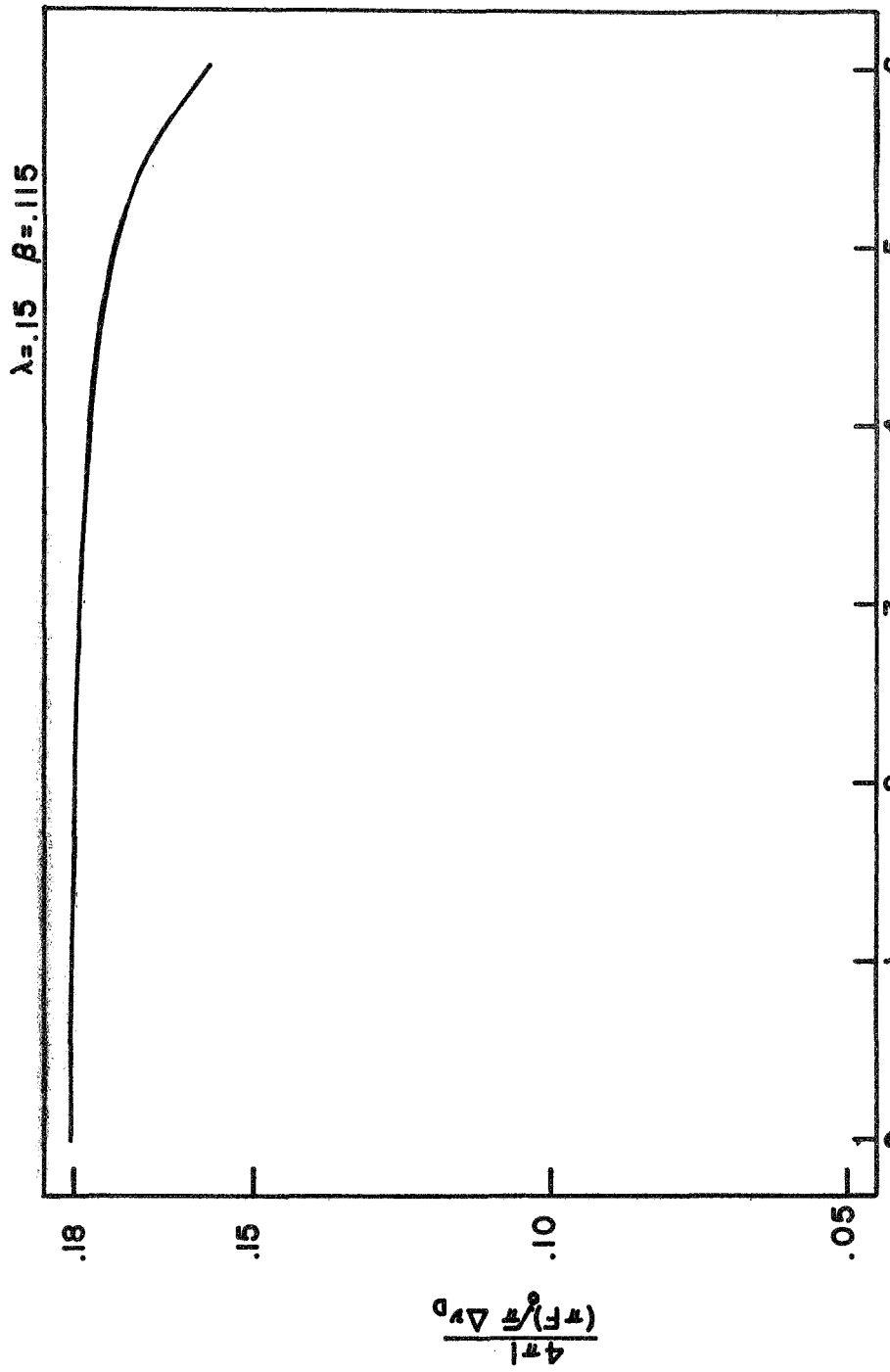
λ=.15 β=.115
.18
.15
.10
.05
0
1
2
3
4
5
6
TIME in HOURS
from LOCAL NOON
4πI / (πF)⊙π Δν_D

Figure XXIX.

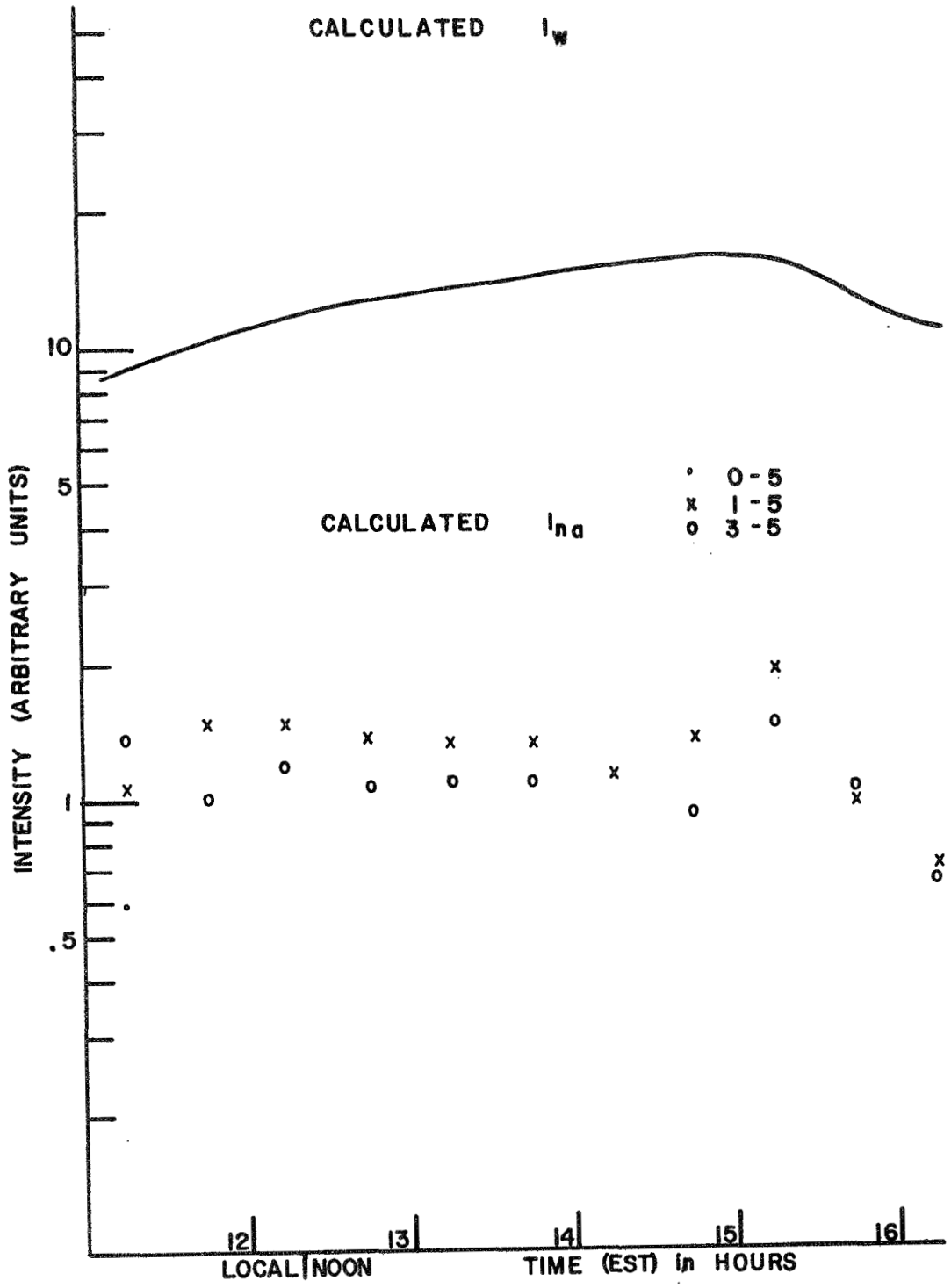
CALCULATED I_w
CALCULATED I_{na}
0 - 5
1 - 5
3 - 5
INTENSITY (ARBITRARY UNITS)
10
5
1
.5
12
LOCAL NOON
13
14
15
16
TIME (EST) in HOURS

Figure XXX.

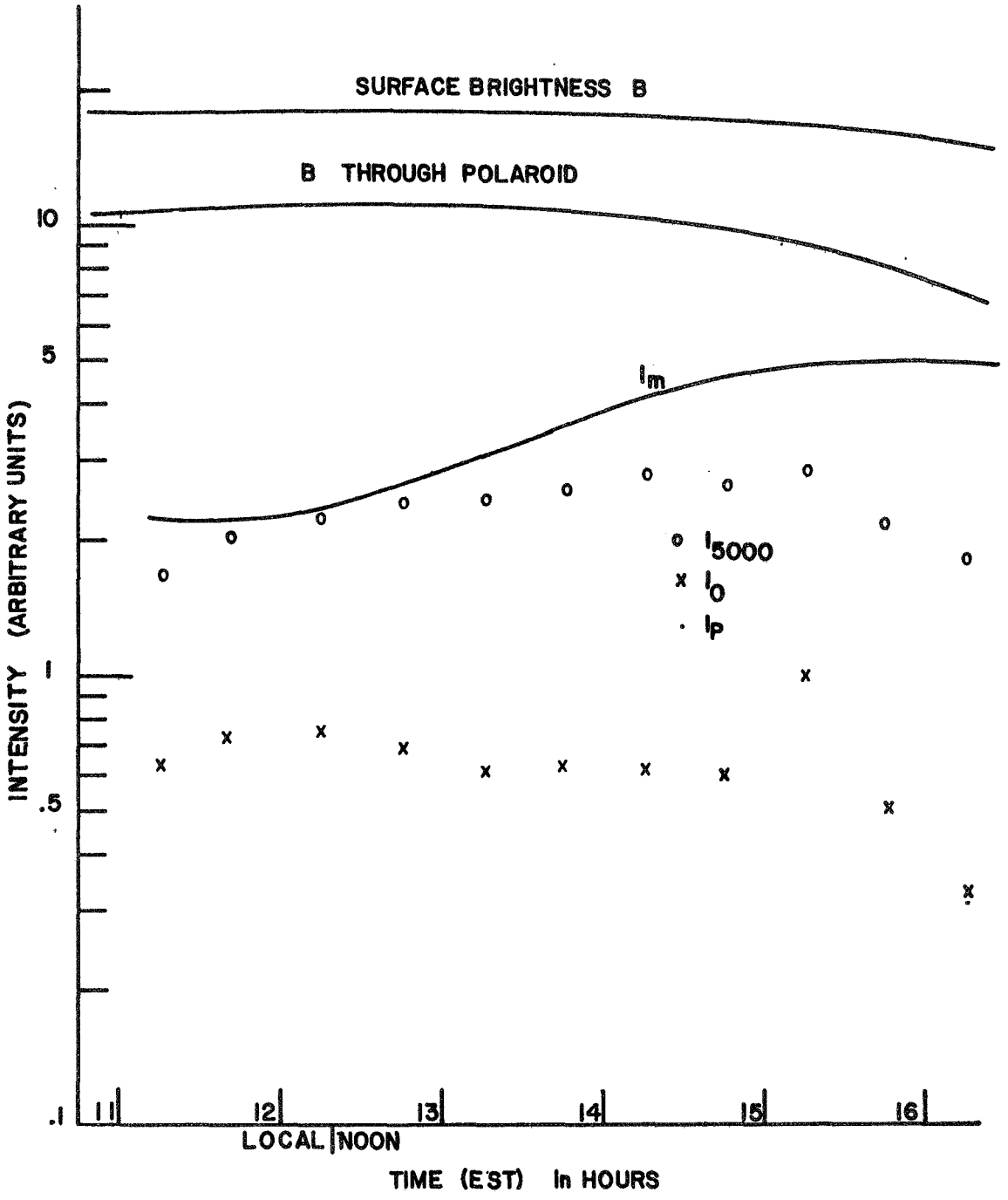
SURFACE BRIGHTNESS B
B THROUGH POLAROID
10
5
1
.5
.1
INTENSITY (ARBITRARY UNITS)
I_m
I_{5000}
I_0
I_P
11
12
13
14
15
16
LOCAL NOON
TIME (EST) In HOURS

Figure XXXI.

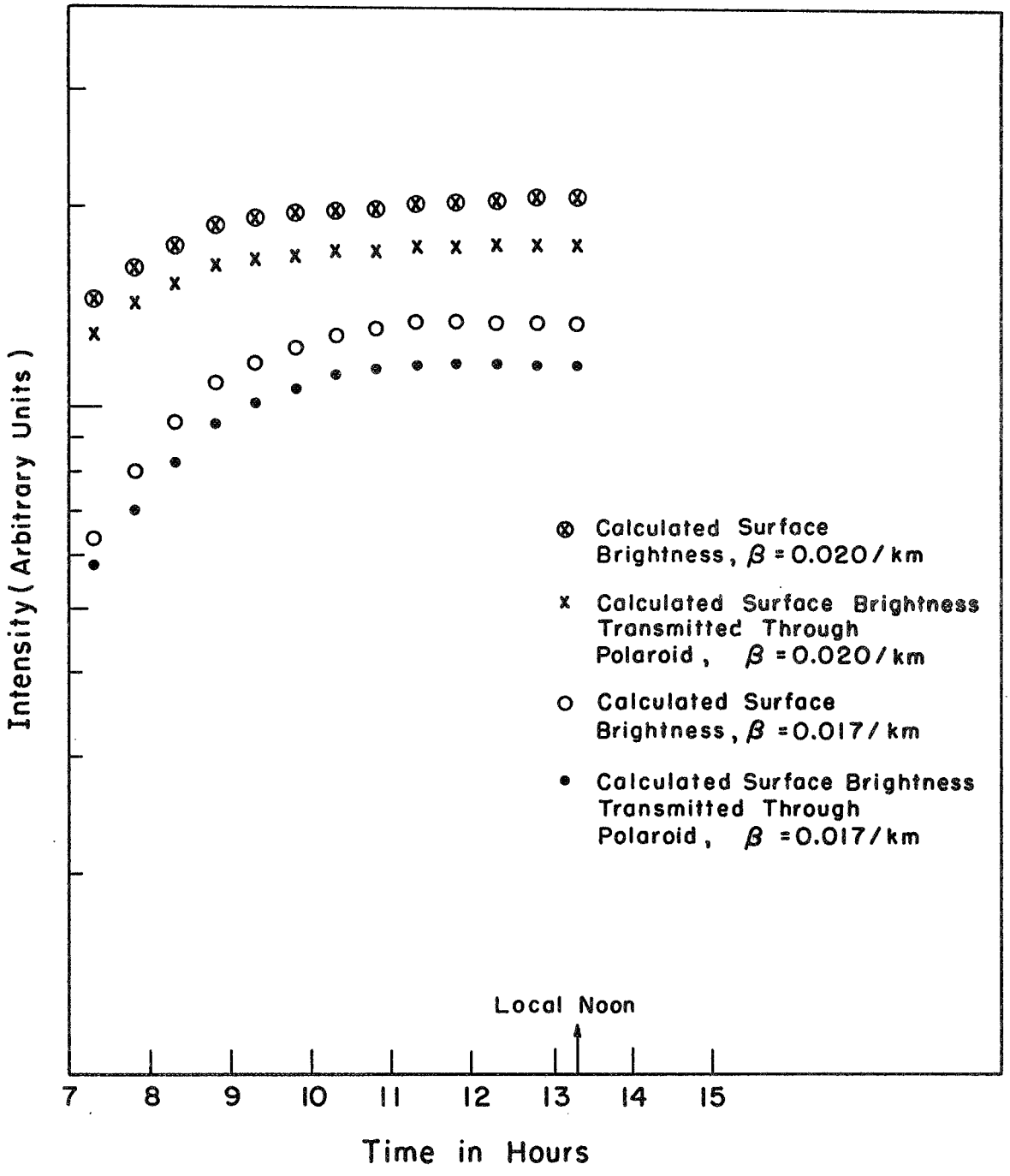

Figure XXXII.

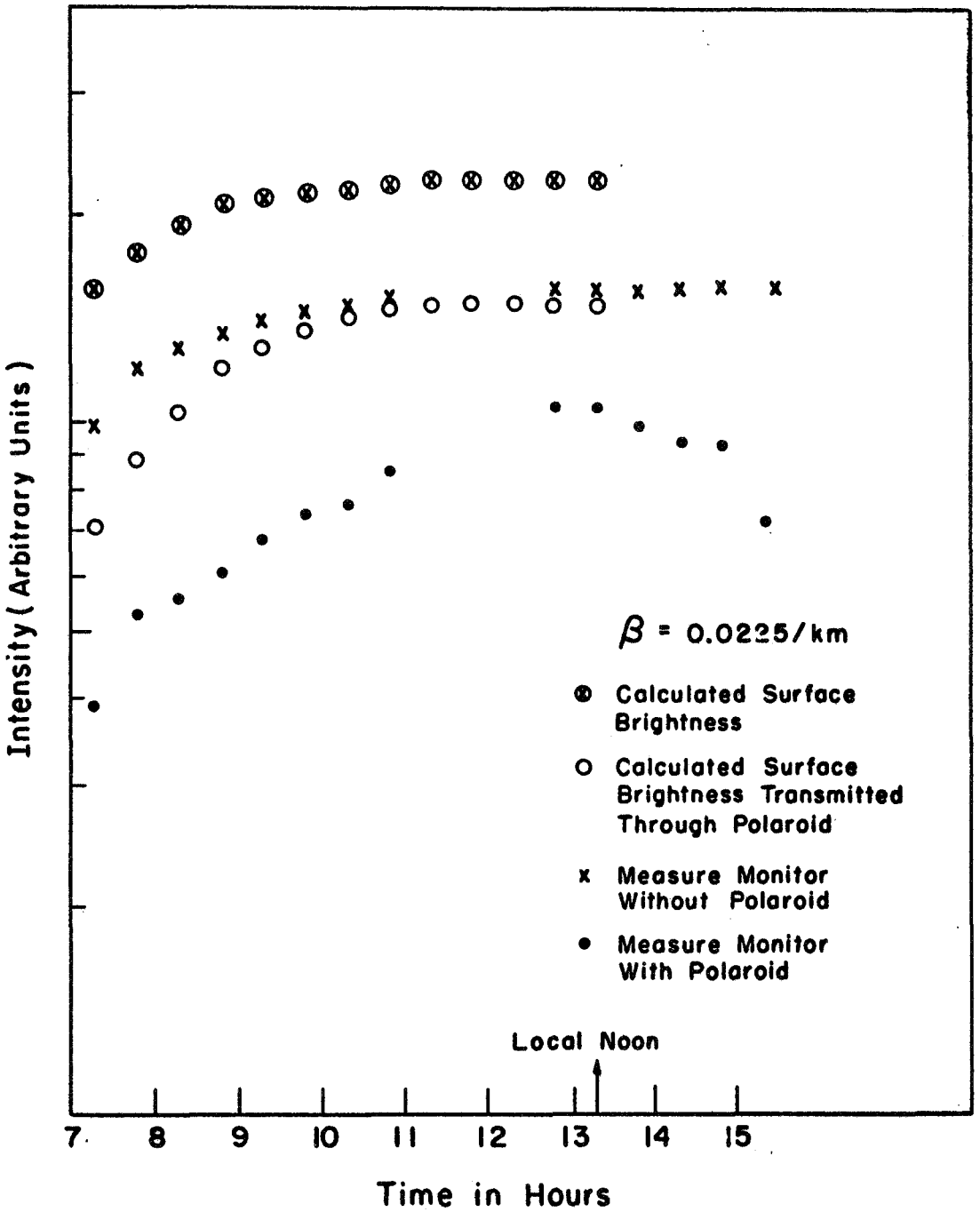

Figure XXXIII.

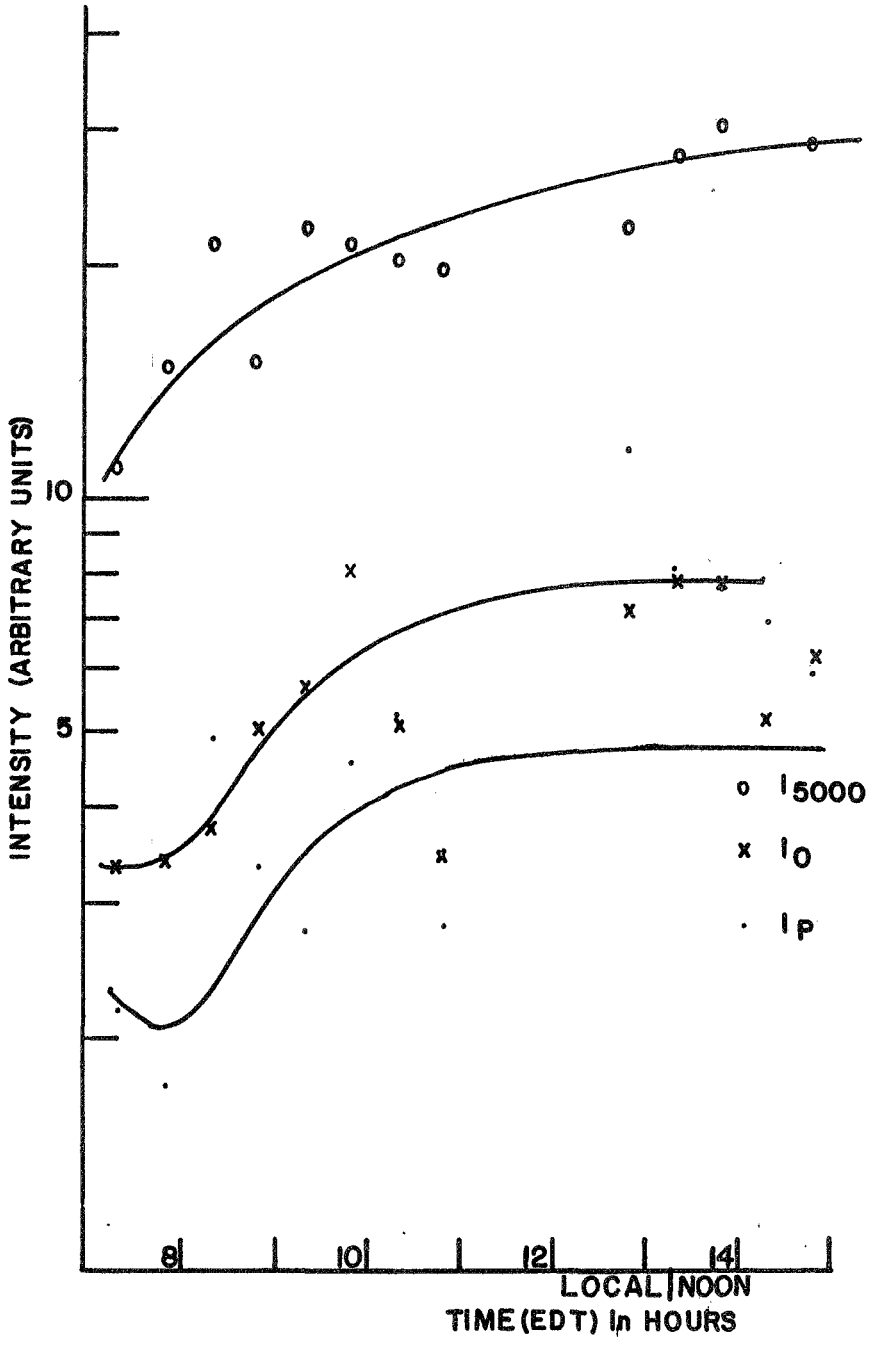

Figure XXXIV.

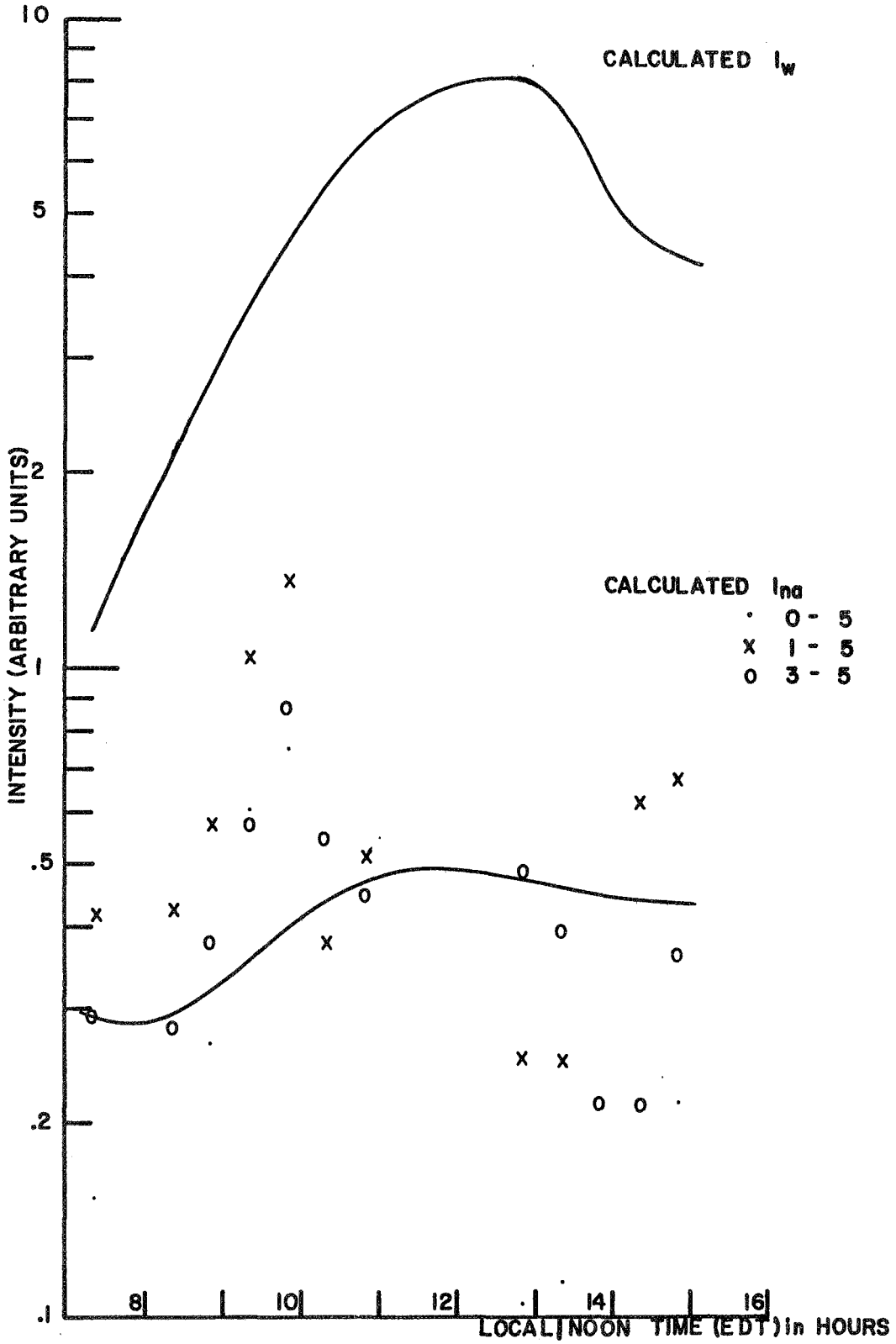
10
5
2
1
.5
.2
.1
INTENSITY (ARBITRARY UNITS)
CALCULATED I_w
CALCULATED I_{na}
· 0 - 5
x 1 - 5
o 3 - 5
8
10
12
14
16
LOCAL NOON TIME (EDT) in HOURS

Figure XXXV.

REFERENCES

Abramowitz, M., and L. A. Stegun, Handbook of Mathematical Functions, U. S. Government Printing Office, Washington, D. C. 1966.

Avrett, E. H., and D. G. Hummer, Non-Coherent Scattering, II., Royal Astronomical Society 130, No. 4, 295 (1965).

Chamberlain, J. W., Physics of the Aurora and Airglow, Academic Press, New York, 1961.

Chamberlain, J. W., D. M. Hunten, and J. E. Mack, Resonance Scattering by Atmospheric Sodium 4, Abundance of Sodium in Twilight, J. Atmospheric Terrest. Phys. 12, 153-165 (1958).

Chandrasekhar, S., and D. D. Elbert, The Illumination and Polarization of the Sunlit Sky on Rayleigh Scattering, Trans. Amer. Phil. Soc., 44, pt. 6, 643 (1954).

Cherniaev, V. I., and M. F. Vuks, The Spectrum of the Twilight Sky, Compt. Rend. 14, 77-80.

Condon, E. U., and H. Odishaw, Handbook of Physics, McGraw-Hill, New York, 1958.

Condon, E. U. and G. H. Shortley, Theory of Atomic Spectra, The MacMillan Company, 1935.

Dawson, L. H., and E. O. Hulburt, J. Opt. Soc. Am. 31, 554-558 (1941).

Donahue, T. M., A Calculation of the Sodium Dayglow Intensity, J. Geophys. Research 63, 663-666 (1956).

Donahue, T. M. , International Dictionary of Geophysics, Pergamon Press.

Donahue, T. M., and R. R. Meier, Distribution of Sodium in the Daytime Upper Atmosphere As Measured by a Rocket Experiment, J. G. R. 72, No. 11, June 1, 1967, 2803.

Donahue, T. M., R. Resnick, and V. Stull, Distribution in the Upper Atmosphere of Sodium Atoms Excited by Sunlight, Phys. Rev. 104, 873-879 (1956).

Donahue, T. M., and V. Stull, Excitation of the Sodium Twilight Glow, Ann. de Geophysique 15, No. 4, 481 (1959).

Gadsden, M., Sodium in the Upper Atmosphere: Meteoric Origin, J. Atm. Terres. Phys. 30, 151-161 (1968).

Gadsden, M., T. M. Donahue, and J. E. Blamont, On the Measurement of Sodium Dayglow Emission by Means of a Zeeman Photometer, J. G. R. 71, No. 21, 5047 (1966).

Goudsmit, S. and R. F. Bacher, The Paschen-Back Effect of Hyperfine Structure, Phys. Rev. , 1499-1500 (1929).

Herzberg, Gerhard, Atomic Spectra and Atomic Structure, Dover, New York, 1944.

Heydenburg, N. P., L. Larrick, and A. Ellett, Polarization of Sodium Resonance Radiation and Nuclear Moment of the Sodium Atom, Phys. Rev. 40, 1041-1042 (1932).

Holstein, T., Imprisonment of Resonance Radiation in Gases, Phys. Rev. 72, No. 12, 1212 (1947).

Hunten, D. M., A Study of Sodium in Twilight, 1, Theory, J. Atmospheric Terrest. Phys. 5, 44 (1954).

Hunten, D. M., Science 145, 26 (1964).

Jackson, D. A., and H. Kuhn, The Hyperfine Structure of the Zeeman Components of the Resonance Lines of Sodium, Proc. R. Soc. 167A, 205 (1938).

Kopferman, H., Nuclear Moments, Academic Press, New York, 1958.

McNutt, D. P., and J. E. Mack, Telluric Absorption, Residual Intensities, and Shifts in the Frauhnofer D Lines, J. Geophys. Res. 68, 3419-3428 (1963).

Millman, S., and P. Kusch, Phys. Rev. 60, 91 (1940).

Mitchell, A. C. G., and M. W. Zemansky, Resonance Radiation and Excited Atoms, Cambridge at the University Press, 1961.

Pauling, L., and S. Goudsmit, The Structure of Line Spectra, McGraw-Hill, New York, 1930.

Pringsheim, P., and E. Gaviola, Zeitschrift fur Physic, 1924.

Shimoda, and J. Nishikawa, Phys. Soc., Japan 6, 512 (1953).

Slipher, V. M., Publ. Astron. Soc. Pac. 41, 263 (1929).

Stull, V. R., The Transfer of Solar Radiation at the Wave Lengths of the Sodium D-lines by the Earth's Atmosphere, Ph.D. Thesis, University of Pittsburgh, 1959.

Tousey, R., and E. O. Hulburt, Brightness and Polarization of the Daytime Sky at Various Altitudes above Sea Level, J. of the Optical Soc. Am. 37, No. 37, 78 (1947).

Walker, S., and H. Straw, Spectroscopy, Science Paperbacks, London, 1961.